Selenium Removal from Power Plant Waste Water with Solid Phase Extraction Materials

by

Man Li

A Dissertation Presented in Partial Fulfillment
of the Requirements for the Degree
Doctor of Philosophy

Approved March 2017 by the
Graduate Supervisory Committee:

Candace Chan, Chair
Mary Laura Lind
Francois Perreault

ARIZONA STATE UNIVERSITY

May 2017

ABSTRACT

As selenium is toxic at low levels, treatment methods to remove selenium from industrial waste waters are needed. In this work, three groups of sorbent materials were investigated in detail for their effectiveness for selenium and arsenic removal from water: 1) nanostructured carbon-based materials, 2) layered double hydroxide (LDH)-based materials, and 3) biopolymer-based sorbents. The materials were investigated in spiked de-ionized water and waters collected from different locations at Salt River Project's (SRP) Santan Generating Station in Gilbert, AZ. The results show that nanostructured carbon-based materials removed ~80% and up to 100% selenium and arsenic, respectively in spiked DI water. Heat treated layered double hydroxides removed close to 100% removal in selenium and arsenic spiked DI water. Isotherms conducted in spiked DI water fit the Langmuir model and showed a maximum selenate adsorption capacity of 67 mg/g for the calcined LDH powder. Results from SRP waters showed that certain LDH sorbents were effective for removing the selenium, but that higher pH and existence of competing ions affected the removal efficiencies. The functionalized biopolymer sorbent from Crystal Clear Technologies: CCT-149/OCI-B showed good removal efficiencies for both selenate and selenite in DI water. Isotherms conducted in spiked DI water for CCT-149 fit the Langmuir model and showed a maximum selenate adsorption capacity of 90.9 mg/g. Column tests using spiked DI water and waters obtained from SRP wells were investigated using both LDH and CCT-149/OCI-B. Removal of sulfate using chemical pre-treatment of the water with barium chloride resulted in about three times higher selenate loading onto the granular LDH and doubled the water volume that can be treated using CCT-149/OCI-B. The results from the column tests are being used to guide

the pilot testing investigating the implementation of LDH sorbents at pilot scale at the Santan plant. The good results in the cooling tower #5 blowdown water and combined discharge waste water of SRP provide valuable information about the efficacy and efficiency of adsorptive media for the removal of selenium. Composites comprising LDH nanosheets with different substrates were successfully synthesized that were able to retain the performance in removing selenate of nanosheet LDH.

ACKNOWLEDGMENTS

This work was done under my advisor Dr. Candace Chan's kind concern and concentrated guidance. I would like to thank her for her instruction and help. She has devoted a large amount of energy to it. It has been an enjoyable experience to work with her.

I would like to thank Lisa Farmen, COO of Crystal Clear Technologies, for offering the biopolymer sorbents, the technology, and the cooperation. Most importantly, the energy, the passion, and the love she devoted to science and research that impressed me. I very appreciate her encourage and guidance.

I would like to thank my committee members, Prof. Mary Laura Lind and Prof. Francois Perreault, for their time and suggestions. I would like to thank my group members Chengwei Wang for synthesizing the carbon nanospheres and carbon foams, and Ran Zhao for helping me on the synthesis of layered double hydroxides nanosheets.

We would like to thank Fred Fuller and Brent Schuster from Salt River Project for their support of this research through the SRP/ASU Joint Research Program and for providing water samples. Partial support from the National Science Foundation Nanosystems Engineering Research Center for Nanotechnology Enabled Water Treatment (ERC-1449500) is also acknowledged. We gratefully acknowledge the use of facilities within the LeRoy Eyring Center for Solid State Science, W. M. Keck Foundation Laboratory (Environmental Biogeochemistry), and Goldwater Environmental Laboratory at Arizona State University.

I would like to thank all my friends here at Arizona State University for their friendship and the moments we spent together, especially Ting Yang and Ying Li who gave me a hand with my research.

The last but not the least, I would like to thank my parents for their eternally immutable love and support.

TABLE OF CONTENTS

CHAPTER Page

CHAPTER Page

CHAPTER Page

CHAPTER Page

CHAPTER Page

LIST OF FIGURES

Figure Page

Figure Page

Figure Page

Figure Page

Figure Page

Figure Page

Figure Page

Figure Page

LIST OF TABLES

Table Page

Table Page

Table Page

Table Page

LIST OF PUBLICATIONS

Chapter 3

1. **Li, M**., Wang, C.-W., O'Connell, M. J. & Chan, C. K. Carbon Nanosphere Adsorbents for Removal of Arsenate and Selenate from Water. *Environmental Science: Nano*. **2015**, 2, 245-250

Chapter 4

2. **Li, M.**, Farmen, L. M., & Chan, C. K. Selenium Removal from Sulfate-Containing Groundwater Using Granular Layered Double Hydroxide Materials. *Industrial & Engineering Chemistry Research.* **2017**, 56(9), 2458-2465

3. **Li, M.**, Farmen, L. M., & Chan, C. K. Calcined Layered Double Hydroxides for Selenium Removal from Power Plant Waters. *CLEAN-Soil, Air, Water*. **2017**. (Submitted)

Chapter 6

4. **Li, M.**, Farmen, L. M., & Chan, C. K. Functionalized Biopolymer used for Selenium and Arsenic Removal from Waste Water. **2017**. (In preparation)

Chapter 12

5. **Li, M.**, and Chan, C. K. Study of Selenate Adsorption by Layered Double Hydroxide and Chitosan Composite Beads. (In preparation)

6. **Li, M.**, and Chan, C. K. Adsorption of Selenate using Layered Double Hydroxide Combined Cellulose Membranes for Power Plant Waters. (In preparation)

Other Publications

7. **Li, M.**, Cheng, Q., Wittman, R. M., Peng, X.-h. & Chan, C. K. Electrochemical and Photoelectrochemical Properties of the Copper Hydroxyphosphate Mineral Libethenite. *Chemelectrochem.* **2014**, 1, 663-672

8. Peng, X.-h., **Li, M.** & Chan, C. K. Investigation of the Optical Absorbance, Electronic, and Photocatalytic Properties of $(Cu_{1-x}Co_x)_2(OH)PO_4$ Solid Solutions. *Journal of Physical Chemistry C*. **2015**, *119* (9), 4684–4693

LIST OF ACRONYMS

ACRONYM	DEFINITION
As	Arsenic
As(III)	Valence +3 Arsenic (found in arsenite ion, AsO_3^{3-})
As(V)	Valence +5 Arsenic (found in arsenate ion, AsO_4^{3-})
BET	Brunauer-Emmett-Teller Surface Area Technique
BRL	Below Reporting Limit
BV	Bed Volume
CCT	Crystal Clear Technology Inc.
CF	Carbon Foam
CNS	Carbon Nanospheres
DI	De-ionized
EBCT	Empty Bed Contact Time
EPA	US Environmental Protection Agency
FGD	Flue Gas Desulfurization
FNOM	Functionalized NOM (Functionalized biopolymer-based sorbents)
FTIR	Fourier Transform-Infrared Spectroscopy
GAC	Granular Activated Carbon
ICP-MS	Inductive Coupled Plasma-Mass Spectroscopy
ICP-OES	Inductively Coupled Plasma-Optical Emission Spectroscopy
LDH	Layered Double Hydroxide
LOD	Limit of Detection (Detection Limitation)
MICB	Metal Oxide Impregnated Chitosan Beads
NMO	Nanocrystalline Metal Oxide
NOM	Naturally Occurring Material (Native substrate)
PAC	Powdered Activated Carbon

PZC	Point-of-Zero Charge
Se	Selenium
Se(IV)	Valence +4 Selenium (found in selenite ion, $HSeO_3^{2-}$)
Se(VI)	Valence +6 Selenium (found in selenate ion, SeO_4^{2-})
SEM	Scanning Electron Microscopy
SRP	Salt River Project
TDS	Total Dissolved Solids
XRD	X-ray Diffraction

1. Introduction

As the demand for electricity increases along with the growing economy, the electric utilities require more and more waters for steam generation and cooling during power generation. However, the blowdown and plant discharge waters may contain trace level metal contaminants harmful to the health and environment.[1] Selenium at trace levels can be an issue for non-coal-fired power plants if these selenium-containing waters are used as make-up waters for the cooling water. A large amount of water is required to extract heat from the power plant condenser on the low pressure side of the steam turbine and dissipate it in the wet cooling towers through evaporation;[2] during the evaporation process, the levels of ions in the water can increase several times in the cooling tower blowdown. Selenium can enter the aquatic environment by contamination from agricultural drainage [3] and industrial wastewaters (e.g. oil refining, mining). As selenium is also found as a constituent of coal (several mg per kg),[4-5] wastewaters from coal-fired power plants can contain high levels of selenium on the order of several hundred ppb. For example, flue gas desulfurization (FGD) waters can contain 1 – 10 mg/L selenium.[6-7] Although selenium is an essential nutrition element for living organisms, excessive levels of selenium can lead to toxicity in humans and wildlife, like organ damages, and particularly in aquatic environments where bioaccumulation can be quite rapid.[8-9] For example, only 2–5 ppb of waterborne selenium species can cause reproductive failure in fish.[10] While the U.S. Environmental Protection Agency's maximum allowable selenium contaminant level for drinking water is 50 µg/L,[11] changes in regulatory limits (as of Nov. 2015, US EPA) for Flue Gas Desulfurization (FGD) wastewater of any steam electric power generating point source discharge have been lowered to only 12 µg/L for selenium

(daily average standard for 30 consecutive days).[12] Hence, there is a need for strategies for selenium removal from power plants waste waters.

Selenium is found in the environment in four oxidation states: Se(VI), Se(IV), Se(0), Se(-II),[13] and the predominant form of selenium present depends on the pH and oxidation reduction potential [14-15] as shown in Figure 1. It is found as selenate, Se(VI), and selenite, Se(IV), in oxidized systems, but Se(0) and selenides in anaerobic zones.[16] Both Se(0) and Se(-II) are insoluble. In pH 6-8, only Se(0), selenite, biselenite ($HSeO_3^{-1}$) and selenate are present. Removal strategies for selenium typically involve reduction of selenate, which is not easily adsorbed onto particulates, to selenite, which can be easily immobilized.[14,15,17-18] This is because selenite tends to bind through inner-sphere surface complexes and binds strongly to metal oxide surfaces while, selenate tends to bind through a mechanism of outer-sphere and adsorbs relatively weakly to metal oxide surfaces.[19-23] For this reason, other ions present in water such as sulfate, which is similar to selenate in structure and physicochemical properties,[24] may compete for the same binding sites, which leads to the difficulty in removing selenate from waters with high concentration of competing ions. Wijnja et al.[21] investigated selenate and sulfate adsorption mechanism on Al oxide in situ, showing that selenate and sulfate adsorb to Al oxide predominantly via the same mechanism, an outer-sphere surface complexation mechanism, at pH 6.0 and above. At pH below 6.0, a small fraction of inner-sphere surface complexes was presented. Yamaguchi et al.[25] studied the volume changes caused by selenate and sulfate adsorption on an amorphous iron oxide suggesting that similar reaction mechanisms were occurring since the volume changes for sulfate and selenate were identical.

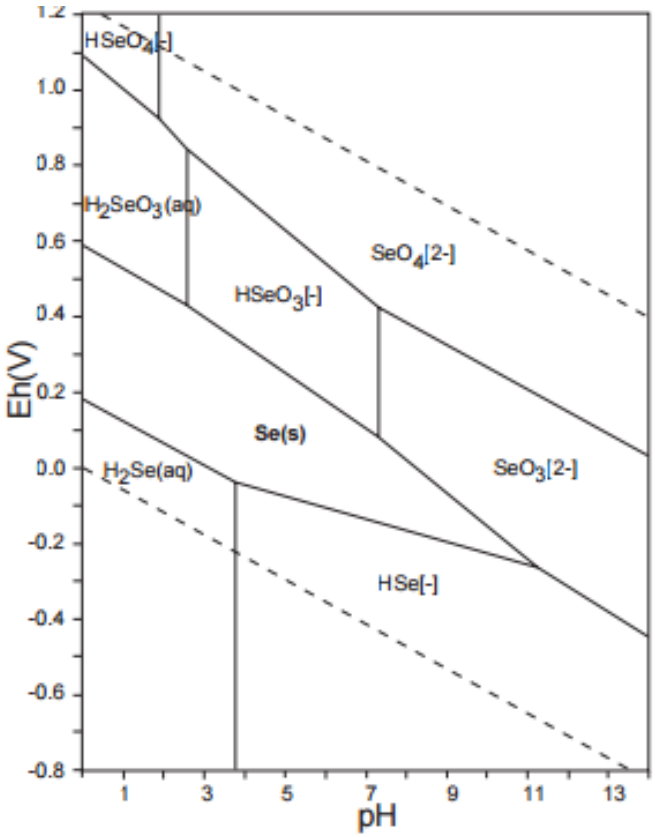

Figure 1. Eh-pH diagram for selenium species.[26]

1.1. Overview of Selenium Treatment Technologies

Several recent reviews have summarized the various chemical, biological, and physical treatment methods that have been investigated for selenium removal from water.[7,27] A summary of the various selenium treatment technologies that are commercially available is reported in Table S1. Biological reduction of Se with anaerobic bacteria or algae has been shown to be very effective, with > 95% selenium removal for influent Se of 0.4 mg/L[16] and a commercially available bioreactor (ABMet®) from GE already demonstrated to remove Se to < 10 μg/L in pilot and full-scale applications.[28]

However, such technologies require substantial real estate, capital/operational costs, and maintenance that may not be appropriate for low influent Se levels or high flow rates. Other technologies that are available but not demonstrated at full scale include activated alumina, BioSolve® (a commercially available technology system consists of a continuously stirred tank reactor with plastic sponge media for biofilm development), electrocoagulation, and fluidized bed reactor etc.[27]

The use of physical methods such as sorption for water treatment is attractive since it is a simple and low-cost process. Various adsorbents have been studied for selenium removal so far, including activated carbon, chitin and chitosan, zero valent iron (ZVI), activated alumina, iron oxyhydroxides.[29] Due to the large surface area and suitable surface functional groups, activated carbons are used as good adsorbents for heavy metal ions removal in water treatment application, but the adsorption of selenium, either Se(IV) or Se(VI), is ineffective.[29] Jeffers et al.[30] had showed < 4% Se(IV) or Se(VI) removal at the initial concentration from 30-100 µg/L using dosages of activated carbons up to 100 mg/L. Selenium and arsenic adsorption on novel polymeric materials with abundant amine groups, such as chitin or chitosan, has also been investigated,[31] but good efficiency only shown in highly acidic solutions. Among the solid phase extraction materials, zero valent iron (ZVI) is one of the most well-known techniques for removing common environmental contaminants such as As, Cr(VI), and NO_3^- due to its moderately strong reducing ability.[17] However, the efficacy of removing selenium is largely dependent on the oxidation state of the selenium and the existence of competing salts.[6] It is also reported that the adsorption of Se(IV) is pH dependent with about 100% Se(IV) removed at pH 4-6 but < 10 % removed at pH 9-10.[17] Adsorption of Se (IV) by alumina

has been reported to be effective, with almost complete removal in the pH range of 3-8 (for concentrations up to 4 mg /L using 3.3 g/L Al_2O_3). However, Se (VI) adsorption by alumina is poor,[32] which drops off rapidly with increasing pH and water that can be treated at pH 7 is less than 50% bed volumes when at pH 5 in column test with synthetic water. Trussel et al.[33] also observed that sulfate and bicarbonate had no effect on Se (IV) removal but greatly affected Se(VI) adsorption. Su et al.[34] had investigated the sorption of Se(IV) and Se(VI) on amorphous iron oxide and goethite (α-FeOOH), in which the amorphous iron oxide showed better performance on selenite sorption, and the greatest sorption of Se(IV) was only found at pH < 8. Selenate is more difficult to remove compared to the lower oxidation state species and there are few effective adsorbents available.[35]

The objective of this project was to lower the selenium level in SRP waters down to below 2 ppb. As introduced above, sorption of selenium onto solid-phase extraction materials is complicated by the fact that selenium is typically found as the oxoanions biselenite ($HSeO_3^-$) or selenate (SeO_4^{2-}) in natural waters.[14,36] This means that positively charged surfaces, such as metal oxides with high point of zero charge (PZC), must be employed in order to facilitate binding of the negatively charged selenium species. In our study, we screened several materials that showed good sorption ability in water treatment applications and investigated three groups of sorbents in detail for their selenium removal performance based on their properties such as high surface area and high point of zero charge. Besides selenium, we also evaluate the adsorption properties of sorbents for removal of arsenic. The toxic and carcinogenic properties of arsenic[37] are well known. Although arsenate, As(V), is less toxic than arsenite, As(III), it is the predominate form

of arsenic in oxygen rich and oxidizing environments such as drinking and surface waters.[38] Hence, most of the arsenic removal experiments were performed on arsenate.

1.2. Materials Characterization Techniques

1.2.1. X-ray Diffraction

The X-ray diffraction (XRD) technique is one of the most useful and straightforward methods to identify phases in crystalline samples and to determining the crystallographic information like atomic and molecular structure for materials such as metals, ceramics, minerals, polymers, and other organic or inorganic compounds as well as biological molecules. The atomic planes in the specimen can cause the incident beam of X-rays to interfere with each other as they leave the crystal and thus diffract into many specific directions. The scattered X-rays are collected by the detector to form a diffraction pattern that made of reflections from the atomic planes in the material. The fundamental diffraction is based on the Bragg's law:

$$n\lambda = 2d \sin\theta$$

Here n is any integer, λ is the wavelength of the incident beam, d is the spacing between two diffracting planes, and θ is the incident angle. By measuring the angles and intensities of these diffracted beams, the signals of the reflections are shown as peaks in the XRD pattern, which can be used to identify the crystal structure of the material.

1.2.2. Scanning Electron Microscopy

The scanning electron microscopy (SEM) is one of the most commonly used technique for imaging of sample surfaces in research area today and developed new areas of study in the physical, chemical or any other science communities. When using a focused beam of high-energy electrons instead of using light to hits the specimen and scans across it, a variety of signals at the surface of specimen are detected by collecting the ejected x-rays, primary backscattered electrons, secondary electrons and so on. These are generated by electron-sample interactions and the signals can be used to reveal information about the samples including external morphology as well as chemical composition.

Because SEM utilizes vacuum conditions and uses secondary electrons to form the image, specimen preparation must be performed appropriately. Water must be removed completely from the samples since the vapor from the water would affect the vacuum condition. Non-conductive samples need to be made conductive by covering the sample with a thin layer of conductive material such as gold or carbon using a sputter coater or adhering them onto a conducting tape. In this work, specimens were prepared by dispersing sample powders into isopropanol and then dropped onto a silicon substrate. For insulated samples, a thin layer of gold was covered on the specimen by sputtering in order to improve the conductivity and hence to obtain better image quality.

1.2.3. Brunauer-Emmett-Teller Surface Area Analysis

Brunauer-Emmett-Teller (BET) surface area analysis was developed in 1938 by Stephen Brunauer, Paul Huge Emmett, and Edward Teller,[39] and named afterwards. BET

analysis provides specific surface area evaluation of materials by measuring physical adsorption, usually using a non-corrosive gas such as nitrogen, argon, and carbon dioxide etc., on the surface of the solid as a function of relative pressure. Physical adsorption results from van der Waals forces, a relatively weak forces, between the adsorbate gas molecules and the sorbent surface area of the sample. The measurement is usually carried out at the liquid nitrogen temperature, which is 77 K. The analysis encompasses external area and internal pore area to determine total specific surface area in m^2/g to study the effects of surface porosity and particle size in many applications.

1.2.4. Fourier Transform-Infrared Spectroscopy

Fourier transform-infrared spectroscopy (FTIR) is an effective analytical technique for identifying the chemical functionality and compounds in the near-surface region of materials. FTIR measures the absorbance of infrared light of a sample and generates an infrared spectrum of absorption or emissioin based on the functional groups at a particular wavelength. The infrared absorption bands can be used to identify molecular components and structures. The signal obtained from the detector is an interferogram, then it is analyzed with a computer using Fourier transforms to obtain a single-beam infrared spectrum.

When a material is irradiated with infrared radiation, absorbed IR radiation can excite molecules into a higher vibrational state. The wavelength of light absorbed by a particular molecule is a function of the energy difference between the excited and at-rest vibrational states so that the wavelengths that are absorbed by the sample can be used to characterize its molecular structure.

1.2.5. Inductively Coupled Plasma Techniques

Inductively coupled plasma (ICP) analysis is a very useful technique that can be used to detecting and analyzing trace elements including metals and some non-metals. The inductively coupled plasma is the excitation source used in optical emission spectroscopy (ICP-OES) and mass spectrometry (ICP-MS). It is a plasma that is ionized by inductively heating the argon gas with an electromagnetic coil, and contains plenty of ions and electrons to make the gas electrically conductive. The sample solutions are introduced into the ICP as an aerosol using a nebulizer and sprayed into the chamber in the center of the plasma. The plasma's extremely high temperature which can reach to 8000-10000 K causes the sample aerosol to separate into individual atoms (atomization). And then the plasma ionizes the atoms (ionization) so that they can be detected. For ICP-OES, the break up atoms recombine and give off radiation at the characteristic emission wavelengths. The characteristic wavelengths that correspond to different elements can be identified and the intensity of the emission lines are quantified to obtain the concentration. For ICP-MS, the generated ions are separated by the mass-to-charge ratios and only the ions with specific mass-to-charge ratio can reach to the detector to generate a signal proportional to the concentration.

2. Methods for Sorbent Evaluation

2.1. SRP Water Sites

Water samples were collected from 7 different sites from Salt River Project's Santan Generating Station, a combined cycle, natural-gas-powered plant in Gilbert, AZ, labelled Sites A through G as shown in Table 1. Water samples from sites A – F were collected on July 29, 2014. The raw canal water (site G) was obtained on August 14, 2014. The boiler and cooling water for the Santan Generation Station are sourced from onsite wells or surface waters. Groundwater in the Salt River Project (SRP) service area contains naturally occurring levels of selenium, which can become concentrated in cooling tower water blowdown. Samples from the make-up water (canal and well water), cooling tower blowdown, and final plant discharge waste were chosen (Figure 2). Detailed information regarding the pH and concentrations of dissolved species of interest to this project are shown in Table 2. The pH values were obtained immediately after sampling and ranged from 6.88 to 8.42. The analytical data with information about metals concentration and total dissolved solids (TDS) were obtained from SRP from samples collected at the same sites but at an earlier date, June 19, 2014.

Barium chloride pre-treatment of the power plant water prior to exposure to the sorbents was investigated. A 1 M $BaCl_2$ solution (Sigma-Aldrich, product no. 34252-1L-R) was added to the water matrix using a 3:1 mol ratio of Ba^{2+} to SO_4^{2-}.

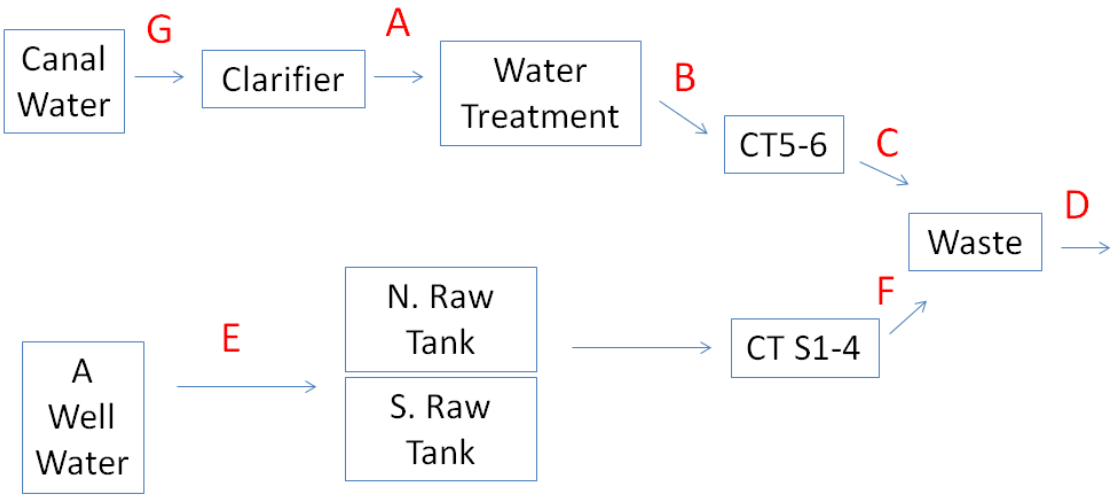

Figure 2. Sample sites for SRP water tests.

Table 1. Description of sample sites for SRP water tests.

Site	Description
A	Raw canal water after clarifier
B	Canal water discharge from service water tank, chlorinated
C	CT-6 blowdown discharge, with bisulfite, de-chlorinated
D	Final plant discharge waste (ST-005)
E	Discharge from A well
F	CT1-4 blowdown discharge, de-chlorinated
G	Raw canal water before clarifier

Table 2. Detailed information of sample sites for SRP water tests.

Site	7/29/14 Sample Date		6/19/14 Sample Date						
	pH	Temp (ºC)	Cr (ppb)	As (ppb)	Se (ppb)	Cu (ppb)	Nitrate (ppm)	Sulfate (ppm)	TDS (ppm)
A	7.95	29.8	BRL	7.1	BRL	BRL	1.41	59.5	698
B	7.99	29.0							
C	6.88	29.3	24	19.6	2.94	12	63.1	708	3200
D	8.42	35	18	15.4	2.37	12	49.4	398	2100
E	7.71	32.7	17	23.9	2.72	BRL	45.3	132	1000
F	7.57	31.8	53	83.6	5.75	83	123	533	2700
G									

BRL= below reporting limit
TDS=total dissolved solids

2.2. Jar Testing Procedures

Initial Se removal tests were performed at room temperature in batch jar tests using sorbents at concentrations ranging from 0.1 – 5 g/L (will be noted below) in ultrapure de-ionized (DI) water or SRP power plant waters spiked with 1 ppm Se(VI) (unless otherwise noted) by diluting 1000 ppm Se(VI) stock solution or 1 ppm Se(IV) by diluting 1000 ppm Se(IV) stock solution. Arsenic removal was also investigated using As stock solution. The synthetic stock solutions were prepared by dissolving sodium selenate, Na_2SeO_4 (Sigma-Aldrich, product no. 71948-100G, purity ≥ 98.0%); or sodium selenite, Na_2SeO_3 (Sigma-Aldrich, product no. S5261-25G, purity ≥ 98%); sodium arsenate, $Na_2HAsO_4 \cdot 7H_2O$; or arsenite, $NaAsO_2$ (Pfaltz&Bauer, item no. S04150, purity ≥ 98%), respectively in DI water.

The sorbents were added to the spiked solutions and stirred at a constant speed with a magnetic stirrer (except for LDH-500C isotherm experiments which is using a rotator at 300 rpm), with sampling performed after different time periods. The amount of adsorbed selenium was calculated using Equation (3), where C_0 (ppm) is the initial selenium concentration in the solution; C_t (ppm) is the selenium concentration at time *t;* Q_t (mg/g) is the amount of selenium adsorbed onto the sorbent at time *t*; and m (g/L) is the dosage of sorbent material used.

$$Q_t = \frac{(C_0 - C_t)}{m} \qquad (3)$$

Ultrapure DI water (18.3 MΩ cm, pH 5.5) was used for synthetic water solutions. The sorbents were removed with filtration by filtered using a 0.2 micron Isopore track etched polycarbonate membrane in a Pall syringe filter. Then 2% nitric acid was added to the filtered sample solutions to preserve for ICP analysis.

2.3. Equilibrium Isotherms

To further study the maximum capacity of loading selenium onto the LDH, adsorption isotherms were conducted using 1 g/L of LDH-500C in 250 mL DI water (pH 6) spiked with Se(VI) solutions ranging from 0.2 - 100 ppm. The samples were agitated for 22 h on a compact digital mini rotator (Thermo Scientific, Catalog no. 88880025) in order to reach equilibrium. The experimental data plotted are the averages of triplicate. The error was calculated using the standard deviation from the mean. The Langmuir model was applied to describe the adsorption behavior at equilibrium since the experimental data did not fit the Freundlich model well. The Langmuir isotherm can be

expressed as shown in Equation (4), where C_e (ppm) is the concentration of Se(VI) at equilibrium; Q_e (mg/g) is the adsorption ability of LDH-500C for loading selenate at each C_e; Q_{max} (mg/g) is the maximum adsorption ability of loading selenate onto LDH-500C; K (L/mg) is the equilibrium constant.[40]

$$Q_e = \frac{Q_{max} K C_e}{1 + K C_e} \qquad (4)$$

The Langmuir equation can also be expressed as shown in Equation (5).

$$\frac{C_e}{Q_e} = \frac{1}{Q_{max} K} + \frac{C_e}{Q_{max}} \qquad (5)$$

Therefore, the slope of the Langmuir plot is $1/Q_{max}$ and the intercept is $1/Q_{max}K$.

2.4. Characterization and Analysis Methods

X-ray diffraction (XRD) characterization was performed using monochromatic $Cu_{k\alpha}$ radiation (λ=1.5405 Å) (Panalytical X'pert Pro). Scanning electron microscopy (SEM) was performed with an FEI XL 30 field emission scanning electron microscope. SEM of LDH-granular was performed with a Nova 200 NanoLab (FEI) focused ion beam, and the sample was coated using Au sputtering for 45 s before use. The specific surface area was using the Brunauer-Emmett-Teller (BET) method under 77 K nitrogen (Micromeritics TriStar II 3020). Thermogravimetric analysis (TGA) was performed on a Setaram TG 92 at a heating rate of 5 ^{o}C/min. Fourier transform infrared (FTIR) spectra of samples were collected on a Bruker IFS66V/S FTIR spectrometer using a diamond ATR sample module.

Preserved sample solutions were analyzed with inductively coupled plasma optical emission spectroscopy (ICP-OES, ICAP-6300, Thermo Co., USA). For solutions containing higher concentrations > 20 ppm selenium, a dilution factor of 50 will be applied for ICP-OES analysis. Unspiked water samples with low-level selenium concentrations were analyzed with inductively coupled plasma mass spectrometry (ICP-MS, iCap Q quadrupole, Thermo Co., USA) at ASU, the sulfur signal from ICP-MS was used to estimate the sulfate concentration in the acidified water solutions used for selenium analysis. Some of the samples were tested at SRP lab.

3. Carbon-based Materials

3.1. Overview of Carbon-based Materials

New sorbent materials are greatly needed in order to remove harmful contaminants from drinking and industrial waste water that can cause negative health effects and adverse consequences to the environment. Activated carbons are commonly used adsorbents for water treatment applications and are a mature technology for the removal of harmful organic compounds [41] and metals [42-43] such as chromium, lead, and mercury. Not only do activated carbons need to have suitable surface functional groups for adsorption of species, but some studies have also shown that a microporous structure can improve the removal of inorganic oxoanions.[44-45] This can be challenging to control due to the wide range of preparation conditions for activated carbon, which can give different structures, porosity, surface chemistry, and surface area.[43] With the development of carbon nanotechnology, there has been interest in exploiting the high surface-to-

volume ratios of these nanomaterials for water treatment. Recently, carbon nanotube and graphene-based sorbents have been demonstrated for removal of metals such as mercury,[46] arsenic,[47-48] chromium,[49-50] and selenium[51] with promising results. However, such carbon nanostructures may have cost prohibitive synthesis methods and also cytotoxicity issues.[52-53] For instance, a recent report found that graphene oxide actually amplified the phytotoxicity of arsenate in wheat plants and affected the plants' natural detoxification processes.[54] Recently, we developed a facile spray pyrolysis method for synthesizing highly porous carbon nanospheres that displayed excellent properties for dye adsorption and electrochemical double-layer energy storage.[55] Unlike carbon nanotubes and graphene, spherical shaped carbon nanostructures have been shown to have good biocompatibility.[56-57] Therefore, carbon nanospheres may be promising materials for environmental remediation applications such as the removal of harmful metals from water. In our study, we investigated the synthesized carbon nanospheres with high point-of-zero charge (PZC) in removing selenate and arsenate from simulated de-ionized (DI) water and SRP power plant waters, and also compared the performance with another synthesized carbon foam as well as commercially obtained activated carbon.

3.2. Carbon-based Materials Tested

Granular activated carbon (GAC) and powdered activated carbon (PAC) have been heavily studied as adsorbents in water treatment processing due to their wide pore size distribution and large pore volumes.[58] Some studies on modified GAC showed good performance with arsenic removal.[59-60] In our studies, we investigated GAC 820 and PAC 20BF obtained from Cabot Norit Americas, and homemade carbon nanospheres (CNS),

carbon foams (CF) for selenate removal and arsenate removal in both spiked de-ionized water and waters from SRP power plant.

3.2.1. Commercial GAC and PAC

GAC 820 granular activated carbon (GAC, 8 x 20 mesh) and Cabot Norit® 20BF powdered activated carbon (PAC, 325 mesh) were obtained and used without further treatment. According to information obtained online, Norit PAC 20BF is a powdered activated carbon derived from bituminous coal with a 325 mesh size. The datasheet for Norit GAC 820 (8 x 20 mesh) could not be found, but that for GAC 830, which is similar in mesh size, is a granular activated carbon produced by steam activation of select grades of coal. Figure 3 shows photographs of GAC and PAC obtained from the Norit website.

Figure 3. Photographs of a) GAC, b) PAC; from www.norit.com

3.2.2. Carbon Nanospheres (CNS) Synthesis

In a typical experiment, precursor solutions were prepared by dissolving sucrose (Alfa Aesar) and $Mn(NO_3)_2$ (Alfa Aesar) in 100 mL de-ionized water. An air brush (Crescendo, Model 175) was used to create a swirling mist of the aqueous precursor solution. Nitrogen was used as the carrier gas with a flow rate of 5 - 8 L/min, with the air brush was adjusted to supply the feedstock at 10 - 15 mL/h into the tube furnace together. The furnace was heated to 1000 ^oC. High temperature annealing was performed by heating the as prepared carbon nanospheres at 1200 ^oC under Ar gas flowing at 150 sccm for 2 h. After annealing, the sample was treated with acid post etching by sonicating in 1 M HCl for 5 min, followed by vacuum filtration and washing in DI water to form the final product consisting of CNS with a median diameter of ~70 nm, with the largest particle size < 1 micron. The specific surface area (SSA) for the carbon nanospheres was around 1000 m^2/g.[55]

3.2.3. Carbon Foam (CF) Synthesis

In a typical synthesis, sugar (sucrose, Alfa Aesar) and $Zn(NO_3)_2 \cdot 6H_2O$ (Alfa Aesar) were gently melted and mixed uniformly with a mass ratio of 1 g : 2 g. Then the mixture was heated to ~180 ^oC on a hot plate, during which the mixture will quickly carbonize and form carbon foam in about 5 min. After the carbonization was completed, the as-prepared carbon foam was crushed into powder and then annealed at 1200 ^oC for 2 h under N_2 gas flowing at 150 sccm. During the annealing process, ZnO was reduced to Zn by carbon and evaporated from the sample, leaving a high surface area carbon foam. The specific surface area (SSA) for the carbon foam was around 1690 m^2/g.[61]

3.3. Physical Properties

The physical properties of the as-prepared carbon nanospheres (CNS) and carbon foams (CF) were characterized using SEM, TEM, and BET. Figure 4A-B show typical scanning electron microscopy (SEM) images of the as-synthesized carbon nanospheres (CNS) and carbon foams (CF). Transmission electron microscopy (TEM) of the CNS after carbonization showed that the CNS contained manganese oxide nanoparticles 2-10 nm in diameter (Figure 4C). After etching, the nanoparticles were dissolved to reveal empty micropores (Figure 4D). Based on the X-ray diffraction (XRD, Figure 5A) and Raman spectroscopy (Figure 5B) analysis, the CNS adopted a disordered amorphous structure with predominately carbon sp^3 bonding.[55] The Raman spectrum for PAC showed a similar disordered structure as that in the CNS (Figure 5B) but the (002) and (100) planes associated with graphitic carbon can be discerned in the XRD pattern (Figure 5A). Thus, the structure of PAC is likely a mixture of disordered carbon with some regions of graphitic, sp^2 carbon.

The specific surface area for the carbon nanospheres (CNS) and carbon foams (CF) using the Brunauer-Emmett-Teller (BET) method was around 1000 m^2/g and 1690 m^2/g,[61] respectively. And CNS shows a pore volume around 0.28 cm^3/g. Gas sorption measurements on PAC determined a BET surface area of 864 m^2/g and pore volume of 0.22 cm^3/g. GAC has been reported with a BET surface area of 908 m^2/g and pore volume of 0.5 cm^3/g.[62] The nitrogen-sorption isotherm for the CNS and PAC are shown in Figure 5C. While PAC shows a type IV isotherm with hysteresis, indicating some mesoporosity,[63] the CNS had a type I isotherm with no hysteresis. This indicates that the

CNS contained mostly micropores < 2 nm and no significant pore volume associated with mesopores (2 - 50 nm) or macropores (> 50 nm), as shown by the Barrett-Joiner-Halenda (BJH) derivative pore distribution plot (Figure 5C, inset).

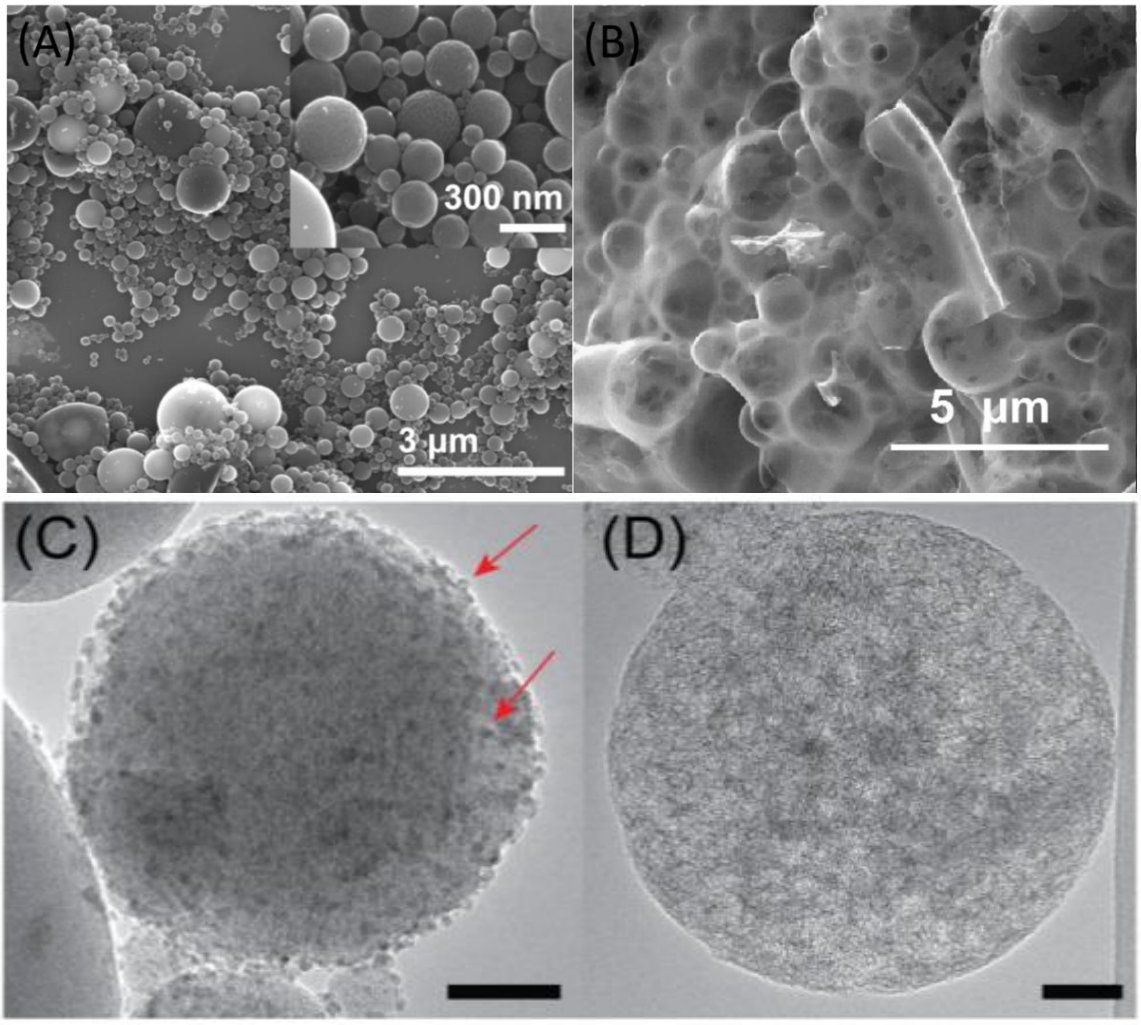

Figure 4. SEM images of (A) carbon nanospheres (CNS),[64] (B) carbon foams (CF).[61] TEM images of CNS (C) after carbonization as a composite with metal oxide nanoparticles (noted with arrows) and (D) after acid etching to dissolve the metal nanoparticles. Scale bar = 50 nm.[64]

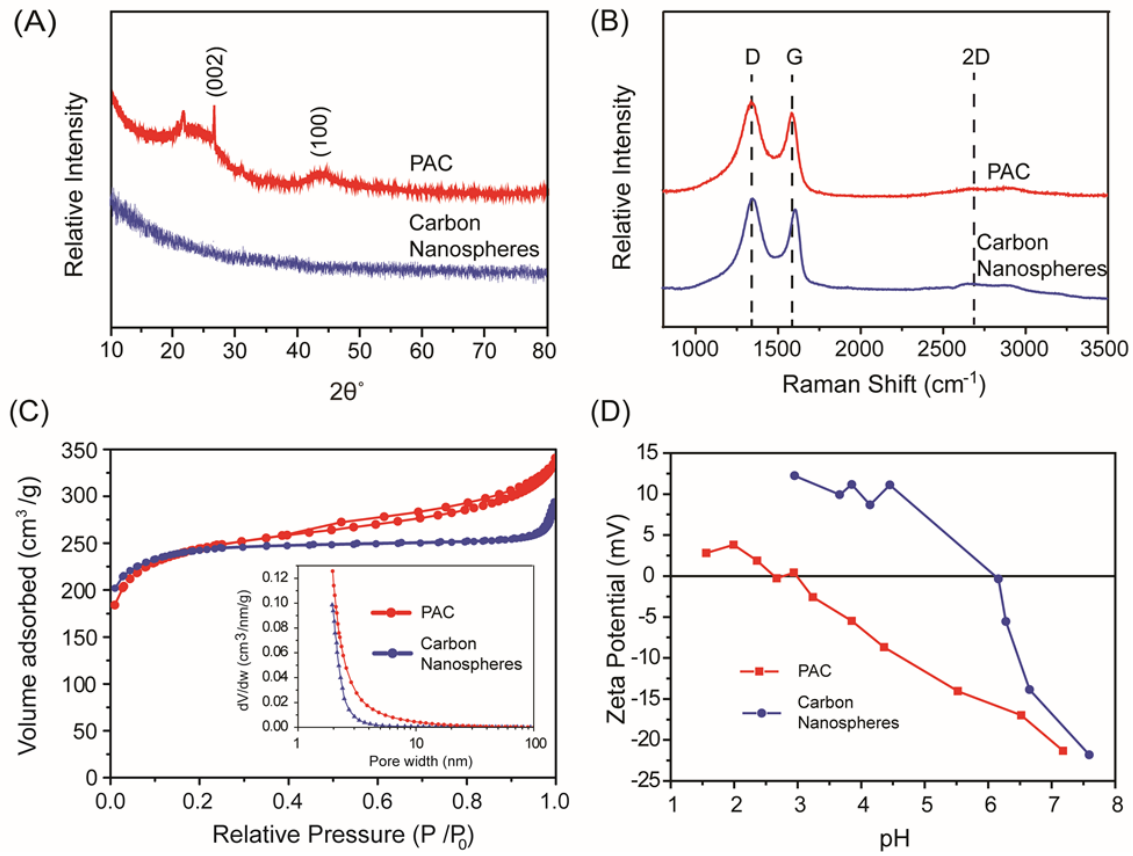

Figure 5. A) XRD, B) Raman spectra, C) N_2-sorption curve with pore size distribution the inset, and D) zeta potential measurement for PAC compared with carbon nanospheres.

Zeta potential measurements were performed on the PAC and CNS (ZetaPALS, Brookhaven Instruments). As shown in Figure 5D the isoelectric point (pH where the zeta potential is zero) for PAC was around pH 2.5 – 3, which is typical for coal-derived activated carbons with acidic surface groups (L-type carbon).[65] In contrast, the isoelectric point for the CNS was around 6.16. The higher isoelectric point in the CNS is a result of the high annealing temperatures in inert atmosphere used in the synthesis, which can remove the oxidized acidic surface groups and create basic carbons with anionic

exchange properties.[66] Basic carbons with anionic exchange properties (h-type carbons) can be obtained when heating >950 ºC in vacuum or inert atmosphere.[65,67]

3.4. Jar Test Results

Figure 6 shows selenate and arsenate removal over time using the different carbons as sorbents at a concentration of 0.44 g/L in DI water spiked with 1 ppm selenate and arsenate, except for the carbon foams (CF), which was used at a lower concentration (0.1 g/L) due to the small density.

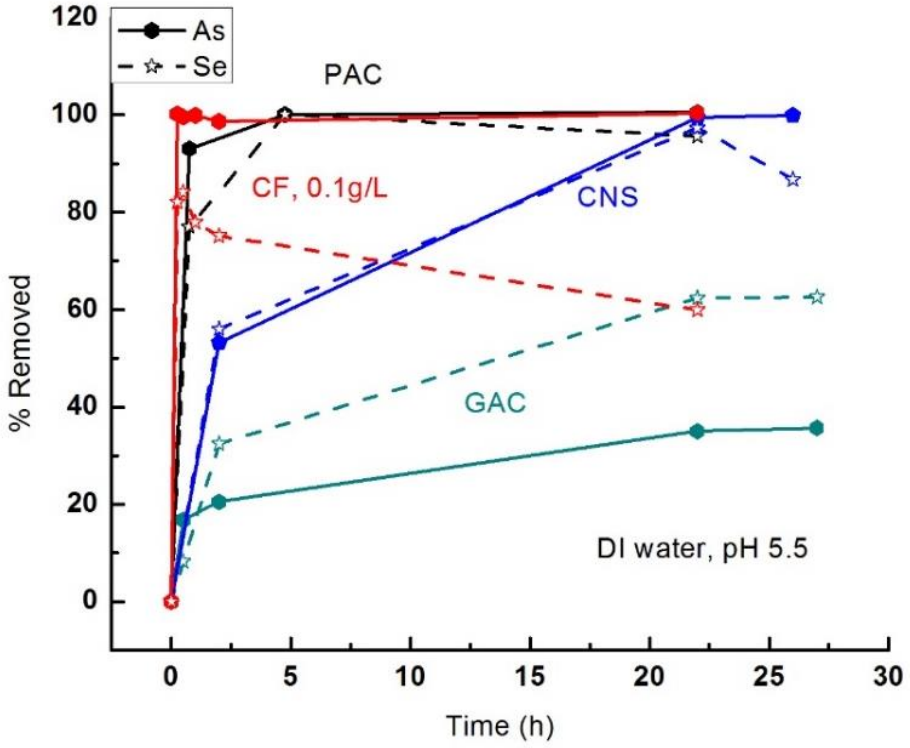

Figure 6. Percent removal of 1 ppm selenate and 1 ppm arsenate on different carbons in spiked de-ionized water.

The carbon nanoshperes (CNS) showed good binding to both metal species. For removing arsenate in DI water, 53% of the arsenate was removed in 2 hours, with 100% removal observed by 22 hours when using the CNS (Figure 6). And 56% of the starting selenate concentration can be removed by CNS in 2 hours (Figure 6). After 22 hours of exposure, 97% of the selenate was removed. However, at 26 hours, the selenate concentration in the water increased, suggesting some desorption of selenate from the CNS surface. Similar desorption behavior has been observed on inorganic sorbents in high ionic strength electrolytes.[68] Since selenate is a weak binding anion and adsorbs through outer-sphere complexes,[69] it can easily become displaced by competing anions. In DI water, which is slightly acidic, the adsorption of protons onto the basic surface groups of the CNS will cause the solution pH to increase. For instance, the DI water solution containing 1 ppm arsenate and selenate had an initial pH of 5.5, which increased to 7.35 after the CNS was added and stirred for 2 hours. The increase of pH in the solution until the equilibrium is reached could result in desorption of some of the selenate. Nonetheless, these results are much better than what was previously observed on other nanocarbon sorbents. For example, graphene oxide evaluated in a similar water matrix (1 ppm selenate in DI water, pH 6) but at a higher dose of 1 g/L could only remove 30 % of the selenate after 24 hours exposure time.[51] This could be due to a number of reasons, including low effective surface area or differences in surface functional groups. Although dilute graphene oxide suspensions have surface area as high as 736 m^2/g, this value decreases due to agglomeration starting at concentrations of 50 mg/L.[70] The surface chemistry of graphene oxide is complex and heterogenous, but is generally accepted to consist of predominately epoxides and tertiary alcohols in the basal plane and ketones,

carboxylic acids, ethers, and enols on the edges.[71] Studies have found that strong hydrogen bonding between water molecules and functional groups in the basal plane play a key role in maintaining the layer stacking of graphene oxide,[72] which may further inhibit the ability for selenate to adsorb, since it may have to intercalate in between the layers or compete with water for binding sites. Furthermore, the graphene oxide surface is acidic in character[73] and would have a low number of suitably charged binding sites for adsorption of selenate at pH 6.

Powdered activated carbon (PAC) could adsorb arsenate and selenate faster than the carbon nanospheres (CNS), with 93% arsenate and 77% selenate removed in 45 minutes. For both PAC and the CNS, all of the arsenate and selenate could be removed at longer exposure times. Carbon foams (CF) was observed to have similar performance with PAC in removing arsenate, but only removed 85% of the selenate. Desorption of selenate was also observed in the carbon foam sample at longer exposure times, which may be due to effects from the large hollow pores in the carbon foam. On the other hand, granular activated carbon (GAC) removed only 35% of the arsenate and 62% of the selenate after 22 hours. Due to the poor performance in DI water, GAC was not tested further.

To further study the performance of the carbon nanospheres (CNS), additional jar tests were conducted using 0.44 g/L PAC, CNS, and 0.1 g/L CF in canal and well waters spiked with 1 ppm selenate and 1 ppm arsenate. The pH of the canal and well waters were 8.54 and 8.30, respectively. In this pH range, the dominant Se(VI) species is SeO_4^{2-} and the As(V) is found as the doubly charged anion, $HAsO_4^{2-}$.[14,74]

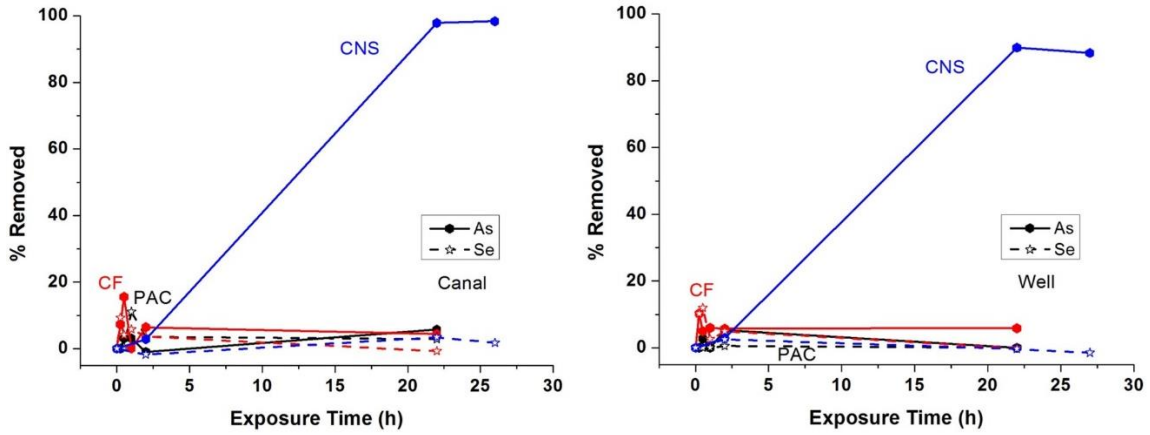

Figure 7. Percent removal of 1 ppm selenate and 1 ppm arsenate on 0.44 g/L carbon nanospheres compared to powdered activated carbon (PAC) at dosage of 0.44 g/L and carbon foam (CF) at dosage of 0.1 g/L in (a) canal water, (b) well water.

When tested in the canal (Figure 7a) and well waters (Figure 7b), the arsenate removal rates of CNS were slower than that in the DI water, with only about 3% removed after 2 hours. However, by 22 hours, > 89% of the arsenate was removed, with the removal efficacy in the canal water very similar as in the DI water. The slightly lower removal efficacy for arsenate in the canal and well waters compared to DI water can be explained by their higher pH. The anionic adsorption capability of carbons is typically attributed to surface functional groups such as –COOH, $–OH_2^+$, $–COO^-$, –OH, $–O^-$, which become protonated and/or positively charged when dispersed into aqueous solutions.[42,75-76] The arsenate adsorption capacities of activated carbons reported in the literature typically reach a maximum at pH 2 – 5,[77-78] where the carbon surface has a more positive charge. Similarly, carbon nanotubes with oxygen-containing surface functional groups showed low arsenate binding capacities due to negative zeta-potentials from pH 3-10.[79]

For this reason, many carbon-based adsorbents rely on modification with iron, which can form inner-sphere complexes with arsenic.[80-81] Here, we see that our carbon nanospheres (CNS) display good arsenate adsorption at pH > 8 without requiring this modification due to their higher isoelectric point. The canal and well waters also contain other competing anion species such as nitrate (typically 60 – 130 ppm) and sulfate (700 – 1000 ppm), which did not appear to have a large effect on the arsenate binding. In canal and well waters, the selenate removal efficacy of the carbon nanospheres (CNS) was very low, about 2-3%, due to the presence of completing anions such as sulfate.[82] However, one way to potentially address this problem is to use a barium salt to precipitate out the sulfate from the water prior to its exposure to the sorbents.[15]

Despite the good adsorption behavior in DI water, PAC and CF could not remove too much arsenate and selenate from the canal and well waters. To further investigate whether the low removal efficacy of PAC in the canal and well waters was due to the higher pH or the presence of competing ions, the pH of the DI water was adjusted to 8.3 by adding NaOH. The results for these tests are shown in Figure 8. Comparing these results to those obtained in DI water without pH adjustment (Figure 6), both arsenate and selenate removal efficiencies by PAC decreased by about half, which means the higher pH of the solution does have a negative effect on the adsorption properties. This suggests that the worse performance of PAC in the canal and well waters is due to a decrease in positively charged surface binding sites as a result of the higher pH.

This also shows that the basic surface properties of the carbon nanospheres (CNS) allows for good arsenate adsorption in the canal and well waters. The exact nature of the

basic sites will require further detailed study, as it is a controversial topic in carbon science, but the sites are likely introduced in our synthesis process, resulting in carbon materials with higher isoelectric point.

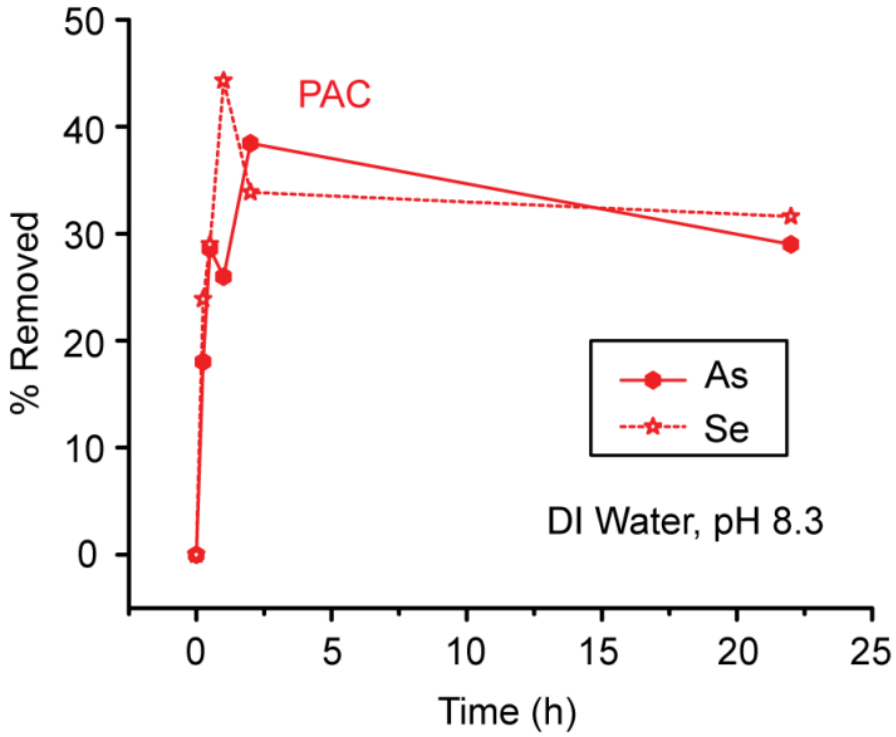

Figure 8. Percent removal of 1 ppm selenate and 1 ppm arsenate on powdered activated carbon (PAC) in DI water, pH 8.3.

Some contributors to basicity have been proposed as: (1) the electron donating character of π-electrons on graphitic basal planes, (2) oxygen surface functionalities such as chromene, diketon, quinone, and pyrone groups, (3) nitrogen-containing functionalities, and (4) inorganic impurities.[83] The contribution of (1) seems to be less likely in this case, since the CNS have little graphitic structure and moreover have very similar disordered carbon structure as PAC, based on Raman spectroscopy and X-ray diffraction. Due to the

lack of nitrogen functional groups in the sucrose precursor used to make the CNS, (3) is also less likely. Instead, the annealing procedures used to prepare the CNS may create basic oxygen-containing functional groups. The last contribution cannot be ruled out since the manganese salt is an important component of the synthesis. However, any manganese compounds should be removed from the CNS after the post-synthesis HCl etching. Also, previous studies have found that manganese oxide species can successfully remove arsenate from water only at pH < 5 due to their low point-of-zero charge.[84-85]

3.5. Conclusions

In summary, we have found that carbon nanospheres (CNS) prepared using a facile spray pyrolysis method can display good activity for arsenate and selenate adsorption in synthetic DI water solution. In water solutions composed of canal and well water at pH > 8, the carbon nanospheres could outperform PAC likely due to the presence of basic functional groups, higher surface area, and suitable microporous structure as a result of the formation mechanism arising from the synthesis method. However, competing anions in these waters completely inhibited selenate adsorption on the carbon nanospheres, whereas the arsenate binding kinetics were only slightly decreased. Further work will focus on addressing this issue, such as by using barium salts [15,86] or lime [87] to remove competing sulfate ions in a pre-treatment step.

As conventional activated carbons and nanostructured carbons such as carbon nanotubes and graphene typically show good adsorption properties in acidic pH, these results highlight the potential for carbon nanospheres to be used as adsorbents for toxic metal treatment at neutral to alkaline pH.

4. Layered Double Hydroxide (LDH)-based Materials

4.1. Overview of Layered Double Hydroxide (LDH)-based Materials

Layered double hydroxides (LDHs) are attractive materials for applications as sorbents for selenium removal as they are layer structured materials containing positively charged layers that can allow for high anion exchange capacities (Figure 9). These materials are also known as hydrotalcite-like compounds and can be represented as $[M^{II}_{1-x}M^{III}_{x}(OH)_2]^{x+}[A^{n-}_{x/n}]^{x-} \bullet mH_2O$, where M^{II} = divalent metals such as Mg^{2+}, Zn^{2+}, Co^{2+}, Cu^{2+}, M^{III} = trivalent metals such as Al^{3+}, Fe^{3+}, Ni^{3+}, etc.[88-89] A^{n-} is an exchangeable anion with a valence of n, and x value is in the range of 0-0.33.[90] LDHs contain positively charged layers of brucite-like octahedral hydroxide sheets, in which partial divalent cations M was substituted by the trivalent metals N that result in the positive charges. The sheets are separated by compensating anions to keep charge neutrality,[91] and the remaining free space of the interlayer region can be occupied by water molecules.[92-93] The interlayer species can be readily exchanged with other anions, as shown in Equation (1) for monovalent cations and Equation (2) for divalent anions:

$$Mg_6Al_2(OH)_{16}CO_3 \bullet 4H_2O + 2A^- \rightarrow Mg_6Al_2(OH)_{16}(A)_2 \bullet xH_2O + CO_3^{2-} \quad (1)$$

$$Mg_6Al_2(OH)_{16}CO_3 \bullet 4H_2O + A^{2-} \rightarrow Mg_6Al_2(OH)_{16}(A) \bullet xH_2O + CO_3^{2-} \quad (2)$$

LDHs are the only known materials with positively charged layers and ion-exchangeable, interlayer anions.[94] As a result, LDHs have been investigated as sorbents and ion-exchange materials to remove anions.[95-96] Previous studies have moreover shown that LDHs have greater affinities for multi-charged anions with high charge density,[90-

[91,97] making them particularly attractive for the removal of the oxoanionic forms of chromium, arsenic, and selenium over other monovalent anions that might be also present in the water (e.g. chloride). However, this feature can make the sorption capacities of LDHs susceptible to interference from carbonate and sulfate anions.

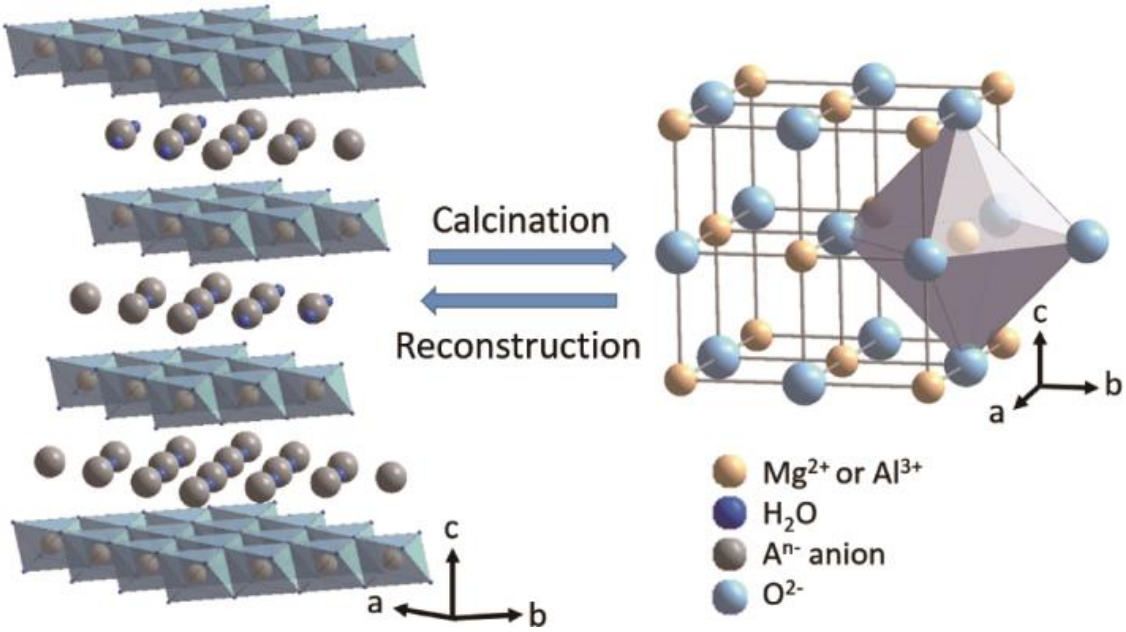

Figure 9. Crystal structure of layered double hydroxide (LDH) and the periclase structure formed after calcination. The layered structure is reconstructed upon exposure to water.

LDHs also display a unique structural feature known as the "memory effect" or "reformation" effect.[98-99] Prior studies have shown that heat treatment can be used to change the structural properties of LDH, wherein calcination can cause decarbonation, dihydroxylation, and loss of crystallinity to form a periclase structure; subsequent exposure of the calcined LDH into water results in rehydration and recovery (reformation) of the initial layered structure from the nonlayered, periclase form (Figure 9.).[100] This is the so called "memory effect". During rehydration, anions present in the water can also

be intercalated or incorporated in the reconstructed LDH,[101] providing another mechanism for anion removal from water. On the other hand, sorption by uncalcined LDH is predominately through ion-exchange, as shown in Equations (1) – (2). Calcined LDHs also display increased surface area, porosity, and fewer interlayer carbonate anions, [1,102-103] features that can improve the sorption capacities of the material compared to the uncalcined LDHs, [1,103-104] which may be particularly useful in complex water matrices where there are high concentrations of competing anions.

Considering the various types of LDHs, the Mg-Al-CO_3 LDHs (i.e., $M^{II} = Mg^{2+}$, $M^{III} = Al^{3+}$, $A = CO_3^{2-}$) are attractive as sorbents due to the absence of heavy metals, which could present a safety or toxicity issue in the event of leaching. Also, the PZC of Mg-Al-CO_3 LDH was measured to be 9.7,[105] which is higher than values reported for other LDHs, e.g. 8.78 for Zn-Al-CO_3 LDH.[106]

Previous work by Yang, et. al. showed that Mg-Al LDH was effective for removing low levels of As and Se (20 ppb) from aqueous solution, even in the presence of competing ions such as CO_3^{2-} and HPO_4^{2-}.[1] In this same study, the LDH displayed similar removal capacities for selenite vs. selenate in isotherm measurements. A detailed study by Chubar, et al. also showed that various Mg-Al-CO_3 LDHs prepared using different methods were effective for removal of selenate and selenite, but that certain physicochemical characteristics such as surface area, pore size, Mg:Al ratio, carbonate content, crystallinity, and moisture content of the starting materials could play a role in the selenium loading capacity.[105] However, most previous studies on LDH removal of selenium species are conducted in simulated waters comprising spiked DI water.

Although there have been many reports investigating the fundamental sorption properties of LDHs in batch tests, there have been limited studies evaluating the implementation of LDHs in packed bed columns, particularly for selenium removal. Recent work by Chubar *et al.* demonstrated that Mg-Al-CO_3 LDH (i.e., $M^{II} = Mg^{2+}$, $M^{III} = Al^{3+}$, $A = CO_3^{2-}$) was effective for removing selenium from spiked de-ionized (DI) water in a packed bed.[107] The LDH was prepared with a novel alkoxide-free sol-gel synthesis that resulted in interlayer carbonate ions that could be easily exchanged with selenate, Se(VI).[108] The study found that 4300 bed volumes (BVs) of water containing 50-60 µg/L Se(VI) could be treated using the LDH. However, the water matrix only contained 0.01 M NaCl as background electrolyte. Introduction of sulfate at a concentration 74 times higher than the Se(VI) level decreased the Se(VI) removal efficiency by 2.6 times due to simultaneous removal of the competing sulfate anions. These results show that although LDHs are effective sorbents for removing Se(VI), sulfate present in the water can interfere with binding sites and decrease the adsorption capacities, particularly in water matrices with high sulfate levels but only trace levels of selenium. There are also limited studies of the performance of LDHs as sorbents in more complex water matrices, where multiple anions and cations might be present.

In this work, the performance of commercially available LDHs in granular or powder forms and several different types of home-made nanosheets LDHs for removing selenate and arsenate was studied. The commercially available Mg-Al-CO_3 LDHs in powdered and granular form were evaluated for the removal of selenate and selenite. The decarbonated/dehydroxylated forms of the commercial LDHs (obtained by calcining) were used in order to evaluate the best possible anion removal capacities. Screening of

selenium removal efficacy was performed using the LDH sorbents in simulated waters comprising DI water spiked with selenium and also selenium containing power plant waste waters. Adsorption isotherms were performed to determine the maximum loading capacities of the calcined LDHs for removing selenate. Fixed bed, small scale column tests were conducted using granular LDH with relative large particle size, which would facilitate its evaluation in small scale column tests, to study the performance in dynamic situations for treatment of well water (the make-up water for the power plant boiler and cooling water investigated in this study). Regeneration of the exhausted sorbents was also explored using heat treatment.

4.2. Layered Double Hydroxide (LDH)-based Materials Tested

Table 3. LDH sorbents investigated and description.

Sample Name	**Sample Description**
LDH-powder	Commercial powder LDH from Sigma-Aldrich, as-received
LDH-granular	Commercial granular LDH from Sasol Germany, as-received
LDH-500C	Commercial powder LDH from Sigma-Aldrich, calcined at 500 ^{o}C for 2 h
LDH-nanosheet powder	Synthesized in-house using urea hydrolysis method
LDH-nanosheet chunk	Synthesized in-house using precipitation method, assembled into chunks
LDH-nanosheet paper	Synthesized in-house using precipitation method, assembled into papers

For this study, several different types of commercially available and home-made nanosheet LDHs were tested (Table 3) in spiked DI water and in SRP power plant waters for the removal of selenate, selenite, and arsenate. Rapid small scale column tests were also conducted using a granular LDH with relative larger particle size, which would facilitate its evaluation in small scale column tests.

4.2.1. Commercial Hydrotalcite-like LDHs

A commercial powdered hydrotalcite Mg-Al-CO_3 LDH (from here on abbreviated as LDH-powder) was obtained from Sigma-Aldrich. This material is sold as "Hydrotalcite – synthetic" and has the part number 652288-1KG. The price was $73.50/kg. The chemical formula for this LDH is reported by the supplier as $Mg_6Al_2(CO_3)(OH)_{16}•4H_2O$. Due to the hydrophobic nature of the LDH-powder, heat treatment is often used to change its surface properties and enable its dispersion into water prior to use in sorption experiments.[109] The LDH was heated at 500 ^oC for 2 h in air in a box furnace (from here on referred to as LDH-500C). Another granular hydrotalcite LDH (from here on abbreviated as LDH-granular) was commercially obtained from Sasol Germany GmbH and has a product code of PURALOX MG 63 HT – Granulate. The composition is reported by the supplier as 38.3 Al_2O_3 and 61.7 MgO and particle size is reported to have a median diameter of 1.46 mm. In jar test, the LDH-granular was used as received. For small scale column tests, it was gently ground into small particles using a mortar and a pestle, and sieved to specified mesh size ranging 250 – 500 µm using sieve mesh No. 35 and No. 60.

4.2.2. Home-made LDH nanosheets

Mg-Al based LDH nanosheet powders were synthesized in-house (from here on abbreviated as LDH-nanosheet powder) using the urea hydrolysis method described by Costantino et al.[110] In a typical experiment, an aqueous solution was prepared by adding $AlCl_3$ and $MgCl_2$ into DI water with the molar ratio of $Al^{3+}/(Al^{3+} + Mg^{2+})$ equal to 0.33. Then solid urea was added until the molar fraction of urea/$(Al^{3+} + Mg^{2+})$ reached 3.3. The solution was refluxed for 36 h. The white precipitate was filtered and washed with de-ionized water and ethanol for several times, and then dried under vacuum at 60 ^{o}C overnight.

We also used a precipitation method to synthesize in-house LDH nanosheets and assembled them into larger particle sizes as chunks and paper.[111] Similar to the nanosheet powder synthesis, an aqueous solution was prepared by adding $AlCl_3$ and $MgCl_2$ into de-ionized water with the molar ratio of $Al^{3+}/(Al^{3+} + Mg^{2+})$ equals to 0.33. The Al-Mg solution was added dropwise into a pH 10 NaOH solution using a syringe pump. Concentrated NaOH solution was also added dropwise to keep the pH at 10. The white cloudy precipitate was stirred at room temperature for 1 h and then washed with DI water. To assemble the white precipitate into large chunks, the cloudy solution was sonicated for 15 min; for large papers, overnight sonication was required. After sonication, the as-prepared precipitate was filtered using a vacuum pump and pumped overnight. The large soft chunks or paper were dried at 50 ^{o}C until they became solid.

4.3. Physical Properties

4.3.1. Commercial Hydrotalcite-like LDH-powder

The physical properties of the as-received LDHs were characterized using XRD, SEM, and BET analysis. The XRD pattern of as-obtained LDH-powder (Figure 10a, (i)) was a good match to the reference pattern for $(Mg_{0.667}Al_{0.333})(OH)_2(CO_3)_{0.167}(H_2O)_{0.5}$ (PDF 01-089-0460).[112] This shows LDH-power had a rhombohedral structure with space group R-3m and lattice constants a = 3.0460 Å, b = 3.0460 Å, c = 22.7720 Å.[112] It contains strong basal (00*l*) reflections at low 2θ values [101] and other associated reflections at high 2θ values, which indicating good crystallinity and confirms the presence of interlayer carbonate and water molecules.[109] As received, the LDH-powder was hydrophobic. This may due to anionic surfactants residue that used during the producing.[113] Some reports show that hydrophobized LDHs have good adsorption ability for organic solvents and the processes can be selective.[113-114] Prior studies showed that heat treatment could be used to remove impurities and change its surface properties to enable its dispersion into water.[115]

As previously described, calcination of LDHs can also lead to improved sorption properties through removal of interlayer carbonate and water molecules. To better understand the required temperatures for decarboxylation/dehydration of LDH-powder, TGA was performed on LDH-powder samples (Figure 10b). The TGA result of LDH-powder showed that interlayer water molecules were removed above 100 ^oC in the first weight loss region, while interlayer anions were removed in the second weight loss region from 325 ^oC – 525 ^oC. Additionally, XRD was performed on LDH-powder

calcined at 300, 400, and 500 ^{o}C in air (Figure 10a, (ii)-(iv)). The XRD results showed that at 300 ^{o}C, the sharp peak at ~11.6^{o} shifted to ~12^{o} and decreased in intensity. This continued until disappear and reach to a stable structure after 400 ^{o}C, which consisted of two broad peaks that can attributed to the formation of poorly crystalline MgO.[100] This indicates that by 400 ^{o}C, all the interlayered waters and carbonate anions have been removed, leaving the solid solution of aluminum oxide with MgO, consistent with previous observations showing dehydroxylation between 70 – 190 ^{o}C and decarbonation above 360 ^{o}C.[100,116] This is also being confirmed by TGA results from Khitous et al. that interlayer water molecules lost from 30 to 180 ^{o}C while the dihydroxylation and decomposition occur at temperature from 250 – 500^{o}C.[117] After subjecting the LDH-powder to heating at 500 ^{o}C for 2 hours to form LDH-500C, the XRD results showed similar amorphous-like pattern as the sample calcined at 400 ^{o}C. Without the strong (00*l*) reflections (Figure 10a, (iv)), the interlayer waters and carbonate anions of the LDH-powder was removed and the layered structure collapsed.[109] The TGA performed on LDH-500C (Figure 10b) showed only 13% weight loss by 600 ^{o}C, confirming the removal of the interlayer species. Yang et al. have done a detailed study on thermal evolution of the structure of Mg-Al LDH. They reported that at 70 – 190 ^{o}C, loosely held interlayer waters were removed, and OH^{-} group bonded with Al^{3+} lost starts at 280 ^{o}C as the peak at ~12^{o} decreases while the LDH structure remain. The layered structure breaks apart above 360 ^{o}C as the CO_3^{2-} groups left and been removed completely at 405 ^{o}C.[116]

The as-received LDH-powder were dispersed in isopropanol and sonicated for 15 min to prepare the SEM samples. SEM imaging showed that the as-obtained LDH-powder consisted of particles about 500 nm in size (Figure 10c). After calcination, the

LDH-500C particles remained similar in morphology and size (Figure 10d). Similar to previous studies, calcination of the LDH-powder was effective for increasing the surface area, with LDH-500C displaying 179 m^2/g compared to only around 7 m^2/g for the as-obtained powder according to the BET measurements (Table 4).

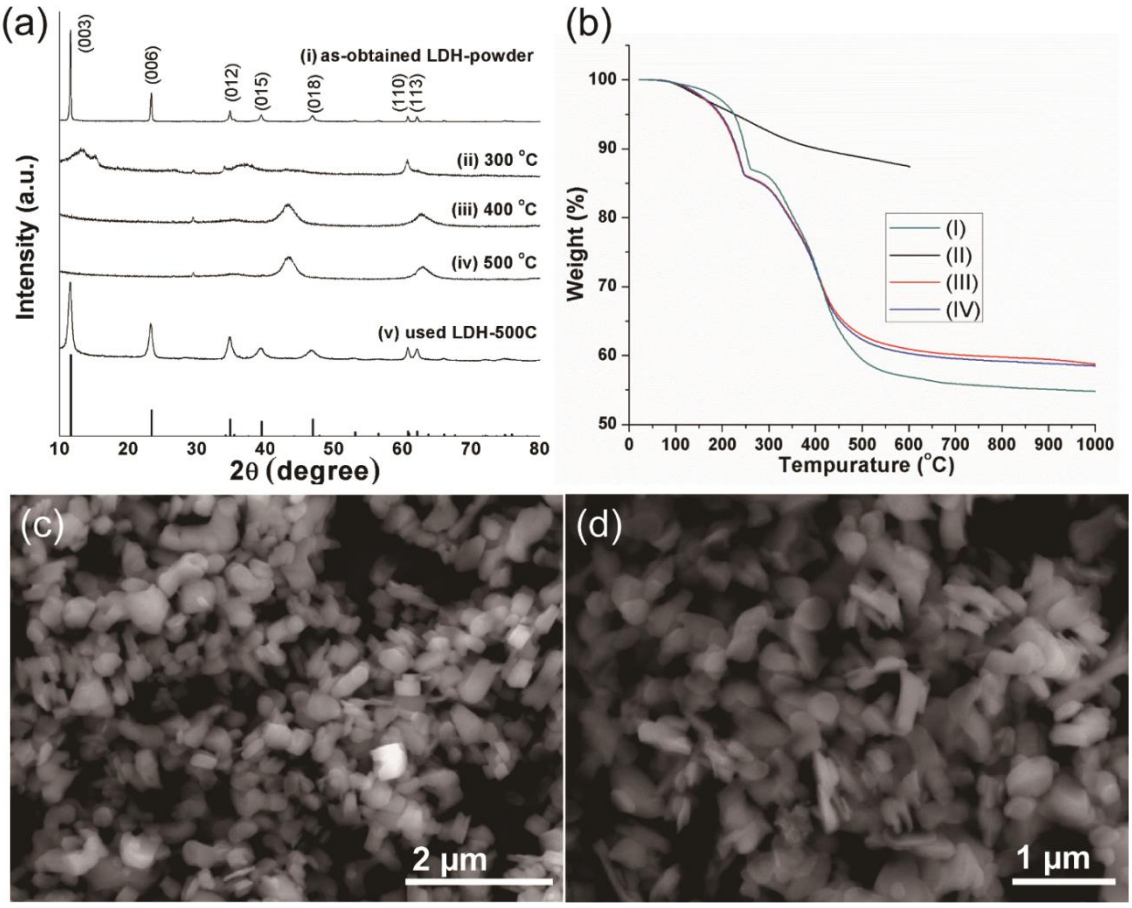

Figure 10. (a) XRD patterns of LDH materials: (i) as-obtained LDH-powder, and after calcination at (ii) 300ºC, (iii) 400ºC, and (iv) 500ºC in air for 2 h; (v) LDH-500C after exposure to 50 ppm Se(VI) in jar test. The pattern for $(Mg_{0.667}Al_{0.333})(OH)_2(CO_3)_{0.167}(H_2O)_{0.5}$ from PDF 01-089-0460 is shown as reference; (b) TGA data of different LDHs: (I) as-obtained LDH-powder; (II) as prepared LDH-500C; LDH-500C after exposure to (III) 50 ppm selenate or (IV) 50 ppm sulfate in jar tests. SEM images of (c) as-obtained LDH-powder and (d) as-prepared LDH-500C.

Table 4. BET surface area of different LDHs.

Sample		Specific Surface Area (m^2/g)
LDH-powder	As-obtained	7
LDH-500C	As-prepared	179
	After jar test	26
LDH-granular	As-obtained	91
	After RSCCT	41

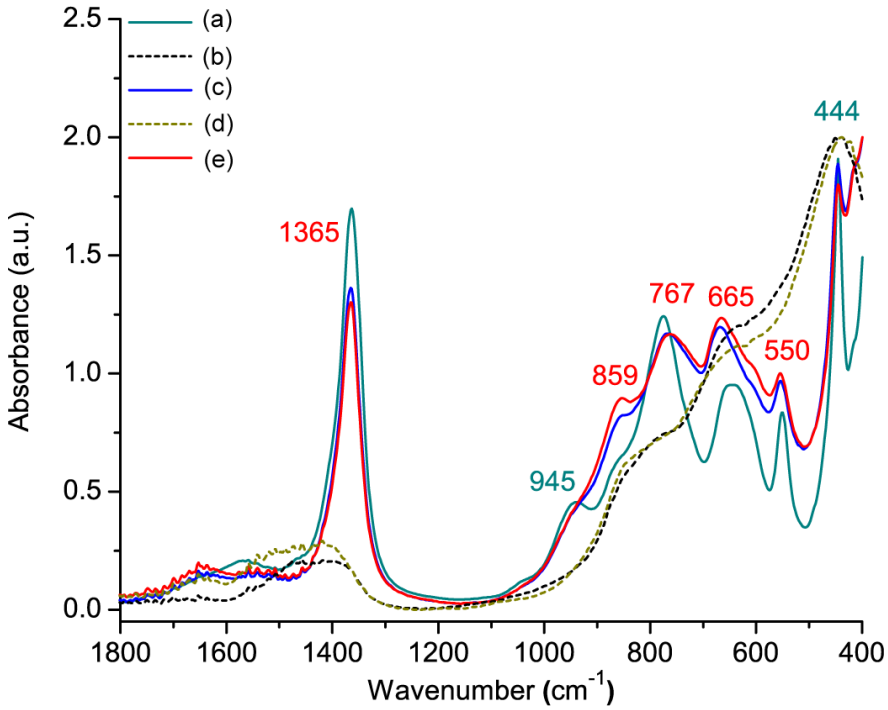

Figure 11. FTIR spectra of (a) as-obtained LDH-powder, (b) as-prepared LDH-500C; (c) LDH-500C after jar test with 50 ppm Se(VI); (d) regenerated sample from (c); (e) LDH-500C after jar test with 100 ppm Se(VI).

FTIR spectroscopy was performed to further characterize the structure of the LDH-powder and LDH-500C. Interlayer carbonate anions can be identified by the band

at 1365 cm^{-1},[96,105] which was pronounced in LDH-powder (Figure 11a) but very weak in LDH-500C (Figure 11b). This is consistent with the removal of interlayer carbonate ions during calcination. The interlayer hydration deformation bands (δH_2O) typically found at around 1635 cm^{-1} [108,118] were absent in the sample LDH-500C, confirming the dehyration. Bands at 444 cm^{-1} assigned to the lattice vibrations of Mg,Al-oxide octahedral sheets, at 550 cm^{-1}, 665 cm^{-1}, and 767 cm^{-1} to Mg/Al-OH translations, and at 945 cm^{-1} assigned to Al-OH deformation were identified in LDH-powder.[105,108,118] These bands were not observed in LDH-500C, consistent with dehydroxylation during calcination.

4.3.2. Commercial Hydrotalcite-like LDH-granular

The as-received LDH-granular displayed a similar XRD pattern as LDH-500C, consisting of two broad reflections (Figure 12a) that are attributed to a magnesium/aluminum oxide solid solution with cubic periclase structure (Figure 9).[100,119] Previous studies showed that calcination of Mg-Al-CO_3 LDHs results in dehydroxylation between 70 – 190 ºC and decarbonation above 360 ºC,[100,116] leaving the non-layered periclase materials, as depicted in equation (8).[120]

$$Mg_{1-x}Al_x(OH)_2(CO_3)_{x/2} \xrightarrow{\Delta} Mg_{1-x}Al_xO_{1+x/2} + x/2\ CO_2 + H_2O \qquad (8)$$

This suggests that the interlayer water and carbonate anions were removed by the manufacturer through calcination.

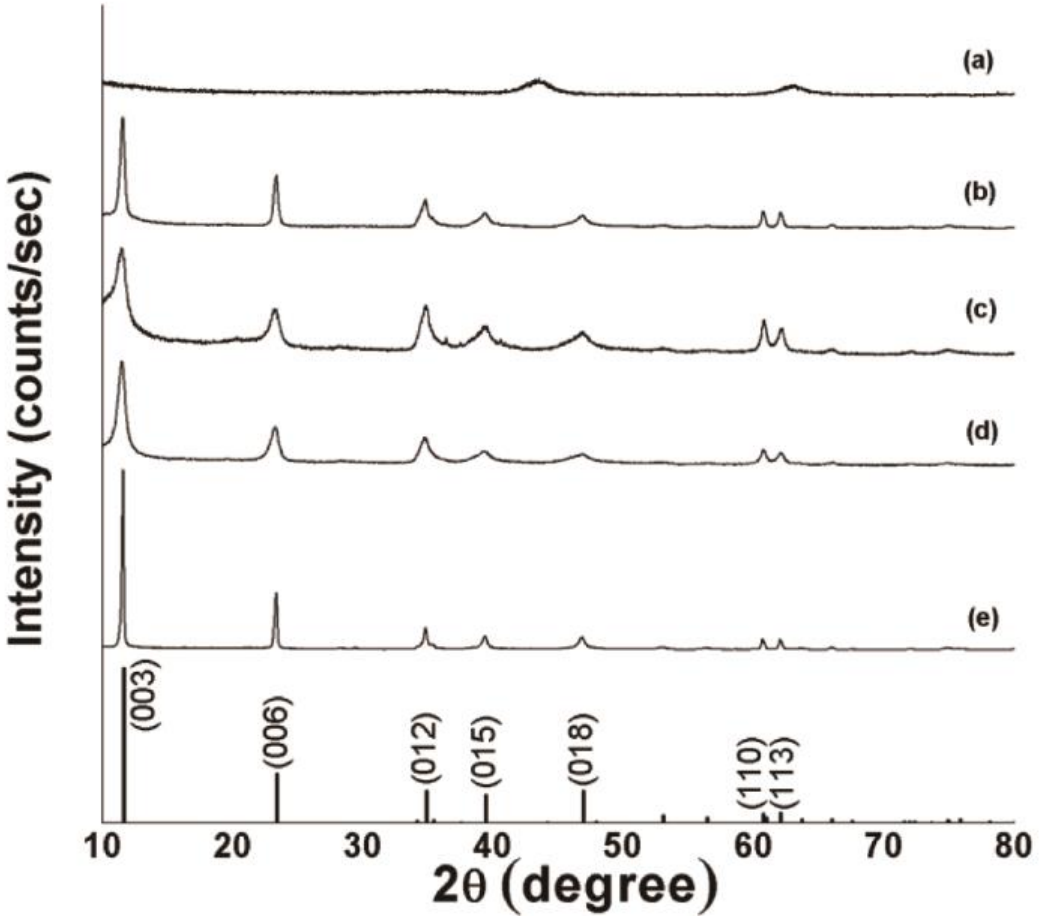

Figure 12. XRD patterns of granular LDH (a) as-obtained sample; (b) after immersion in DI water; exhausted media from column test conducted in (c) groundwater, (d) groundwater pre-treated with $BaCl_2$; (e) powdered LDH with layered structure and reference pattern of $Mg_{0.667}Al_{0.333}(OH)_2(CO_3)_{0.167}(H_2O)_{0.5}$ from PDF 01-089-0460 (bottom).

The as-received LDH-granular were dispersed in isopropanol and sonicated for 15 min to prepare the SEM samples. SEM imaging (Figure 13) showed that the material consisted of micron-sized granules formed from aggregated particles. The specific surface area obtained from the BET measurement was ca. 91 m^2/g (Table 4). Sonication of the material resulted in nanosheet-like particles about 200 nm in size (Figure 13, inset).

FTIR spectroscopy of the LDH (Figure 14a) showed that the interlayer hydration deformation bands (δH_2O) typically found at around 1635 cm^{-1} [108,118] were absent in the sample, confirming the absence of water molecules inside the interlayer space. Interlayer carbonate anions were identified by the band at 1365 cm^{-1}.[96,105]

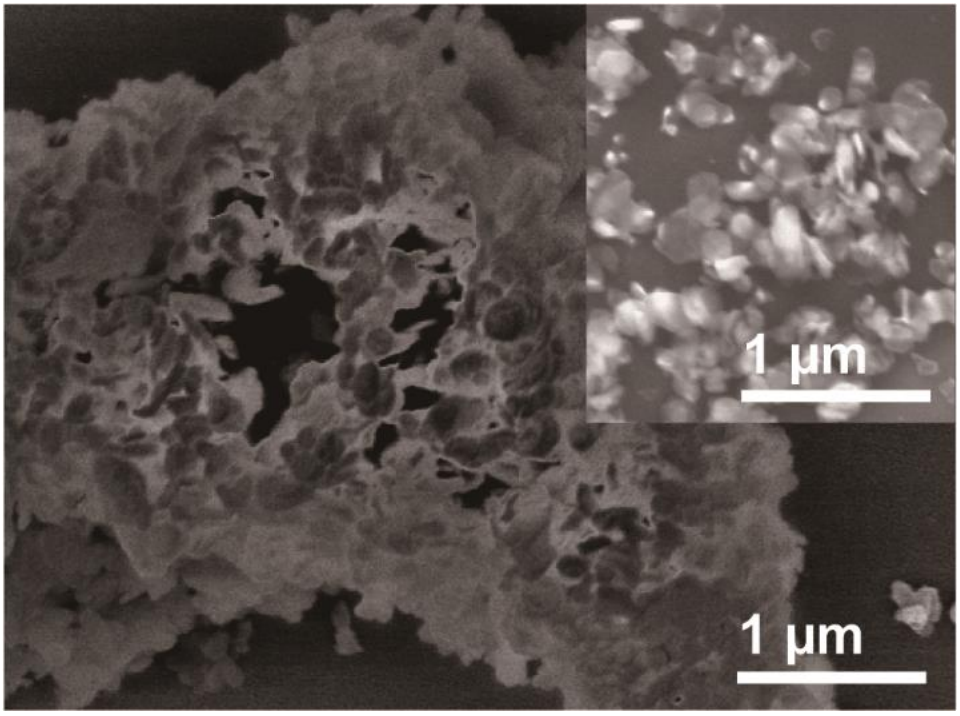

Figure 13. SEM image of granular LDH; particles obtained after sonication shown in inset.

Immersing the granular LDH into DI water confirmed the ability of the material to regenerate the layered structure, which would also be important for its capacity for oxoanion removal. As shown in Figure 12b, the XRD pattern showed the reflections associated with the layered rhombohedral crystal structure of LDHs.[101-112,117] However, the reflections for the reconstructed granular LDH samples were broad, suggesting a low

crystallinity. The reference XRD pattern for powdered LDH with layered structure showed much sharper reflections in comparison (Figure 12e). FTIR analysis (Figure 14b) of the granular LDH reconstructed in DI water revealed bands at 450 cm^{-1} from the lattice vibrations of Mg,Al-oxide octahedral sheets, at 550 cm^{-1}, 670 cm^{-1}, and 772 cm^{-1} from Mg/Al-OH translations, and at 940 cm^{-1} from Al-OH deformation.[105,108,118]

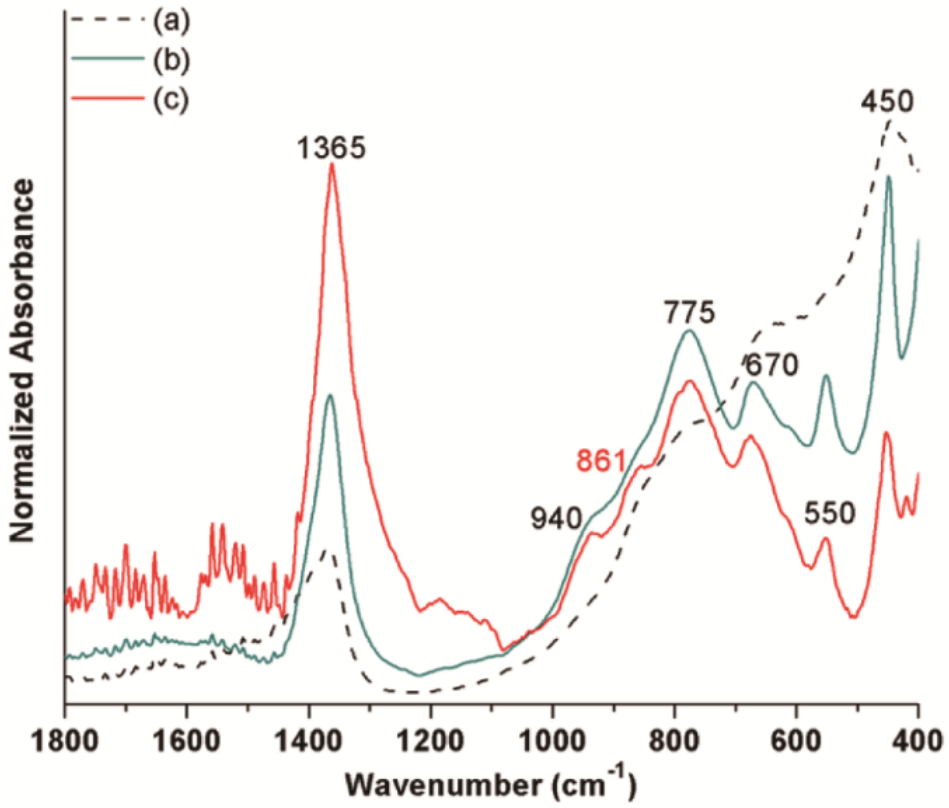

Figure 14. FTIR spectra of granular LDH (a) as-obtained, (b) after reconstruction and rehydration in DI water, (c) exhausted media from column test conducted in $BaCl_2$ pre-treated well water.

4.3.3. Home-made LDH nanosheets

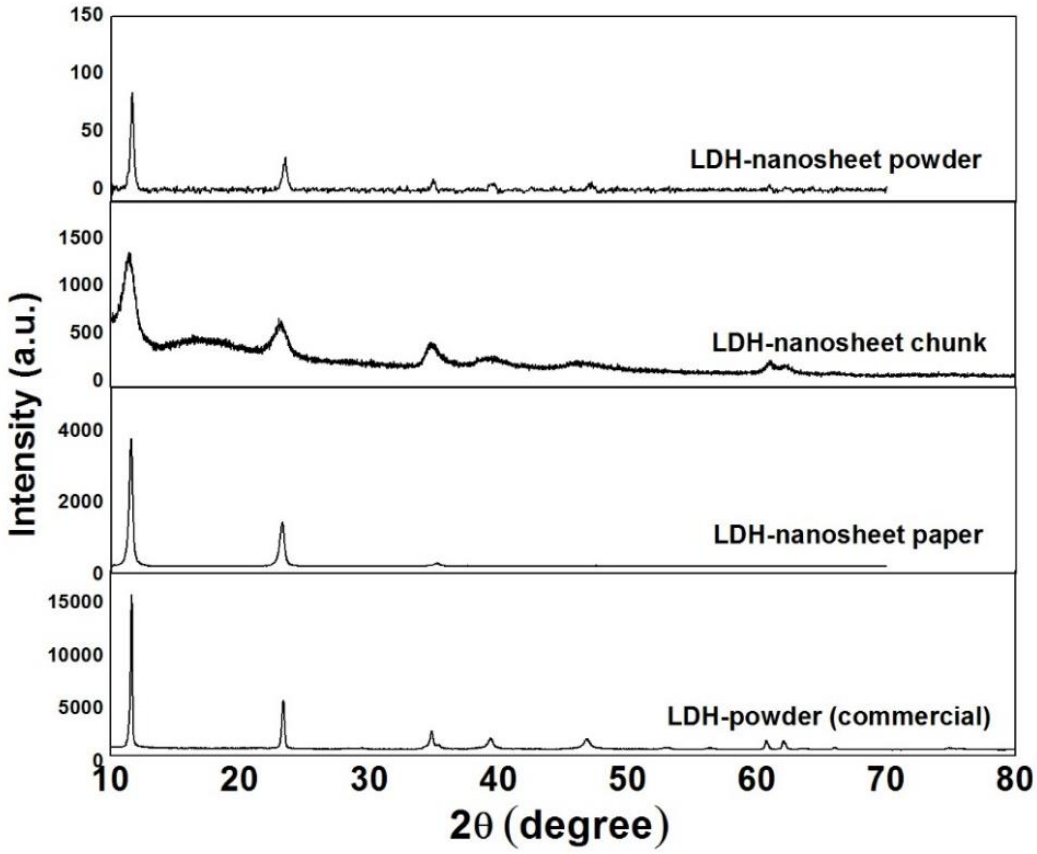

Figure 15. XRD of home-made LDH nanosheets compare with commercially obtained LDH-powder from Sigma-Aldrich.

The X-ray diffraction (XRD) showed that the home-made LDH-nanosheet paper prepared using the precipitation method (Figure 15) had peaks at the same position with LDH-powder but with relatively lower intensities, which indicates that that LDH nanosheet paper was synthesized successfully and included the water molecules in its structure. XRD of the LDH nanosheet chunk showed a similar pattern with the commercially obtained LDH-powder but with lower intensities and broader peaks, which

indicates that nanosheet chunk was successfully made but the crystalline quality is not as good as the commercial LDH-powder. The LDH-nanosheet powder prepared using the urea hydrolysis method also showed similar XRD patterns but with much lower intensity of the basal reflections (Figure 15). All of the home-made LDHs showed a lower intensity and broader peaks compared to commercial LDH-power, which also suggests that the home-made LDHs have smaller particle sizes than commercial LDH-powder. This can be confirmed by scanning electron microscopy (SEM) imaging.

The SEM image (Figure 16) shows the LDH nanosheet powder was made up of nanosheets with particle size less than 500 nm. SEM of LDH-nanosheet paper shows nanosheets with sizes smaller around 250 nm, and they all lay down in one direction and assembled into a large paper-like structure (Figure 17).

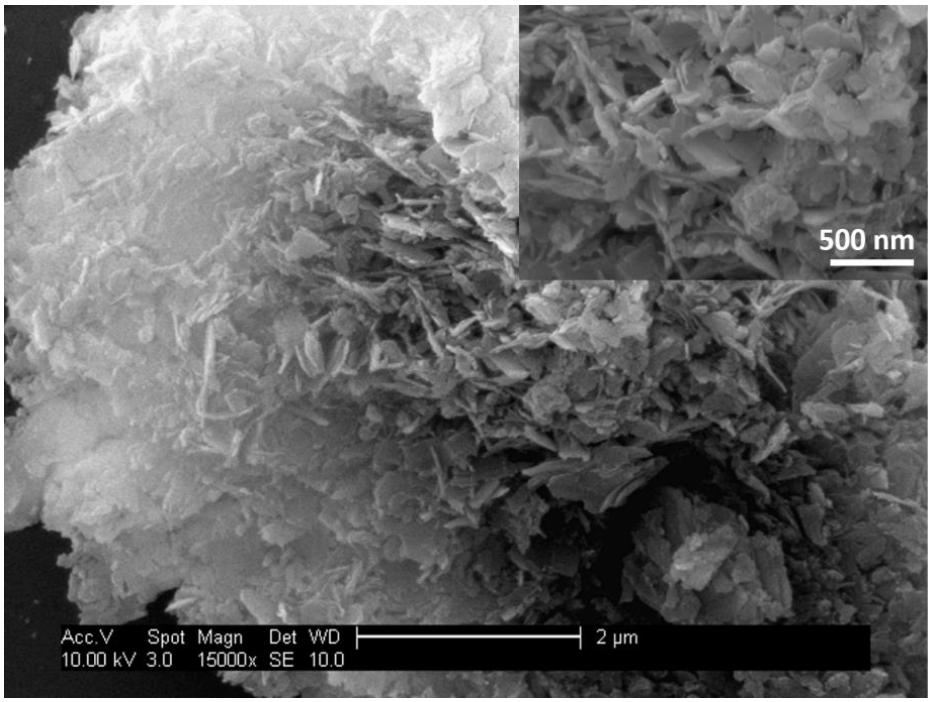

Figure 16. SEM of home-made LDH-nanosheet powder using urea hydrolysis method.

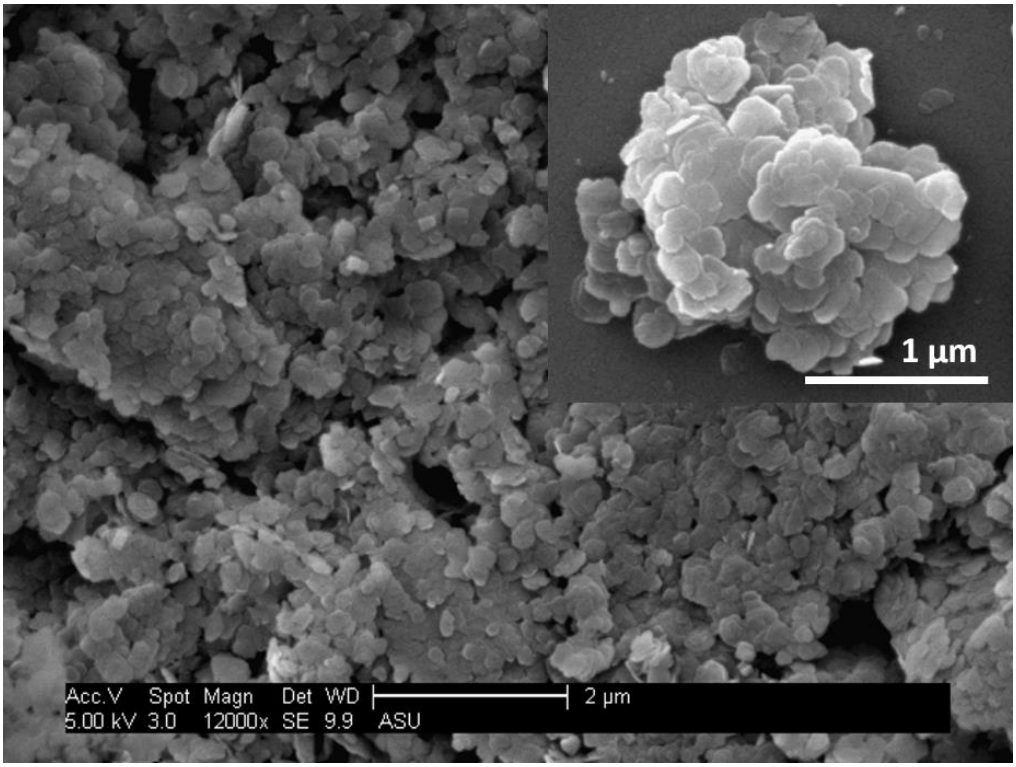

Figure 17. SEM of home-made LDH-nanosheet paper using titration method.

4.4. Jar Test Results

4.4.1. Spiked DI Water Solutions

To study the performance for removing selenate and arsenate, the LDHs were first evaluated in jar tests at a loading of 5 g/L in de-ionized water spiked with 1 ppm initial concentration of selenate, Se(VI), or 1 ppm arsenate, As(V). The as-obtained commercial LDH-powder displayed very little efficacy for Se(VI) removal in spiked DI water (Figure 18, dark yellow curve). Only ca. 17% of the Se(VI) was removed after 26 h of exposure, corresponding to 0.044 mg Se/g loading. The LDH-powder was observed to be quite hydrophobic and difficult to disperse evenly in water, which may be the reason for its low selenate removal efficiency. Additionally, since LDH-powder was in the form of Mg-Al-

CO_3 LDH, which has low ion-exchange properties due to the strong selectively of the material for carbonate anions,[97,102] only surface adsorption of selenium would be possible. The low BET surface area (Table 5) of as-obtained LDH-powder is consistent with a low capacity for selenium removal. After heat treatment to make LDH-500C, the material was easier to disperse into the solution, with 94% Se(VI) and 100% Se(IV) removed by LDH-500C after 2 h of exposure (Figure 18, black curve). The high removal efficiency of LDH-500C confirms that the surface properties play a large role in both selenate and arsenate removal. And also by calcination, the interlayer water was removed resulting higher surface area for LDH-500C than that of LDH-powder (Table 5), which allows more anions to go inside the interlayer structure.

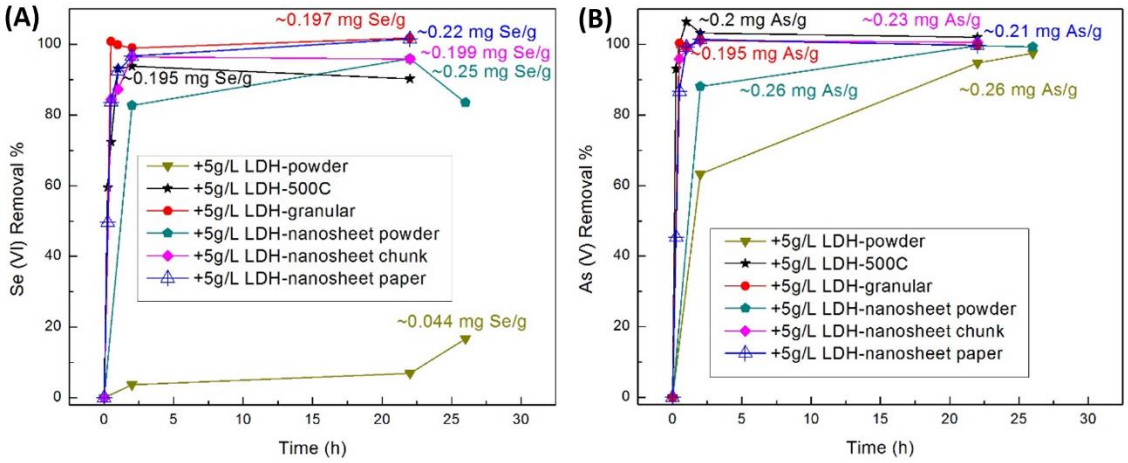

Figure 18. Percent removal of 1 ppm (A) selenate, (B) arsenate on different forms of LDH materials at a concentration of 5 g/L in spiked DI water.

Table 5. Maximum selenate loading using different layered double hydroxide (LDH) sorbents in jar tests (1 ppm Se, 5 g/L LDHs).

Sample Name	**Specific Surface Area (m^2/g)**	**Loading (mg Se/g)**	**Loading (mg Se/m^2)**	**Loading (mg As/g)**	**Loading (mg As/m^2)**
LDH-powder	7.67	0.044	0.0057	0.26	0.0339
LDH-500C	179.35	0.195	0.0011	0.20	0.0011
Used LDH-500C	25.78				
LDH - granular	91.5	0.197	0.0022	0.195	0.0021
Used LDH-granular	40.95				
LDH nanosheet powder		0.25		0.26	
LDH nanosheet chunk 3	19.45	0.199	0.0102	0.23	0.0118
LDH nanosheet paper	20.08	0.22	0.0110	0.21	0.0105

Aside from the LDH-powder (as-received LDH from Sigma-Aldrich), all the other forms of LDHs could remove more than 90% of the selenate and arsenate in DI water in 2 h. Furthermore, the nanosheet LDH paper and chunk (LDH nanosheets assembled into larger particles) as well as commercially obtained LDH-granular could reach 100% selenate and arsenate removal efficiency after 22 h (starting concentration 1 ppm Se, 5 g/L LDHs). Due to the concentration used and absence of competing ions in the DI water, the maximum loadings within 22 h observed for the LDH materials are around ~ 0.2 mg/g, as shown in Table 5. From these results, we can see that the different forms of LDHs have similar performance to each other, and the removal efficiency for selenate or arsenate is not affected too much when the nanosheets are assembled and stacked together to form larger particles. We attribute it to the unique layered structure of

LDH, which allows for water molecules and anions to diffuse through the material, even if its overall surface area is lower than compared to the LDH-powder. But whether it is the surface adsorption or the interlayer ion-exchange dominate in the Se(VI) binding mechanism requires further jar test study. Since the as-obtained LDH-granular was comprised of the dehydrated, periclase-form of the LDH, jar test studies were performed to elucidate the Se(VI) removal mechanism in DI water containing trace levels or high concentrations of Se(VI) at room temperature using sorbents at concentration of 1 g/L with sampling performed after different time periods.

For comparing the trace level removal and high level Se(VI) removal mechanism, the as-obtained periclase-form LDH-granular and layered LDH samples were evaluated in water samples that were agitated using a compact digital mini rotator (Thermo Scientific, Catalog no. 88880025) shaking at 300 rpm. The performance of the as-obtained LDH-granular media (confirmed to have the nonlayered, periclase structure by XRD) was evaluated by spiking DI water to the desired Se(VI) level and shaking overnight prior to the initial sampling point at 0 min to establish the baseline [Se] level. Then, the as-obtained LDH-granular was added to the DI water solution and water samples were taken at different time points. To evaluate the performance of LDH with the layered structure, the as-obtained LDH-granular was immersed in DI water and agitated with the mini rotator overnight so that the layered structure could be reconstructed. Then, the appropriate amount of Se(VI) was added to the solution and the first sample was taken after 2 minutes. As the spiking procedure was the same for the as-obtained LDH-granular and the layered LDH-granular, the initial Se levels are assumed to be the same.

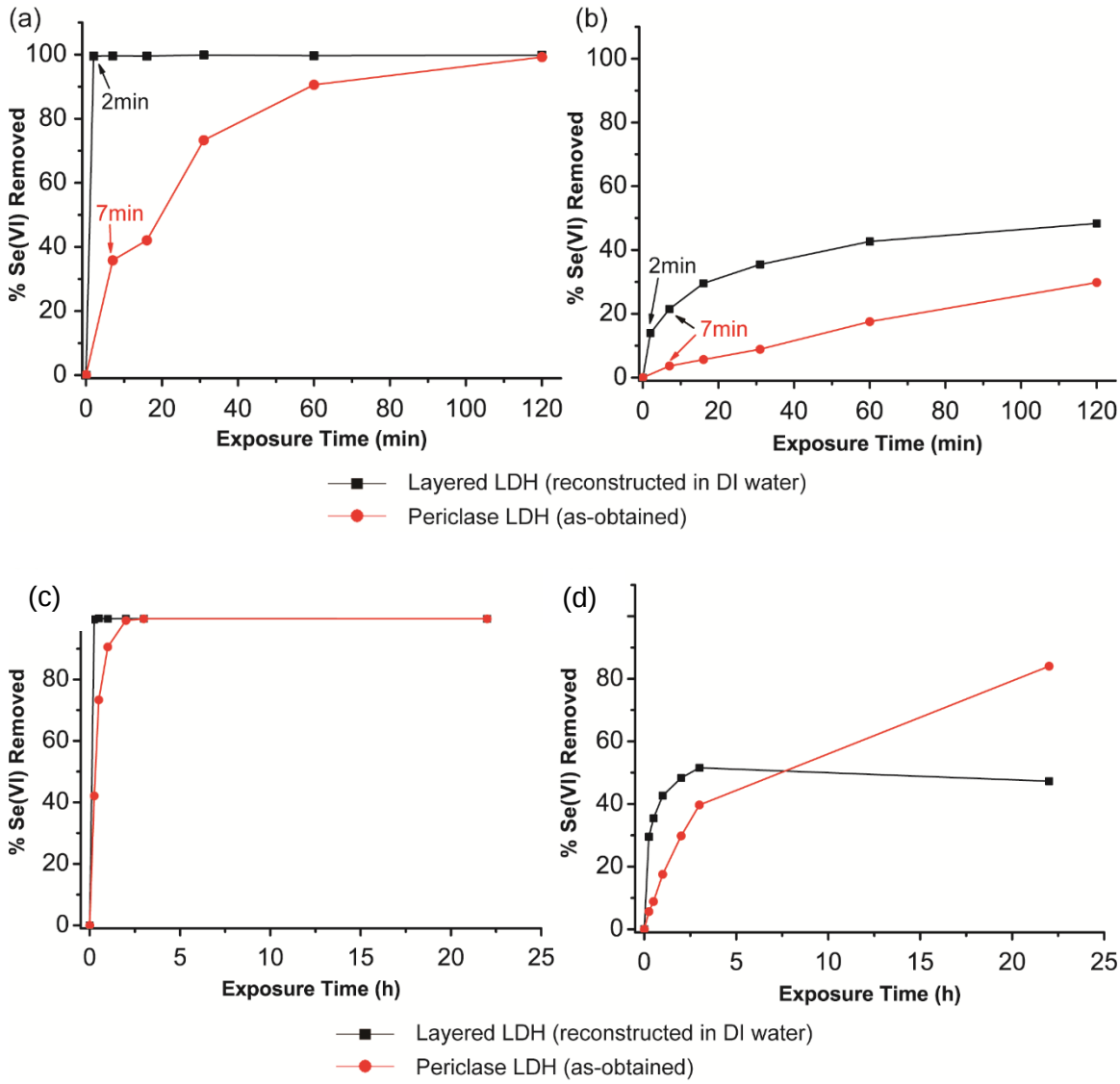

Figure 19. Jar test results in 120 min using 1 g/L LDH in DI water spiked with (a) 3.43 ppb, (b) 72.9 ppm Se(VI). Total 22 h results of (c) 3.43 ppb, and (d) 72.9 ppm. The as-obtained LDH had the non-layered, periclase structure. The layered LDH was obtained by reconstructing the as-obtained LDH in DI water.

For the layered LDH, it is expected that the Se(VI) will bind on the particle surfaces and can also be removed via anion-exchange with the interlayer anions and water molecules. However, when the as-obtained media (with periclase structure) is immersed into a solution containing Se(VI), the Se(VI) can also become incorporated

into the material as the layered structure is reconstructed. At trace levels (initial [Se] = 3.43 ppb), the jar test results showed that the periclase-form of the LDH required 120 min for 100% removal of the Se(VI) (Figure 19a). However, the Se(VI) could be removed within 2 min of exposure to the layered LDH that was reconstructed in DI water. This implies that the Se(VI) removal was predominately through fast surface adsorption in the layered LDH, while the reconstruction of the layered structure in the periclase-form slows the removal of Se(VI). When the Se(VI) level was increased (initial [Se] = 72.9 ppm), the Se(VI) removal was also slower for the periclase- form over the layered one (Figure 19b). Due to the high Se(VI) levels in this case, there are insufficient surface sites for Se(VI) adsorption available and anion-exchange in the LDH interlayer space is required, which is a slower process. However, based on the results in Figure 19d, it appears that at long exposure times, the periclase-form can remove more Se(VI) than the layered form. This is likely due to the combination of Se(VI) being removed via anion-exchange in addition to incorporation into the reconstructed layered structure, rather than just anion-exchange alone.

The adsorption isotherms for Se(VI) binding onto LDH-500C (1 g/L) in spiked DI water are shown in Figure 20. The linear fit of the experimental data to the Langmuir model (Figure 20, inset) was $y = 0.072 + 0.015x$, where $y = C_e/Q_e$ and $x = C_e$, with a correlation coefficient value $R^2 = 0.9896$. This shows a good fit to the model, indicating that Se(VI) adsorbed on defined sites on the surface of LDH-500C as a monolayer. [117,121] The maximum capacity, Q_{max}, calculated by the Langmuir isotherm model was 67 mg/g and the equilibrium constant K was 0.21 L/mg. This demonstrates the large adsorption ability of LDH-500C for removing selenium.

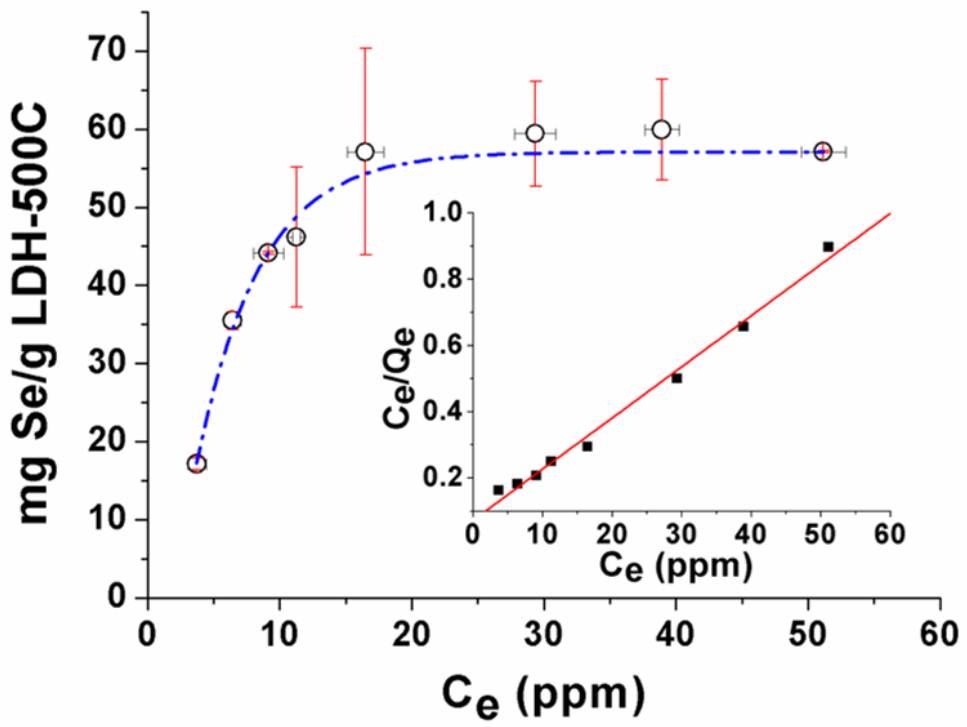

Figure 20. Selenate sorption isotherms using 1 g/L LDH-500C for 22 h exposure time. Plots are averages of triplicate, with standard deviation for the error bar. Langmuir plots using average of triplicate in inset.

Due to differences in sorbent dosages and pH conditions used for performing isotherm experiments, it is not straightforward to compare the Q_{max} obtained here to other values from the literature. Nonetheless, reported Se(VI) adsorption capacities for sorbents based on aluminum oxides,[122] iron oxides,[123-124] manganese oxides,[125-126] chitosan/clay,[127] and silica [128] have all been below 20 mg/g. A study on crystalline Mg-Al LDHs prepared using alkoxide sol-gel, alkoxide-free sol-gel, and hydrothermal precipitation methods reported adsorption capacities of 4, 45, and 18 mg/g, respectively, at pH 7.[105] From these results, we can see that the calcined LDH displays a superior adsorption capacity compared to other metal oxide and LDH-based sorbents for selenate.

4.4.2. Spiked Power Plant Waters

Analysis of the obtained SRP groundwater (site E) showed that the total selenium concentration was 1.75 ppb Se and the amount of sulfate was 36.6 ppm, or more than 20,000 times higher. The determination of selenium speciation at trace levels requires advanced analytical techniques [129-130] and was not conducted for the groundwater samples. However, previous studies have shown that LDHs are effective for removing both oxoanionic forms of selenium.[95,105] Our jar test data also confirmed the efficacy of the granular LDH and LDH-500C for removal of Se(IV) and Se(VI) from spiked DI water solutions (Figure 21).

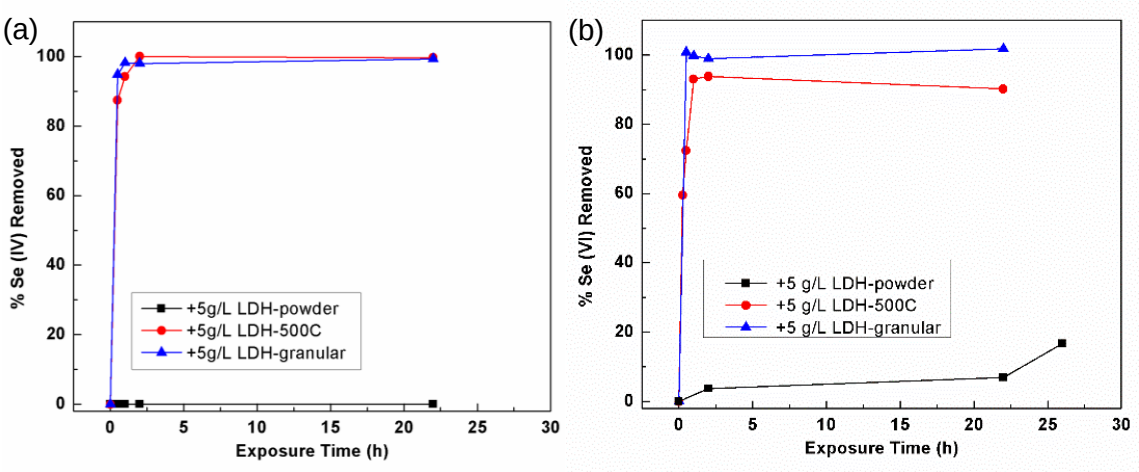

Figure 21. Removal of 1 ppm (a) selenite and (b) selenate from DI water in jar test using LDHs at 5 g/L.

LDH-500C was first studied for removal of selenate from the power plant waters obtained from Salt River Project (SRP). Due to the low-ppb natural levels of selenium in the as-obtained water samples (Table 2), jar tests were performed in SRP water samples from site A to site G spiked with 0.2 ppm Se(VI). 1 g/L to 5 g/L LDH-500C were tested.

Figure 22 shows the amount of Se(VI) removed over time, while Table **6** presents the final percentage of Se(VI) removed after 22 h of exposure to the LDH. As shown in Table 6, when using a sorbent dosage of 1 g/L (Figure 22A), it was effective for removing close to 30% of the selenate in the upstream waters (Site A, B, E), but not in the blowdown waters (Site C, D, F). The highest loading rate was about 0.07 mg Se/g LDH-500C when using 1 g/L sorbent. The differences in removal efficacy correlated with the sulfate levels in the water (Table 2), with more Se(VI) removed in the upstream waters that had lower sulfate levels (site A, B, E, G) compared to the downstream waters including cooling tower blowdown (C, D, F). Due to the similar properties between sulfate and selenate, the two oxoanions can compete with the same sites on the LDH, [6,107,122,131] which means that higher dosages of sorbent are required to fully remove the Se(VI).

Using the water from site E as an example, the LDH-500C dosage was increased from 1 to 5 g/L and the Se(VI) removal efficacy after 22 h exposure was compared. As shown in Figure 22C, the amount of Se(VI) removed after 22 h increased from only 22% to 89% when the dosage was increased from 1 to 2 g/L, with 100% of the Se(VI) removed when using dosages of 4 and 5 g/L. However, at short exposure times, the 5 g/L dosage was more effective for removing higher amounts of selenate, with 83% removed after 30 min compared to <14% for dosages < 4 g/L. When using 5 g/L LDH-500C in the other spiked power plant waters, the removal efficacy was increased to 100% for almost of all of the waters (Figure 22B). Even in the cooling tower blowdown (site C) with the highest sulfate and TDS levels (Table 2), close to 80% of the Se(VI) was removed. This is particularly notable considering the much higher levels of sulfate (hundreds of ppm-

level) compared to the amount of Se(VI) added (0.2 ppm) to the waters. These results show that the calcined LDH-500C can be a good candidate to remove Se(VI) from all of the SRP power plant waters.

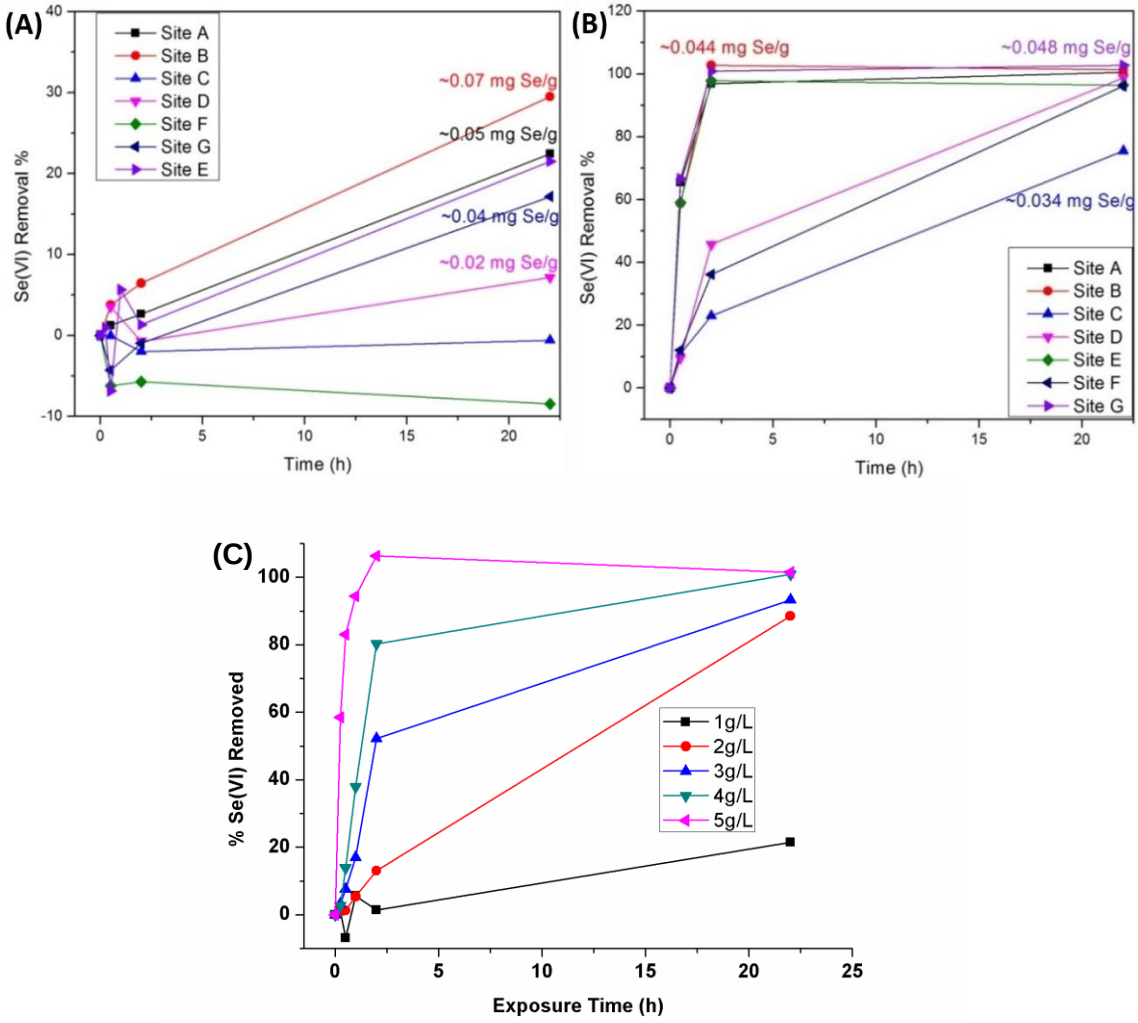

Figure 22. Jar test results from power plant waters spiked with 0.2 ppm selenate. Removal of 0.2 ppm selenate spiked into different power plant waters using LDH-500C at (A) 1 g/L, (B) 5 g/L dosage; (C) removal of 0.2 ppm selenate from spiked well water (E site) using different dosage of LDH-500C. For identification of the waters, please see Figure 2.

Table 6. Percent selenate removed using LDH-500C sorbent in spiked SRP water samples with a starting concentration of 0.2 ppm.

Sorbent conc.	**% Selenate removed**						
	Site A	**Site B**	**Site C**	**Site D**	**Site E**	**Site F**	**Site G**
1 g/L	22	30	0	7	22	0	17
5 g/L	100	100	75	99	97	96	100

To understand the role of sulfate in the groundwater on the selenium removal characteristics of the as-obtained granular LDH, jar tests were performed in water solutions intentionally spiked with large amounts of Se(VI), namely 100 ppm. The sorbent dosage was 1 g/L and the exposure time was 22 h to decrease the likelihood of kinetic limitations for adsorption. As shown in Table 7, the LDH-granular could remove 74% of the Se(VI), which corresponded to an adsorption capacity of 89.5 mg/g. This displays a superior adsorption capacity compared to other inorganic sorbents such as aluminum oxides,[122] iron oxides,[123-124] manganese oxides,[125-126] chitosan/clay composites,[127] and silica,[128] which have been reported having Se(VI) capacities below 20 mg/g. A study on materials prepared using alkoxide sol-gel, alkoxide-free sol-gel, and hydrothermal precipitation methods to synthesize LDH reported adsorption capacities of 4, 45, and 18 mg/g, respectively, at pH 7.[105]

As shown in Table 7, when the LDH was exposed to the groundwater spiked with 100 ppm Se(VI), the adsorption capacity decreased by more than half and only 33% of the Se(VI) was removed. The much lower removal efficacy suggests the presence of competing species in the water. Therefore, removing the sulfate from the water using a chemical pre-treatment step was investigated. Barium chloride, $BaCl_2$, can precipitate out

sulfate as $BaSO_4$ and can also co-precipitate selenate at the same time.[29] Performing the jar test in groundwater pre-treated with $BaCl_2$ to remove the sulfate showed that the amount of Se(VI) that could be removed was almost the same as what was observed in DI water, with loadings of 72.8 mg/g observed. These results confirm that sulfate removal from the water can be effective for improving the Se(VI) adsorption capacity of LDH sorbents.

Table 7. Jar test results using 1 g/L as-obtained LDH and 22 h exposure time in solutions spiked with 100 ppm Se(VI).

Water	**% Se removed**	**Se loading (mg/g)**
DI water + 100 ppm Se(VI)	74%	89.5
Groundwater + 100 ppm Se(VI)	33%	41.1
Groundwater + $BaCl_2$ + 100 ppm Se(VI)	65%	72.8

4.5. Characterization of used LDH after Selenate Removal Tests

The LDH sorbents after exposure to Se(VI) solutions were further characterized using BET, XRD, and FTIR. The BET surface area for LDH-500C after exposure to 100 ppm Se(VI) in a jar test decreased to 26 m^2/g confirming the surface adsorption processes (Table 5). The XRD analysis showed the reflections associated with the basal (00*l*) spacings were present in the pattern for the exhausted LDH-500C after exposure to 50 ppm Se(VI) in a jar test (Figure 10a, (v)), and the pattern looked very similar to that for the as-obtained LDH-powder (Figure 10a, (i)). This confirms the memory effect and recovery of the crystalline LDH structure after the test, indicating that the water

molecules together with the anions were incorporated back into the LDH to form the crystalline layered structure.[101,117]

FTIR characterization also confirmed the recovery of the LDH crystal structure. As shown in Figure 11c, the LDH bands associated with interlayer carbonate and Mg,Al-OH bonds were observed in the LDH-500C after the jar test. The band associated with the ν(Se-O) vibrations of Se(VI)-O-Mg,Al-LDH complexes [108] at 859 cm^{-1} was observed in LDH-500C after exposure to selenate. This band increased in intensity as the concentration of Se(VI) used in the LDH-500C jar test increased from 50 to 100 ppm (Figure 11e), confirming the sorption of Se(VI) on the LDH.

4.6. Regeneration

The memory effect of LDH materials enables the regeneration of the original layered crystal structure after calcined LDHs are re-exposed to water and other anions.[101,109] To investigate whether this phenomenon can be exploited to regenerate the exhausted LDH sorbents using calcination,[132] LDH-500C (5 g/L) was exposed to a DI water solution containing 50 ppm Se(VI); in parallel, another sample of LDH-500C was exposed to 50 ppm sulfate (from Na_2SO_4) with the intent to prepare sorbents saturated with Se(VI) or sulfate. TGA of these samples showed a similar weight loss curve as what was observed for LDH-powder, except with more weight loss > 400^oC attributed to the removal of the interlayer oxoanions (Figure 10b). Therefore, 550^oC was chosen as the calcination temperature and regeneration was performed by heating the samples for 2 h in a box oven.

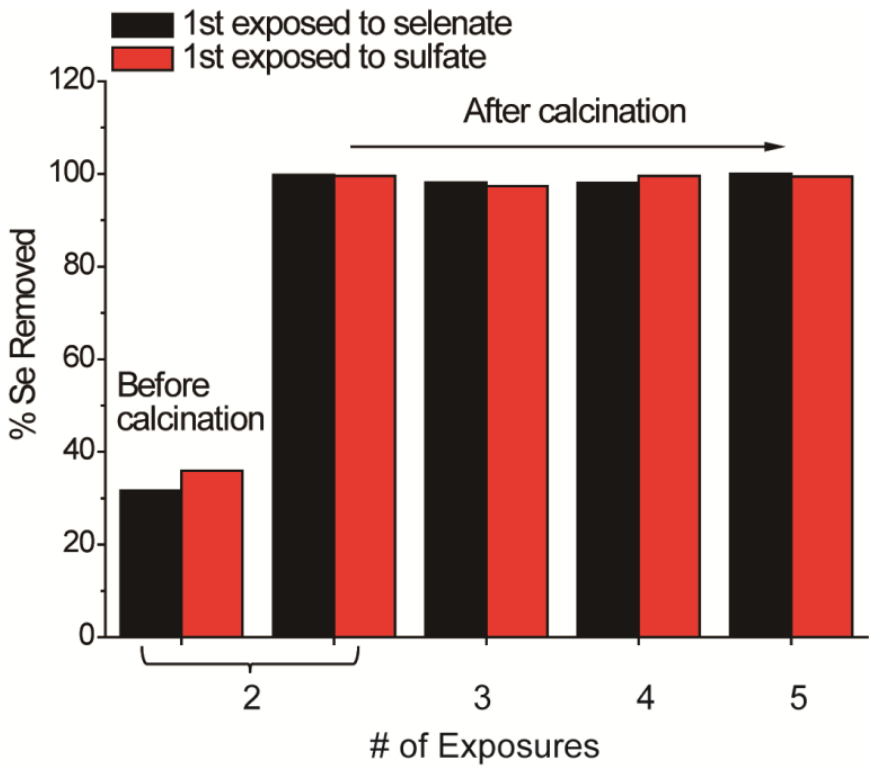

Figure 23. Removal of selenate using 5 g/L used LDH-500C that exposed to 50 ppm selenate or sulfate solution. For each calcined cycle, the used LDH-500C was calcined at 550^{o}C for 2h.

The aforementioned LDH-500C samples containing interlayer Se(VI) or sulfate were exposed to fresh solutions containing 50 ppm Se(VI). Without using calcination to remove the species adsorbed in the first exposure, less than 40% of the oxoanions could be removed from the waters in the second exposure, as shown in Figure 23. Interestingly, the removal efficacy for Se(VI) was similar irrespective of which oxoanion the LDH-500C was previously exposed to. The samples were then calcined and then subjected to a third exposure to solutions with 50 ppm Se(VI). Both samples showed 100% removal of Se(VI) even after the fifth cycle, indicating that the calcination was effective for regenerating the LDH. FTIR analysis of the LDH after regeneration (Figure 11d) showed

a spectrum very similar to the as-prepared LDH-500C (Figure 11b), confirming the removal of the adsorbed selenate during decarboxylation/dehydration. These results show that after calcination to remove the interlayer anions, LDH can be reused for subsequent exposures, with the layer structure regenerated each time after adsorbing more selenate anions from water.

4.7. Conclusions

In summary, the calcined LDH-500C and the as-obtained LDH-granular exhibit a great removal efficacy for selenium from synthetic DI water. Isotherms conducted in spiked DI water showed LDH-500C fit the Langmuir model for adsorption and had a maximum selenate adsorption capacity of 67 mg/g, which is higher than literature values reported for other metal oxide and LDH sorbents. LDH-500C showed good capacity in removing selenate from SPR power plant waters that contain very high competing ions such as sulfate and high total dissolved solids. By using a dosage of 5g/L, LDH-500C could reach close to 100% of the selenate removal efficiency for almost all of the SRP water sites.

Due to the non-layered, periclase structure of the LDH-granular, reconstruction of the layered structure occurs when the media is immersed into water. For trace levels of selenate, surface adsorption of selenate can occur quickly on the layered form of LDH, while at higher levels the ion-exchange plays a larger role due to the insufficient amount of surface sites. For the non-layered periclase form, the reconstruction of the layered structure is a slow process, but ultimately improves the capacity for Se(VI) removal. The LDH was effective in jar tests for removing selenium from groundwater that contained

very high levels of competing sulfate anions, with removal capacities > 41 mg/g if the selenate and sulfate concentrations were roughly the same (100 ppm vs. ca. 40 ppm, respectively). Lowering the sulfate levels through addition of $BaCl_2$ resulted in a higher selenate adsorption capacity > 72 mg/g.

5. Other Metal Oxide Sorbents

Table 8. Characteristics of tested materials for selenium removal.

Sorbent Material	**PZC**	**Comment**
P90 TiO_2	6	Proven photocatalyst for Cr(VI) reduction and sorbent for selenate < pH 6
ZnO	8.8	Proven photocatalyst for Cr(VI) reduction
WO_3	< 3	Proven photocatalyst for dye degradation and water oxidation; stable in acidic/neutral pH
Fe_2O_3	7 – 9.2	Proven photocatalyst for dye degradation and water oxidation
H_2/P90 (Hydrogen treated P90 TiO_2)	Not known	More active photocatalyst for water splitting than P90 without H_2 treatment
Ebonex® (titanium suboxides, Ti_nO_{2n-1}, n = 4-10)	Not known	Used as electrode materials in fuel cells and electrochemical remediation applications
Cu_2O	7-9.5	Proven sorbent for selenate
CuO	9.5	Proven sorbent for selenate

Metal oxide materials with relatively high point-of-zero charge (PZC) values may have potential selenate adsorption properties at around neutral pH solution. Using TiO_2 photocatalysts to reduce selenate to selenite under UV-illumination with organic hole scavengers has also been reported.[133] Several different metal oxides were chosen in an initial screening as sorbents for selenate removal and the description of the materials tested with some of their characteristics are given in Table 8. These materials were

chosen based on their high PZC (for Cu_2O, CuO, and Fe_2O_3),[134] proven performance as photocatalysts for chromium reduction or water splitting (TiO_2, ZnO, WO_3, Fe_2O_3), and their catalytic activity as cathodes or photocathodes (H_2 treated TiO_2, Ebonex®).

5.1. Experimental Methods

Sodium selenate solution was prepared at a concentration of 1 ppm in DI water. The sorbents were used at a dosage of 1.1 g/L (except Fe_2O_3, which was used at 1 g/L) and exposed to the selenate solution for 30 min with the pH adjusted using HCl and NaOH.

H_2 treated P90 TiO_2 was prepared by heating P90 TiO_2 under under H_2 gas (from here on referred to as H_2/P90). Temperature ramp stage for 1h from 0 to 400 ^oC, and hold at 400 ^oC for 1 h.

A pretreatment was employed to modify the surface of the Cu_2O and increase its hydrophilicity and dispersion in the water using a slightly acid medium solution.[135-136] Briefly, Cu_2O was immersed in a pH 4 hydrochloric acid (HCl) for 12 h, and then was washed with DI water, filtered, and dried at 35 ^oC under vacuum over one week (the acid pretreated sample from here on abbreviation as T-Cu_2O). For regeneration, the used Cu_2O after exposed to 1 ppm selenate solution at a dosage of 30 g/L was washed with DI water, then filtered and dried at 35 ^oC under vacuum over one week for the next cycle exposure to the same fresh 1 ppm selenate solution with a same dosage at 30 g/L.

5.2. Jar Test Results

The results showed that P90 TiO_2 and H_2/P90 (H_2 treated P90) had close to 100% removal at pH 6 and below (Figure 24). The removal efficiency decreased at higher pH, consistent with the PZC of TiO_2 being at around 6. The other sorbents did not display high removal efficiencies at pH 6-8, despite their high PZCs. For instance, Fe_2O_3 only displayed 60% removal at pH 3. Increasing the Fe_2O_3 concentration to 5 g/L improved the removal efficiency only very slightly, as shown in Figure 25. Interestingly, the removal efficiency of those metal oxides such as TiO_2, WO_3, and Fe_2O_3 under irradiation with a Xe arc lamp did not improve (Table 9), indicating that they can act as a sorbent for selenate removal without needing the photocatalytic reduction step. Therefore, all subsequent tests were conducted in the dark in order to evaluate these metal oxides as sorbents.

Table 9. Percent selenate removed from spiked DI water with neutral pH under illumination (Light) and without illumination (Dark).

Exposure Time	**15 min**		**30 min**	
	Light	Dark	Light	Dark
TiO_2	11.9 %	9.2 %		
WO_3	0 %	0 %		
Fe_2O_3			6.7 %	6.3 %

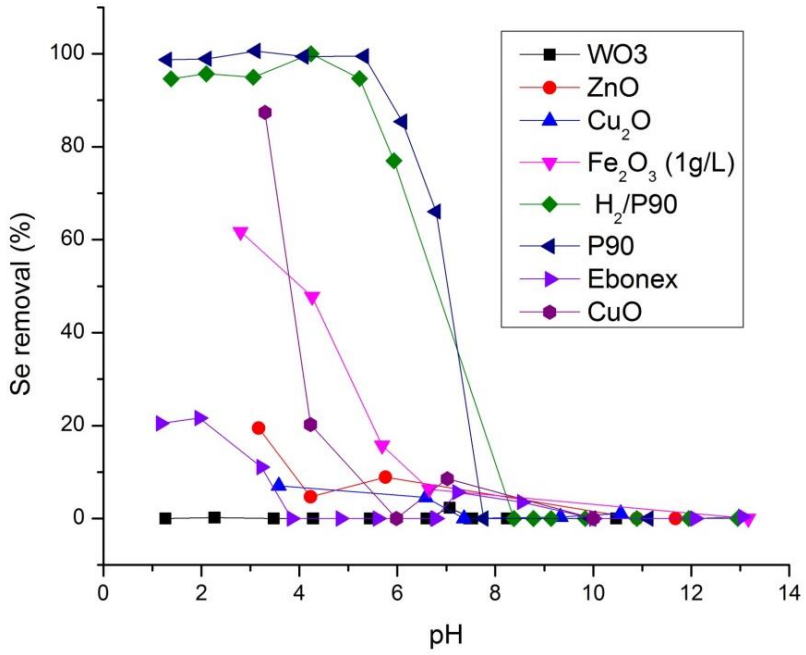

Figure 24. Removal of 1 ppm selenate from DI water in jar tests using different sorbents at 1.1 g/L (except Fe_2O_3 for 1 g/L) for 30 min exposure time along with different pH. pH adjusted using HCl or NaOH.

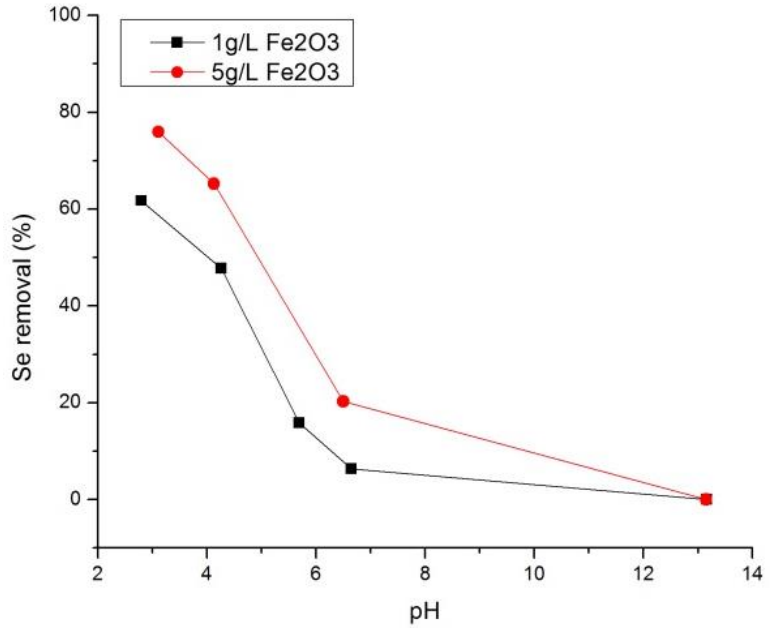

Figure 25. Removal of 1 ppm selenate from DI water using 1 g/L and 5 g/L Fe_2O_3 for 30 min exposure time along with different pH. pH adjusted using HCl or NaOH.

CuO displayed about 90% removal efficacy at pH 3, which dropped to 20% at pH 4 (Figure 24). Previous work[137] using CuO sorbents found that 30 g/L CuO could remove 100% of selenate (spiked at 2 ppm into groundwater) after 4 hours at pH 5-7; reducing the CuO concentration to 10 g/L resulted in only ~ 25% of the selenate removed at pH 7. Our results showed that a much lower concentration of CuO (1.1 g/L) is effective for selenate removal at pH 3, but not at higher pH.

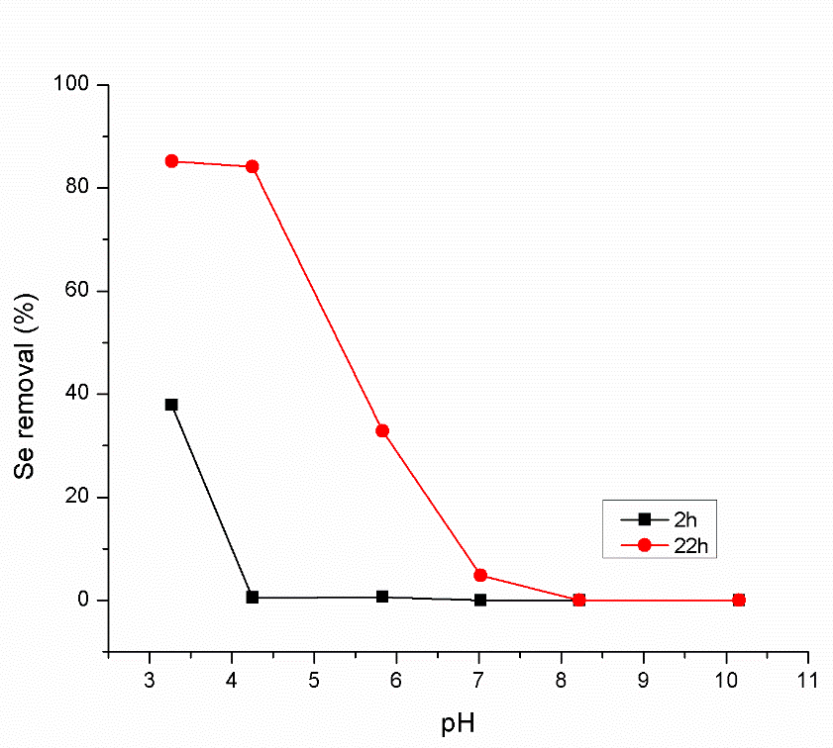

Figure 26. Removal of 1 ppm selenate from DI water using 1.1 g/L Cu_2O for 2 h and 22 h exposure time along with different pH. pH adjusted using HCl or NaOH.

The data in Figure 24 showed that the Cu_2O was not effective for removing selenate in the conditions used, despite the concentration of Cu_2O being similar to that used in previous studies.[135] Additional tests were performed with the sorption time

increased from 30 minutes to 2 h and 22 h. As shown in Figure 26, the 22 h sorption time resulted in more than 80% of selenate removed at pH 4-5 and ~30% at pH 6. Although the removal efficiency was improved with longer sorption time, the removal amounts at neutral pH were still not adequate.

T-Cu_2O (acid pretreated Cu_2O) was used to eliminate the effect of hydrophobic surface of Cu_2O. Besides, the dosage was increased to 30 g/L. The removal results were shown in Figure 27 for the acid treated Cu_2O (T-Cu_2O) using 30 g/L at 2 h and 22 h sorption times. The T-Cu_2O was able to remove 100% of the selenate at pH 3-7.5 after 22 h.

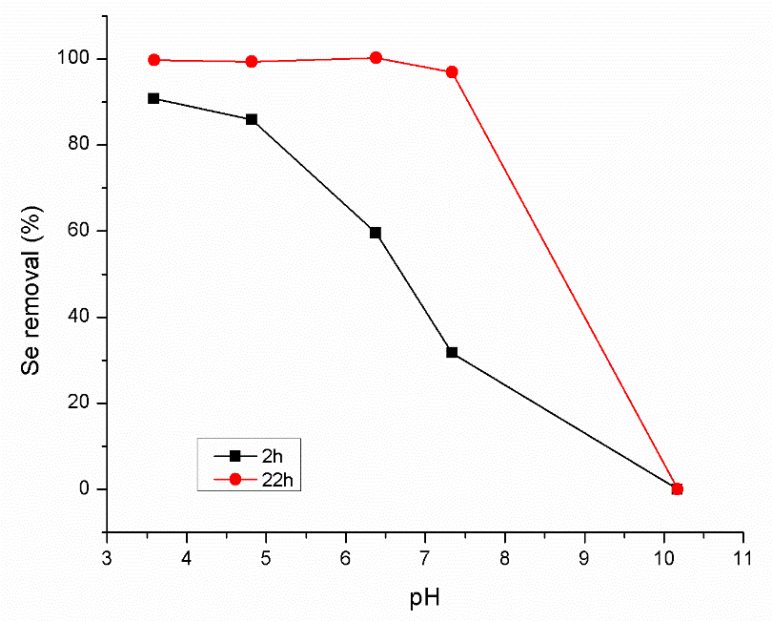

Figure 27. Removal of 1 ppm selenate from DI water using 30 g/L acid treated Cu_2O (T-Cu_2O) for 2 h and 22 h exposure time along with different pH. pH adjusted using HCl or NaOH.

To further investigate the sorption properties of Cu_2O, the amount of selenate adsorbed over time was measured in DI water at pH 6. Figure 28A shows the amount of selenate adsorbed (mg) per g of sorbent material, comparing P90 TiO_2, Cu_2O, and T-Cu_2O (at 1.1 g/L). Figure 29B shows the concentration of selenate remaining (left axis, solid lines) and % removed (right axis, dashed lines) at different times periods. Compared to the TiO_2, the Cu_2O took longer times to adsorb the selenate, but had similar removal efficiencies at 1.1 g/L.

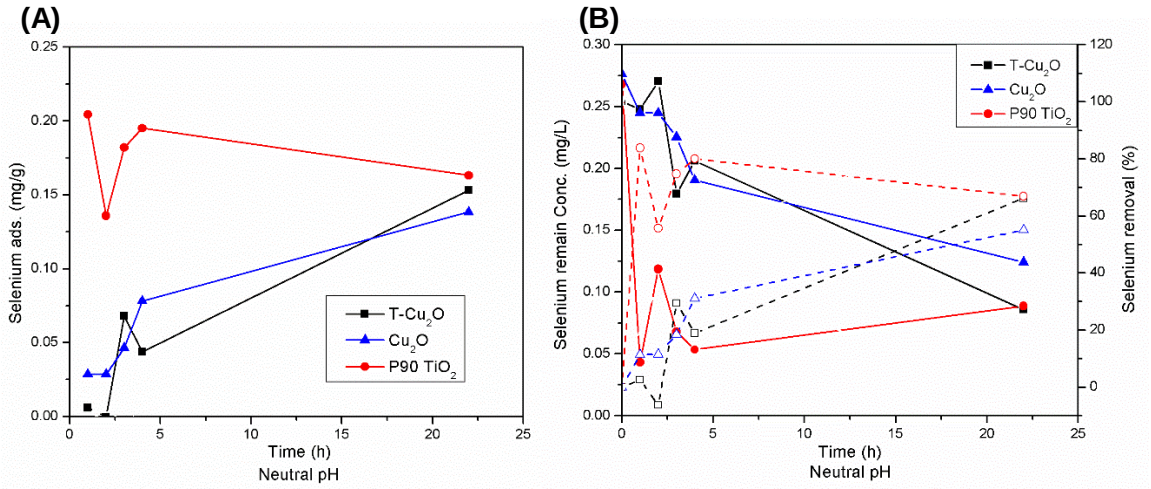

Figure 28. (A) Selenate adsorbed (mg) per g of sorbent materials, and (B) concentration of selenate remaining (left axis, solid lines) and % removed (right axis, dashed lines) along with time using 1.1 g/L different sorbent from spiked DI water. Initial selenate concentration: 1 ppm, neutral pH

Experiments were also conducted to determine if the Cu_2O could be reused multiple times. As shown in Figure 29, the Cu_2O could indeed be reused, with the selenate removal efficiency actually increasing with each cycle. The reason for this is not yet understood, but it likely due to an increase in surface area due to the treatment to remove the adsorbed selenate and regenerate the clean Cu_2O. This will be further studied

to better understand this, since it could have an effect on the dosage of Cu_2O sorbent needed.

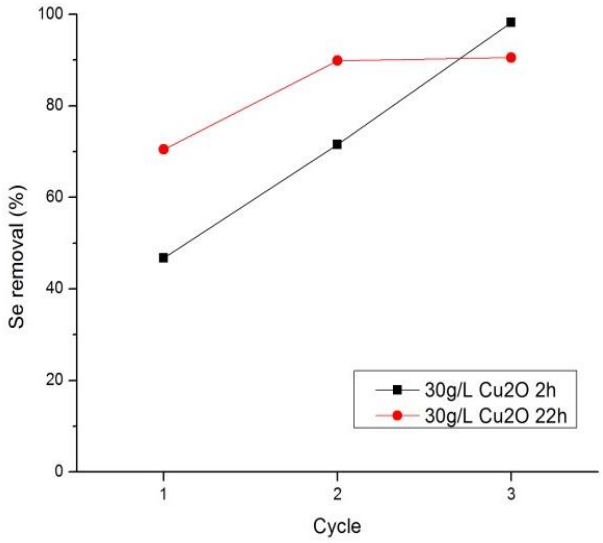

Figure 29. Removal of 1 ppm selenate from DI water using 30 g/L Cu_2O for 2 h and 22 h exposure time for different cycles. For each cycle, the used Cu_2O was washed and dried at 35 ^oC under vacuum for regeneration.

Because adsorption of the selenate onto the positively charged Cu_2O surface can be affected by competing anions in the water matrix, the selenate removal efficiency was tested in the presence of sulfate and nitrate for 2 h sorption times. The T-Cu_2O was used in DI water as a control sample and is shown in the black lines in Figure 30. Addition of 0.1 M Na_2SO_4 or 0.1 M $NaNO_3$ was observed to decrease the selenate removal efficiency, with sulfate completely inhibiting the sorption of selenate. These results indicate that selenium treatment using Cu_2O for SRP waters must be done on waters that have low concentrations of competing anions.

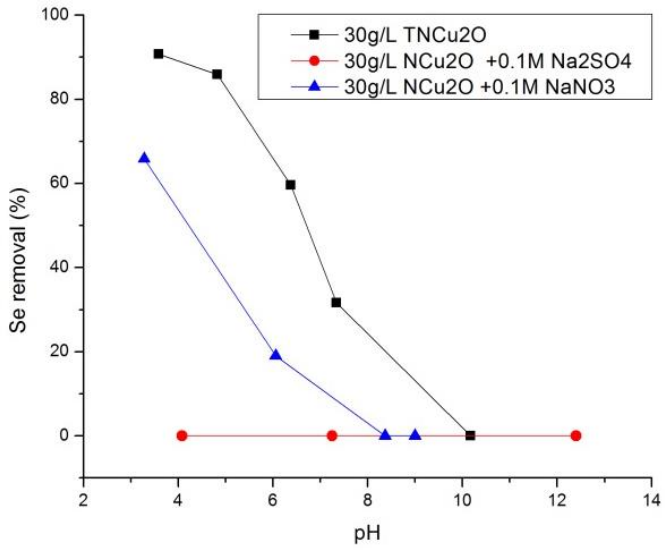

Figure 30. Removal of selenate using 30 g/L Cu_2O from DI water spiked with 1 ppm selenate alone compared with the presence of competing anions. (NCu_2O is the newly obtained Cu_2O)

5.3. Conclusions

Different metal oxides with relative high point-of-zero charge (PZC) were investigated in simulated DI water with sodium selenate spiking. Among them, two sorbent materials showed promising performance in the spiked DI water: Titania (TiO_2) shows 100% selenate removal in spiked DI water when pH < 6; Cuprous oxide (Cu_2O), which is effective at higher pH, requires long contact times (22 h) to achieve close to 90% of the selenate removal in laboratory jar tests using a dosage of 1.1 g/L. Although Cu_2O can demonstrate 100% selenate removal at a use of 30 g/L even when the pH increased up to 8, the high dosage of Cu_2O used is not economic and may cause Cu leaching problem in the water for practical application.

6. CCT Sorbents (offered by Crystal Clear Technologies)

Crystal Clear Technologies, Inc. (CCT) is a R&D company based in Portland, OR, that has $1.5M worth of past funding for R&D and testing of adsorptive media for water treatment applications. CCT has developed solid phase extraction materials with high binding constants to metals in complex wastewater streams such as flue gas desulfurization (FGD) wastewater from coal fired power plants. Furthermore, CCT has a patented nano-layering solid phase extraction technology that can be used to recharge exhausted media in-situ, allowing for multiple exposures of the sorbent to the metals. Figure 31 depicts a functionalized substrate with 2 layers. The first layer of metals is bonded to the metal grabbing group of the ligand; then to recharge the bed, a solution of bi-functional ligand is run through the bed and a second ligand layer is formed. This can be repeated multiple times.

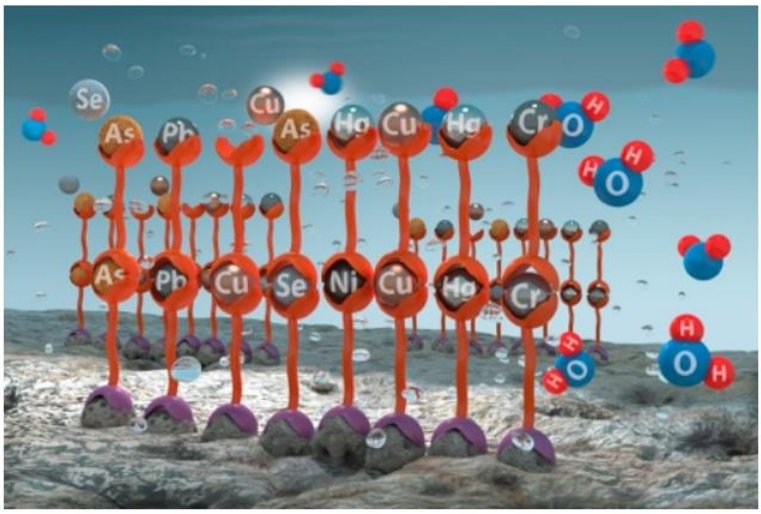

Figure 31. Illustration of CCT layering technology.

In this work, three classes of sorbents prepared by CCT were investigated based on titania, alumina, and zeolite materials to compare with the fourth class that based on biopolymer. Both the native substrates (unfunctionalized) and the corresponding functionalized sorbents were evaluated for a preliminary screening of selenium and arsenic removal in spiked de-ionized water, and afterwards the promising biopolymer-based sorbents for selenate removal in spiked SRP power plant waters in jar tests as well as in small scale column test.

6.1. Overview of Bio-sorption

Bio-sorption, a naturally occurred physiochemical process that is used to bind contaminants onto the cellular structure, can be an alternative way for conventional wastewater-treatment facilities to remove toxic heavy metals for environmental control and remediation. In recent years, bio-sorption has been found as an effective method for reducing metal contamination from surface water and industrial effluents.[138-139] Natural biopolymers are industrially attractive due to their capability of lowering transition metal ion concentrations to ppb levels.[140] Biomaterials that are certain waste from agricultural operations are available in large quantities that may have huge potential to be used at low cost as adsorbents.[141]

6.2. Overview of Functionalized Sorbents

Functionalized biopolymer sorbents are materials functionalized on naturally occurring materials offered by Crystal Clear Technologies, Inc. (CCT) using a nano-layered solid phase extraction (SPE) technology. CCT uses multi-functional organic ligands to 1) bind multiple types of metals, 2) improve sorbent specificity to metals in the

presence of competing ions, and 3) increase the loading of bound metals. In this work, we tested some biopolymer sorbents and functionalized biopolymer sorbents offered by Crystal Clear Technologies, Inc. (CCT) for the selenium and arsenic removal efficacy from simulated DI water and spiked SRP well water. Small scale column tests were also investigated (discussed in chapter 8).

6.3. Jar Test Results

The preliminary screening for CCT sorbents was performed using a dosage of 1 g/L (or otherwise noted) of the native sorbents in DI water containing 1 ppm of metals respectively: arsenite, As(III); arsenate, As(V); selenite, Se(IV); selenate, Se(VI). Sorbents dosage were increased to 5 g/L in spiked SRP waters considering the high concentration of potential competing ions and high total dissolve solids (TDS). The results show all the native sorbents can remove 100 % of the arsenate, and it is easier to be removed than arsenite. This was also reported by Bissen et al. that As(III) is more difficult to be removed than As(V) so that pretreatments of oxidizing As(III) to As(V) is always applied.[142] Selenate is the most difficult one to be removed among the four species.

6.3.1. Titania-based Sorbents Jar Test Results

The native substrate CCT-M1 is the Metsorb® material used to remove arsenic from drinking water. In DI water solutions, 1 g/L M1 could remove 100% of arsenite and arsenate, 76% of selenite, but only 12% of selenate from a 1 ppm starting concentration of each metal (Table 10). In blowdown water (Site C) spiked with 1 ppm Se(VI) and As(V), there was negligible selenate removal (Table 11) even at loadings of 5 g/L, while

the arsenate removal efficacy was not affected and could still can be removed up to 100%. These results show that the interference of competing ions makes native titania sorbents ineffective for selenate removal.

Table 10. Percentage of metals removal in spiked DI water solutions using 1 g/L titania sorbent in 1 ppm starting solution

Sorbent	**Material**	**Se^{+4}**	**Se^{+6}**	**As^{+3}**	**As^{+5}**
CCT-M1	TiO_2	76	12	100	100

The effect of CCT functionalization technology on the Se removal efficacy on the titania sorbent was explored. Three different ligands were tethered onto the surface of the native M1, resulting in the samples CCT-215, -216, and -217. When using the functionalized substrates at 5 g/L in blowdown water (Site C) spiked with 1 ppm selenate, the removal efficiencies increased for CCT-215 and -217 as shown in Table 11. These results show that functionalization can be used to improve the efficacy of selenate removal in real water samples, and that the L6 ligand used on CCT-217 may be the best at binding selenate.

Table 11. Selenate removed from spiked (0.2 ppm) SRP blowdown water (CT5-6, site C) using native titania (M1) and functionalized titania-based sorbents at 5 g/L.

Sorbent	**Functionalized Ligand**	**% Selenate removed**
CCT-M1	none	0
CCT-215	L5	5.6
CCT-216	L8	0
CCT-217	L6	17

6.3.2. Alumina-based Sorbents Jar Test Results

Native alumina-based sorbents were found to display better binding to both selenate and selenite in spiked DI water samples (Table 12) compared to the native titania (Table 10). The boehmite (AlOOH) sorbent (S1) displayed maximum selenate and selenite removal at 30 minutes of exposure time, but showed selenium desorption after longer times (Figure 32). In contrast, for the Al_2O_3 sorbents (S5), the maximum selenite and arsenite removal was observed at 22 hours of exposure time, while the selenate and arsenate removal occurred by 2 hours. Similar to the titania sorbent (M1), selenite removal was higher than selenate for the native alumina sorbents. The ability for the Al_2O_3 sorbent CCT-S5 to remove selenate improved upon functionalization with the ligand L7, as shown in Table 12. However, the arsenite removal ability decreased with functionalization, which will require more study. From these results, we can conclude that native AlOOH (S1) and functionalized Al_2O_3 (S5-L7) are both suitable sorbents for removal of selenate and selenite from DI water solutions.

The efficacy of the alumina based sorbents in SRP water samples was also investigated (Table 13). Although arsenate removal from the well (Site E) and canal water (Site G) was similar to that observed in the DI water, the selenate removal rates dropped significantly. This shows that competing ions in the real water matrices play a large role in selenate adsorption on native alumina substrates. Even after functionalization with ligand L7, no more improvement on selenate removal in both well water (Site E) and raw canal water (Site G) was observed. This suggests that ligand L7 is

not selective on selenate from water contain high total dissolved solids and other competing ions.

Table 12. Percentage of metals removal in spiked DI water solutions using 1 g/L alumina-based sorbents in 1 ppm starting solution

Sorbent	**Material**	**Se^{+4}**	**Se^{+6}**	**As^{+3}**	**As^{+5}**
CCT-S1	AlOOH	95	73	79	100
CCT-S7	Al_2O_3	90	47	59	100
CCT-S5	Al_2O_3	92	51	63	100
CCT-S5-L7	Al_2O_3 functionalized with L7	96	97	48	100

Table 13. Percent removal of selenate and arsenate removal from spiked (1 ppm) solutions of A well discharge (Site E) and raw canal water (Site G) using 5 g/L alumina-based sorbent.

Sorbent	**Material**	**Site E**		**Site G**	
		Se^{+6}	**As^{+5}**	**Se^{+6}**	**As^{+5}**
CCT-S1	AlOOH	17	100	16	100
CCT-S7	Al_2O_3	0	100	10	96
CCT-S5	Al_2O_3	13	96	18	99
CCT-S5-L7	Al_2O_3 functionalized with L7	10	100	11	100

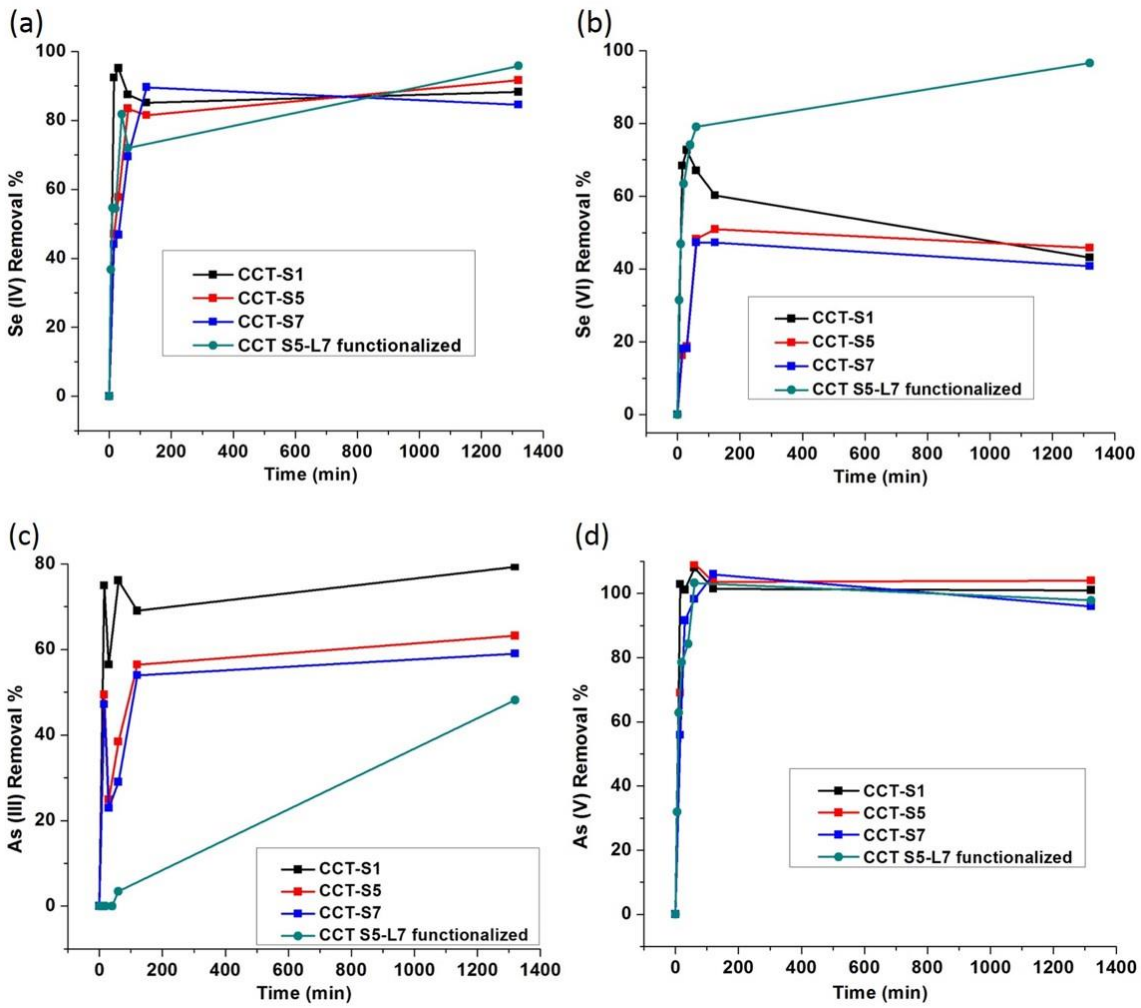

Figure 32. Percent removal of 1 ppm a) selenite, b) selenate, c) arsenite, and d) arsenate on different alumina-based sorbents at a concentration of 1 g/L in spiked DI water.

6.3.3. Zeolite-based Sorbents Jar Test Results

Natural zeolite from St. Cloud mine, New Mexico (CCT-Z) and a surface modified zeolite with functionalization (CCT-SMZ) were also investigated for selenate and selenite removal in spiked DI water. As shown in Table 14, the efficacy of natural zeolite for selenium removal was low, with more selenate removed than selenite. The

functionalized zeolite also displayed low efficacy, with more selenite removed than selenate. Due to the low removal rates in DI water, no further tests on the zeolite based sorbents were performed.

Table 14. Percentage of selenium removal in spiked DI water solutions using 0.5 g/L sorbent in 0.2 ppm starting solution.

Sorbent	Component	Type	Se^{+4}	Se^{+6}
CCT-Z	Zeolite	Native	0	8
CCT-SMZ	Surface modified zeolite	Functionalized	10	0

6.3.4. Biopolymer-based Sorbents Jar Test Results

Native biopolymer substrates are naturally occurring materials (NOM). Similar to the alumina sorbents, functionalization was found to improve the efficacy of biopolymer substrates for selenium removal. Table 15 shows the maximum percentage of selenium and arsenic removed from spiked DI water samples using native biopolymer substrate (NOM) and two forms of functionalized biopolymer sorbents (FNOM). Figure 33 shows the removal at different exposure times for the three samples. These results show that the native biopolymer sorbent (NOM) have high efficacy for selenite and have fair efficacy for selenate removal in spiked DI water, and that selenate removal is greatly improved with functionalization.

Table 15. Percentage of metals removal in spiked DI water solutions using 1 g/L biopolymer-based sorbent in 1 ppm starting solution.

Sorbent	Material	Se^{+4}	Se^{+6}	As^{+3}	As^{+5}
CCT-CN	Naturally Occurring Materials (NOM)	76	34	44	100
CCT-AB7	Functionalized NOM	98	100	33	100
CCT-149	Functionalized NOM	84	100	19	100

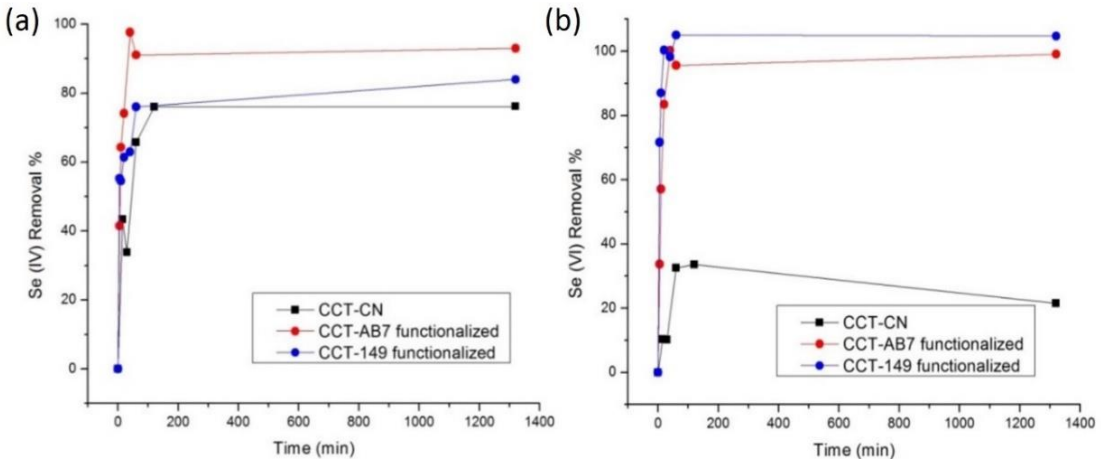

Figure 33. Percent removal of 1 ppm selenite (a) and selenate (b) on different CCT substrates at a concentration of 1 g/L in spiked DI water.

To further study the maximum capacity of loading selenium onto the functionalized biopolymer sorbents (FNOM), the isotherms of CCT-149 was investigated. By using 1 g/L CCT-149 in selenate spiked DI water, the Se loading in mg Se/g CCT-149 increased dramatically as the equilibrium Se concentration (Se(VI) Eq Conc.) increases, and then reach to a saturate platform of a very high Se loading, which is about 90 mg Se/g CCT-149 (Figure 34). As shown in Figure 35, the Langmuir model was applied to describe the adsorption behavior at equilibrium. The experiment data can be plotted and fitted well in the Langmuir equation shown in Figure 35.

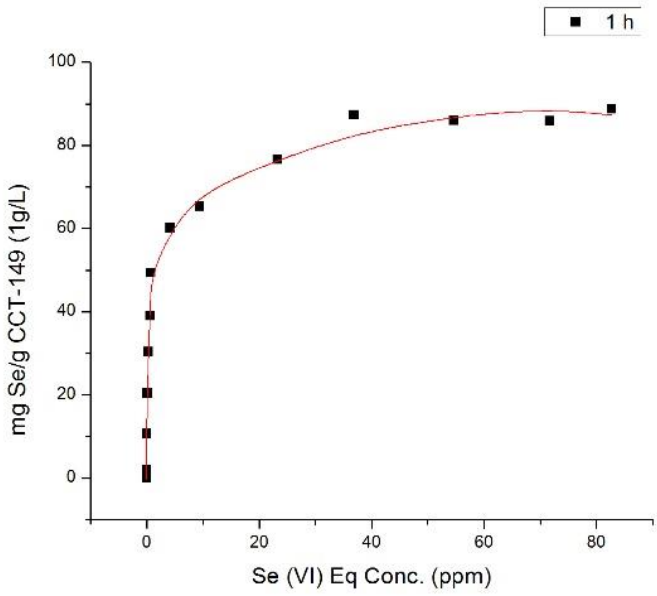

Figure 34. Se(VI) sorption isotherms on 1 g/L CCT-149 for 1 h.

The fitted linear equation is $y = 0.016 + 0.011x$, in which $y = \frac{C_e}{Q_e}$ and $x = C_e$. The correlation coefficient value R^2 obtained from the fitted model is 0.998, which shows that our experimental data fits the Langmuir model very good. This indicates that selenate is adsorbed on definite sites on the surface of CCT-149 and it is a monolayer sorption.[117,121] The maximum capacity Q_0 calculated by the Langmuir isotherm model is 90.9 mg/g, and is close to that obtained at equilibrium (Figure 34). This demonstrates the large adsorption ability of CCT-149 in removing Se(VI).

The functionalized sorbent CCT-149 was tested for selenate removal in spiked water samples from SRP's Santan facility. With a 1 g/L sorbent concentration, CCT-149 was able to remove up to 43% of selenate in the upstream water sources - sites A, B, E, and G, with a loading rate as high as ~0.1 mg Se/g sorbent, but displayed lower removal

efficiencies at both cooling tower locations (Site C and F). These results are shown in Figure 36. Although this loading rate was obtained from the jar test instead of a flowing water test (column test), the result still demonstrates the good selenate adsorption ability of CCT-149 in a high concentration of competing ions like sulfate.

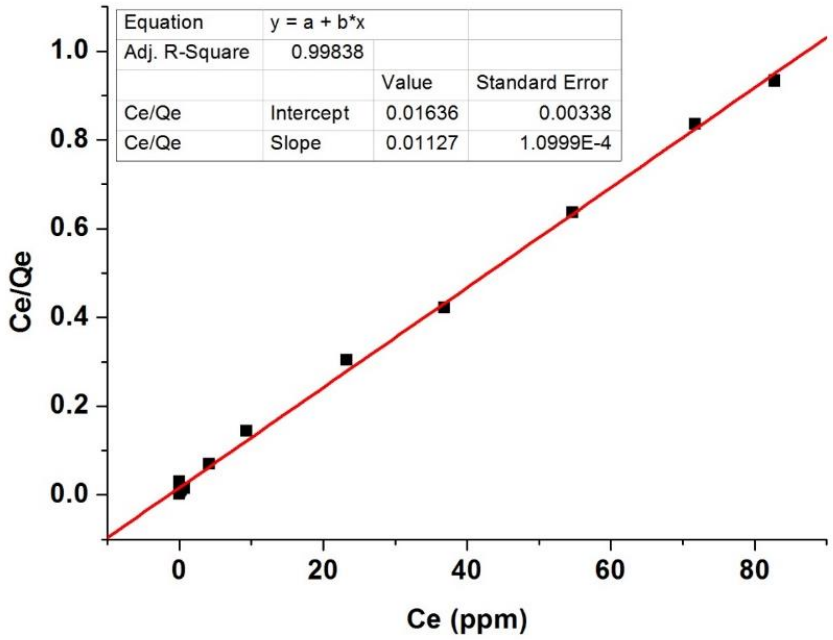

Figure 35. Langmuir plots for the sorption of Se(VI) by CCT-149.

Increasing the sorbent dosage to 5 g/L was found to increase the removal rate (Figure 37). 100% of the selenate was removed in 30 minutes, with over 90% removed in 5 minutes in the well discharge (Site E). The selenate removal in cooling tower 5 and 6 blowdown (Site C) was also increased from 9% to 46% with the higher sorbent concentration. These results show that CCT-149 can be effective for removing selenate in the SRP water matrices if the appropriate sorbent concentration is determined. The maximum selenate removed with CCT-149 in the conditions tested are shown in Table 16.

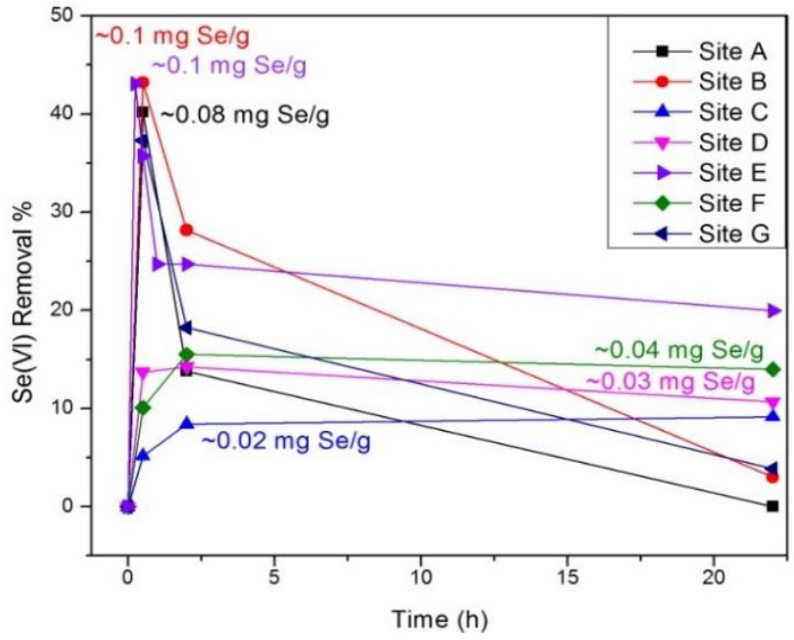

Figure 36. Percent removal of 0.2 ppm selenate on CCT-149 at a concentration of 1 g/L in spiked SRP water sites.

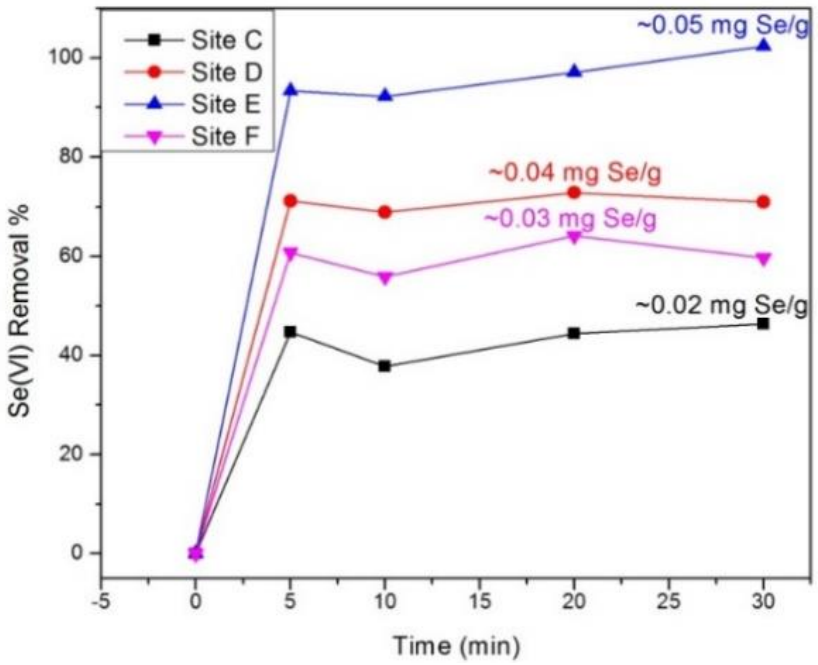

Figure 37. Percent removal of 0.2 ppm selenate on CCT-149 at a concentration of 5 g/L in spiked SRP water.

Table 16. Selenate removed using functionalized chitosan sorbent CCT-149 in spiked SRP water samples with a starting concentration of 0.2 ppm.

Sorbent conc.	**% Selenate removed**						
	Site A	**Site B**	**Site C**	**Site D**	**Site E**	**Site F**	**Site G**
1 g/L	40	43	9	14	43	15	37
5 g/L			46	73	100	64	

6.3.5. Modified Biopolymer-based Sorbents

As the functionalized biopolymer-based sorbents CCT-149 showed good results in removing selenate from spiked DI water, and even in some sites of the SRP power plant waters, modification of the synthesis procedure of CCT-149 was applied to try to improve the performance of biopolymer based sorbents in SRP waters containing high concentrations of competing ions and high total dissolved solids (TDS). Different functionalized biopolymer-based sorbents were synthesized based on modifications to the original preparation of CCT-149 and provided by CCT. For a preliminary screening, 1 g/L of each sorbent was used in selenate spiked DI water with a very high initial concentration ranging 160 – 180 ppm (Table 17). Figure 38 compares the adsorption ability of selenium onto each biopolymer-based sorbent. Among all the biopolymer-based sorbents, OCI-A, -B, -h, -I, K, -L, -N, -O, and -P exhibit higher capacities in loading selenium in mg Se/g than CCT-149. Based on the availability of sufficient amounts of material, OCI-A, -B, -h, and -L were chosen for further study in SRP well water (Site E) and cooling tower 1 water (Site F).

Table 17. Different modified functionalized biopolymer-based sorbents tested in spiked DI water with high initial Se(VI) concentration using a dosage of 1 g/L.

	Initial Se concentration (ppm)	Se Removal %	Loading (mg Se/g)
CCT-149	171.5	53.0	90.9
OCI-A	179.6	55.7	100.0
OCI-B	175.8	64.5	113.3
OCI-Bw	177.0	39.6	70.1
OCI-B2	163.7	51.2	83.6
OCI-C small	182.4	39.9	72.8
OCI-D	180.3	2.3	4.2
OCI-E	169.3	23.8	40.3
OCI-F	177.6	30.2	53.7
OCI-G small	158.9	77.5	123.2
OCI-h small	173.5	76.3	132.4
OCI-Hw	160.2	66.9	107.2
OCI-I	182.5	65.4	119.4
OCI-J small	165.6	51.8	85.8
OCI-K small	175.9	64.9	114.2
OCI-L	166.2	62.8	104.5
OCI-Md	166.6	36.8	61.4
OCI-N	186.8	66.9	125.0
OCI-Nw	190.0	50.7	96.4
OCI-O	183.7	66.9	123.0
OCI-P	186.8	75.6	141.3
OCI-Q	184.5	51.4	94.9
OCI-R	184.9	55.0	101.8

Figure 39a shows the Se(VI) percentage removed using the different biopolymer-based sorbents using a dosage of 1 g/L as a function of exposure time in 0.2 ppm selenate spiked SRP well water (site E). Similar to CCT-149, about half (50%) of the spiked selenate can be removed by OCI-A, -B, and –h in SRP well water, which indicates the ability of these biopolymer-based sorbents to remove selenate from a high concentration of sulfate. However, in SRP cooling tower 1 water, which contained even higher sulfate levels (Figure 39b), the selenate removal percentages were decreased. However, OCI-B

still demonstrated good selenate adsorption ability from water with even higher concentrations of sulfate and TDS.

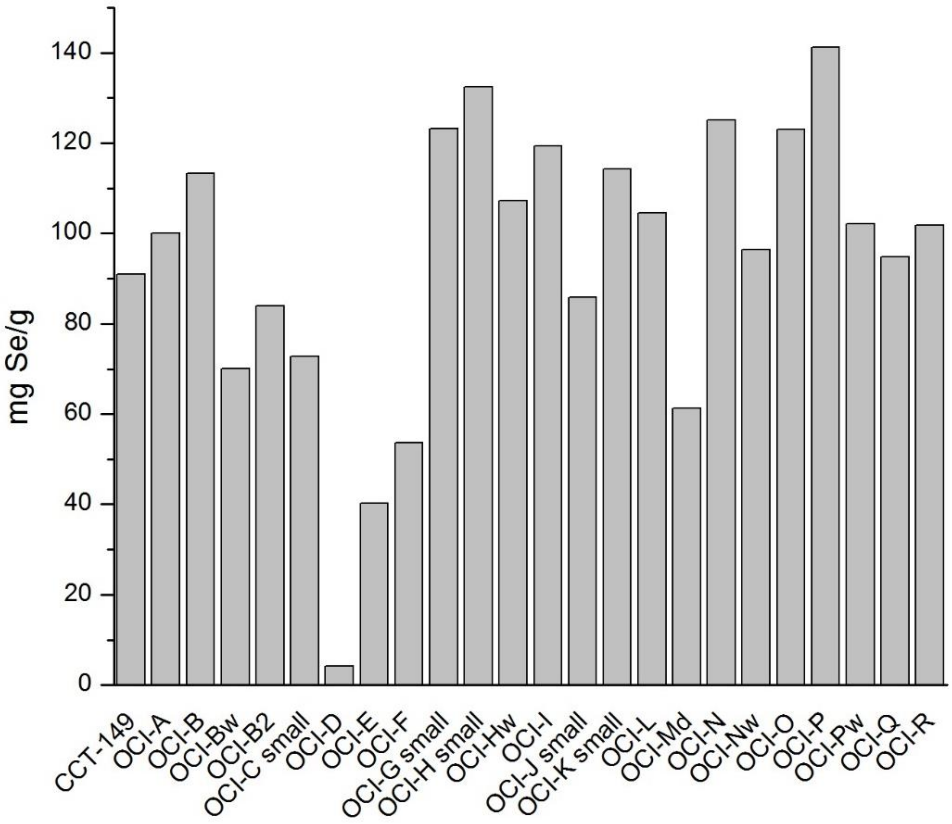

Figure 38. Se(VI) sorption comparison on 1g/L different functionalized biopolymer-based sorbents (FNOM) in spiked DI water. (Initial Se(VI) concentration: 160-180 ppm).

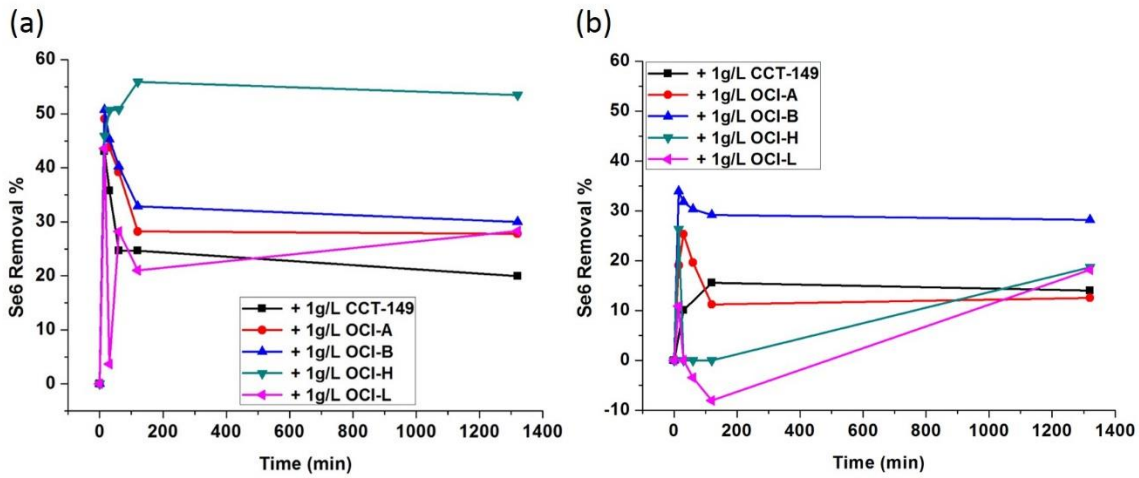

Figure 39. Percent removal of 0.2 ppm selenate on different FNOM sorbents at a concentration of 1 g/L in spiked (a) A well water (Site E) and (b) CT-1 water (Site F).

6.4. Conclusions

In summary, the functionalized biopolymer-based sorbent made by Crystal Clear Technologies is the second promising material for removing selenate in SRP water among the other inorganic-based sorbents screened. CCT-149 was able to adsorb ~0.1 mg Se/g in a 30 min jar test from SRP waters. CCT-149 could remove 100% selenate in A well discharge waters (site E) spiked with selenate.

7. Pretreatment for Removal of Competing Ions

7.1. Competing Ions

To study what ions competed with selenate removal in SRP waters, some of the ions that are present in SRP waters were chosen to spike together with selenate in DI

water. Figure 40 shows the selenate removal percentage at different time exposures with and without other ions present in water. The results show that Fe, Al, and Cr did not compete with selenate, with only sulfate is the biggest challenge for selenate removal.

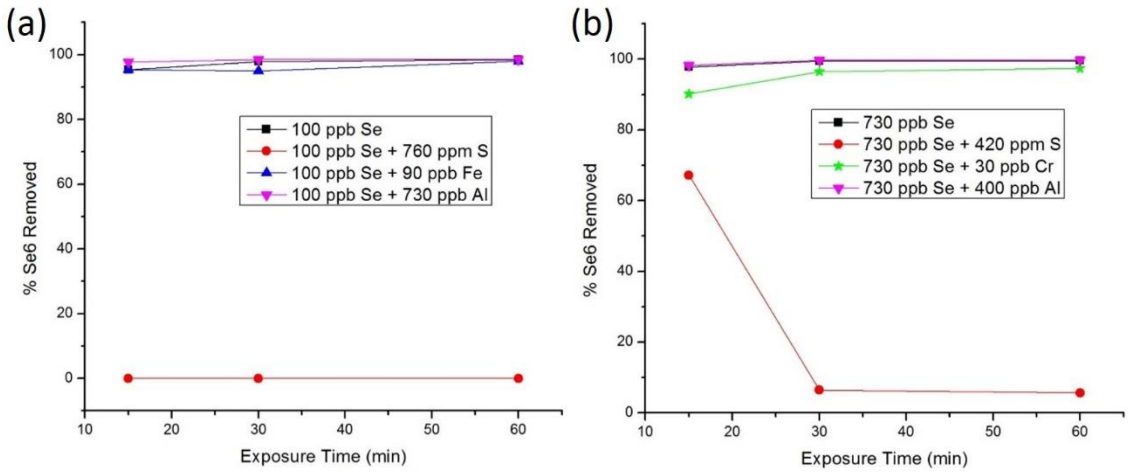

Figure 40. Percent removal of (a) 100 ppb selenate and (b) 730 ppb selenate of OCI-B at a dosage of 1 g/L in spiked DI water with Na_2SO_4, $K_2Cr_2O_7$, $FeCl_3$ or $AlCl_3$.

7.2. Efficacy of Barium Salts for Sulfate Removal

From the results above obtained from spiked SRP water, the most important issue that affects the selenate removal on sorbents is the existence of competing ions. According to the results on the simulated waters to try to figure out the biggest competing ions, sulfate stands out as the biggest problem that prevents selenate removal, probably due to the similar size and properties of sulfate and selenate. It is reported that selenate adsorption can be strongly affected by the presence of sulfate, bicarbonate, and aqueous silica species.[143] Sorbent materials were less successful at removing selenate from water samples that contained high sulfate concentrations (such as the cooling tower blowdown)

unless used at very high dosages (e.g. 5 g/L). Therefore, removing sulfate from the water using a pre-treatment step is one way to improve selenate removal.

Soluble barium salts are usually considered for sulfate treatment by chemical precipitation as $BaSO_4$. Barium carbonate, $BaCO_3$, is one of the frequently-used barium salts for treating sulfate-rich waters. However, it can only be used for removing sulfate when calcium is present so that $CaCO_3$ can precipitate out in the meanwhile to facilitate $BaSO_4$ precipitation. The $BaSO_4/CaCO_3$ precipitate can be thermally treated to reduce it to BaS/CaO, and BaS can be converted back to $BaCO_3$ for re-using by passing CO_2.[86] A $Ba(OH)_2$ process was reported to be technically and economically feasible for the treatment of sulfate-rich industrial effluents.[144] Barium chloride, $BaCl_2$, can precipitate out sulfate as $BaSO_4$. It has also been found to be able to co-precipitate selenate at the same time.[29] Unlike sulfate removal via lime precipitation, which can only reduce sulfate concentrations to 1,500 – 2,000 mg/L, the barium treatment is only limited by the amount of barium available and its relatively high chemical cost of about $2/lb.[145]

In this study, $BaCO_3$, $BaCl_2$, and $Ba(OH)_2$ were investigated for sulfate removal efficacy in SRP CT-1water. For $BaCl_2$ and $Ba(OH)_2$, the mole ratio of Ba/S was calculated to be 3.6. For $BaCO_3$, the mole ratio of Ba/S was calculated to be 8. Additionally, $Ca(OH)_2$ was added prior to $BaCO_3$ treatment for 2 hours of retention time to offer the calcium ions. The results showing the amount of S remaining over time in the CT-1 water after different barium treatments are compared in Figure 41.

Even though giving a high mole ratio of Ba/S = 8, $BaCO_3$ treatment with $Ca(OH)_2$ could only remove 97 % of the sulfate after 3 h. Both $BaCl_2$ and $Ba(OH)_2$ treatment could

remove more than 98% sulfate in 1 h with a relatively lower mole ratio of Ba/S = 3.6. However, after adding $Ba(OH)_2$, the pH of the CT-1 water was dramatically increased to higher than 12, which is probably not a suitable treatment for SRP power plant as it will require pH adjustment afterwards. Therefore, $BaCl_2$ would be a proper pre-treatment for removing sulfate in our case.

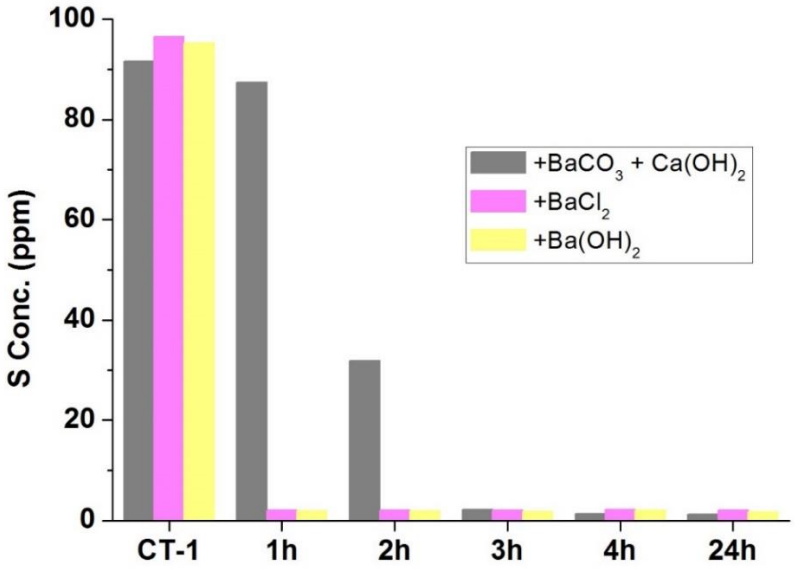

Figure 41. S remaining over time in SRP CT-1 water with different barium treatments.

7.3. Efficacy of $BaCl_2$ for Selenate Removal

To test the ability of $BaCl_2$ to co-precipitate selenate, 4000 ppm sodium sulfate and 1 ppm sodium selenate were added to DI water. A white precipitate formed immediately once 4000 ppm $BaCl_2$ was added. The amount of selenate remaining in the

solution after the precipitate was filtered out was tested. Figure 42 shows the % selenate removed over time after addition of $BaCl_2$. There was 77% removal of the selenate after 15 min, but desorption or re-dissolution of Ba-Se species appeared evident. This result confirms that $BaCl_2$ can co-precipitate selenate while precipitating sulfate out. On the other hand, use of $BaCl_2$ in conjunction with an adsorbent may be needed to avoid re-dissolution of the selenium.

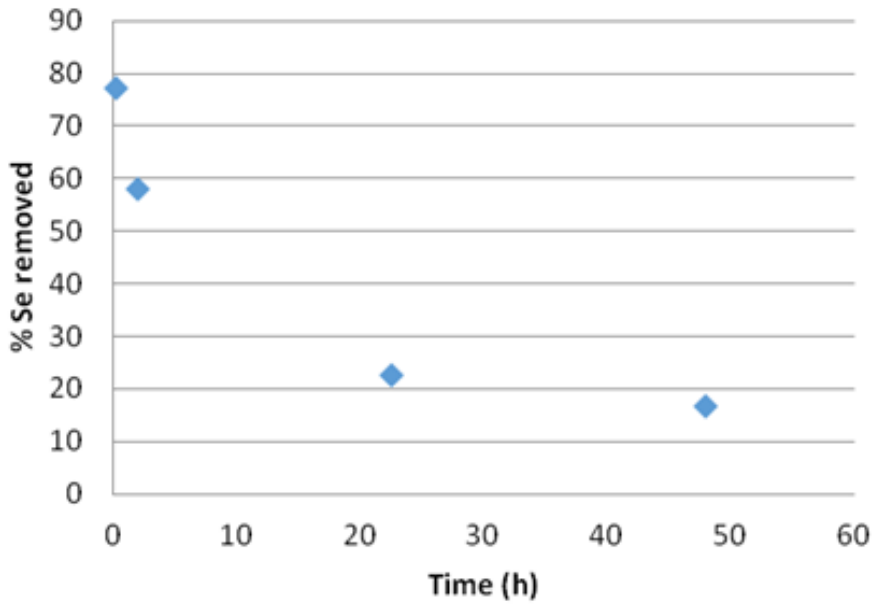

Figure 42. Percent removal of 1 ppm selenate by $BaCl_2$ treatment at a concentration of 4000 ppm in spiked DI water with 4000 ppm Na_2SO_4.

7.4. Efficacy of $BaCl_2$ Pretreatment with Sorbent in Unspiked SRP Waters

The efficacy of the most promising materials, CCT-149 and LDH-500C, for removing the actual selenium species found in SRP waters (i.e. without spiking) were investigated using Sites D (waste effluent), E (well discharge), F (cooling tower

discharge) and G (raw canal water) as the water matrices. For each water matrix, the preserved water was analyzed to determine the baseline selenium concentration. Then, 0.5 g/L $BaCl_2$ was added to determine the efficacy for selenate removal via co-precipitation with $BaSO_4$ and in conjunction with CCT-149, LDH-500C and LDH-granular. Due to the low selenium levels in these waters, ICP-MS was used for analysis. Table 18 summarizes the details of the samples.

The samples tested in SRP waters site D, site E and site G were sent to SRP's analysis lab for ICP-MS results. The detection limit (LOD) of ICP-MS from SRP lab was 1 ppb, so we also performed some of samples tested in water site E and site F in the ICP-MS at ASU's W. M. Keck Foundation lab, which has a lower LOD for more accurate results (details shown in Table 18). The ICP-MS results obtained from the SRP lab are shown in Figure 43 with the left axis referring to selenium concentration (ppb) in the water matrices and the waters after treatment. Although the selenium concentration in SRP water Sites D and E is very low, only around 3 ppb, LDH-500C and the combination of LDH-500C with $BaCl_2$ could still lower it further to around 2.5 ppb in site D. In Site E, using $BaCl_2$ and CCT-149 can reduce selenium levels to below 2 ppb, which already achieves SRP's goal. Furthermore, by using $BaCl_2$ in conjunction with LDH-500C in Site E, the resulting selenium level was below the reporting limit (BRL = 1 ppb). For Site G, the selenium concentration in the water was already below the reporting limit, so it will not be the focus of our further treatment studies.

Table 18. Sample description for selenate removal tests in unspiked SRP water.

Water Matrix	Sample Name	Treatment	Exposure Time (h)
Site D (Waste effluent, Oct. 2014) SRP lab (LOD = 1 ppb)	D	None	n/a
	D-Ba	0.5 g/L $BaCl_2$	0.5
	D-Ba-LDH	0.5 g/L $BaCl_2$ + 5 g/L LDH-500C	1
Site E (Well discharge); SRP lab (LOD = 1 ppb)	E	None	n/a
	E-Ba	0.5 g/L $BaCl_2$	0.5
	E-Ba-LDH	0.5 g/L $BaCl_2$ + 5 g/L LDH-500C	1
	E-149	1 g/L CCT-149	0.5
Site E (Well discharge, Apr. 2015); ASU lab (LOD = 0.07 ppb)	E	None	n/a
	E-LDH	1 g/L LDH-500C	1
	E-L-149	1 g/L LDH-500C + 1 g/L CCT-149	0.5
ASU lab (LOD = 0.1 ppb)	E-Sa	1 g/L LDH-granular	1
	E-Sa-149	1 g/L LDH-granular + 1 g/L CCT-149	0.5
	E-Ba	0.5 g/L $BaCl_2$	0.5
	E-Ba-149	0.5 g/L $BaCl_2$ + 1 g/L CCT-149	0.5
Site F (Cooling tower 1-4); ASU lab (LOD = 0.07 ppb)	F	None	n/a
	F-Ba	0.5 g/L $BaCl_2$	0.5
	F-Ba-149	0.5 g/L $BaCl_2$ + 1 g/L CCT-149	0.5
ASU lab (LOD = 0.1 ppb)	F-LDH	1 g/L LDH-500C	1
	F-L-149	1 g/L LDH-500C + 1 g/L CCT-149	0.5
	F-Sa	1 g/L LDH-granular	1
	F-Sa-149	1 g/L LDH-granular + 1 g/L CCT-149	0.5
	F-149	1 g/L CCT-149	0.5
Site G (Raw canal) Oct. 2014; SRP lab (LOD = 1 ppb)	G	None	n/a
	G-Ba	0.5 g/L $BaCl_2$	0.5
	G-Ba-LDH	0.5 g/L $BaCl_2$ + 5 g/L LDH-500C	1
LOD: Limit of detection			

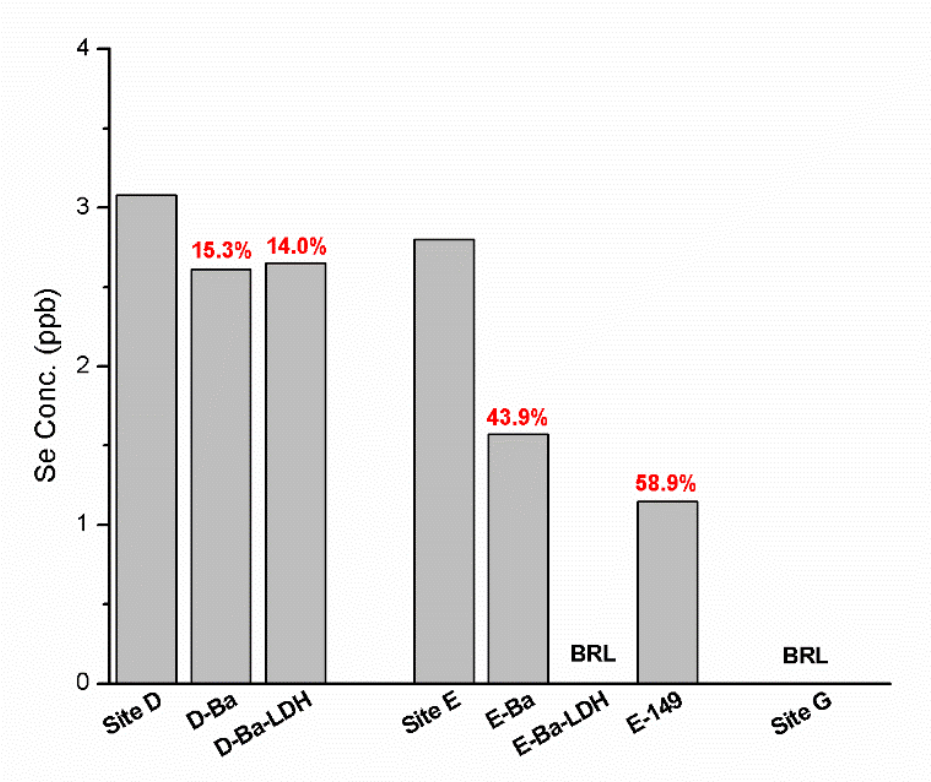

Figure 43. Selenium concentration detected in different SRP water sites and waters after treatment.

These results show that CCT-149 is effective for removing selenium to the desired levels in the well water (E site). The LDH-500C is also effective when used in conjunction with the $BaCl_2$ pretreatment. Further tests were focused on SRP well water (E site) and cooling tower 1-4 water (F site) regarding the efficacy of CCT-149 and LDH-500C with and without $BaCl_2$ pretreatment in the unspiked water matrices. Figure 44 shows the ICP-MS results obtained from ASU lab with the left axis referring to selenium concentration (ppb) in the water matrices and the waters after treatment.

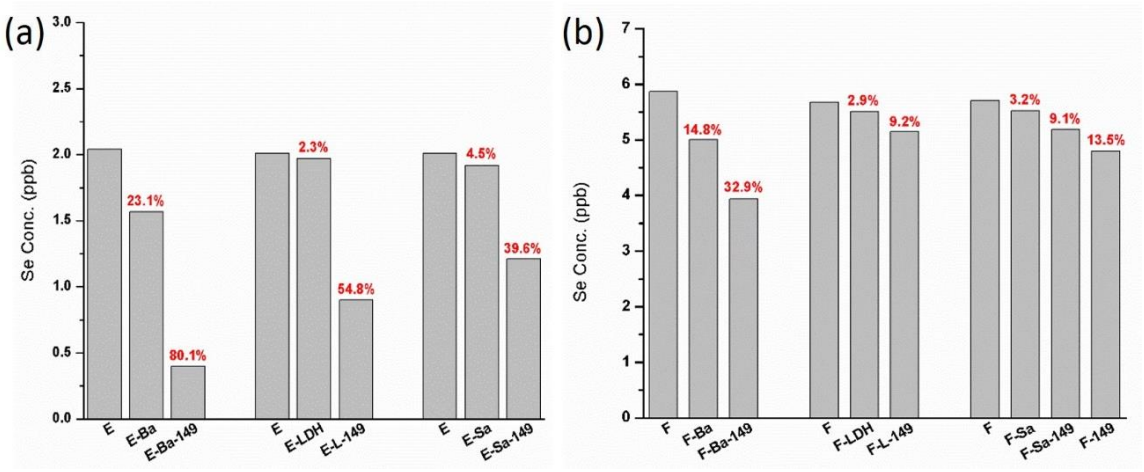

Figure 44. Selenium concentration detected before and after treatment in SRP water site E (a) and water site F (b).

In site E, the $BaCl_2$ itself could lower the selenium concentration further to around 1.5 ppb probably due to the co-precipitation of $BaSO_4$ with Ba-selenium species, and in conjunction with CCT-149, the resulting selenium level was even below 0.5 ppb (LOD = 0.07 ppb, ASU lab), with 80% of the selenium removed (Figure 44a). However, using LDH-500C or LDH-granular (E-L-149, E-Sa-149) in conjunction with CCT-149 did not improve the removal much, compared with only using CCT-149 in site E (Figure 43). In site F, using LDH-500C or LDH-granular combined with CCT-149 also did not make much difference, and not much Se was removed. Even with using $BaCl_2$ as pretreatment with CCT-149, though the % Se removal increased from 13.5 % (F-149) to 32.9 % (F-Ba-149), the result was still not as good as that in site E. This is likely because of the presence of high TDS and competing ions in site F. To confirm whether it was because of the high concentration of competing sulfate ions, the sulfur concentration was also tested by ICP-MS. These results are shown in Table 19.

Table 19. Sample results for S removal in unspiked SRP water.

Water Matrix	Sample Name	34S (ppm)	% S Removal
Site E (Well discharge)	E	47.6	
	E-Ba	0.3	99.3%
	E-Ba-149	4.0	90.1%
	E	52.0	
	E-LDH	50.7	2.4%
	E-L-149	37.3	28.2%
	E	50.7	
	E-Sa	47.1	7.1%
	E-Sa-149	38.9	23.2%
Site F (Cooling down)	F	268.9	
	F-Ba	142.4	47.0%
	F-Ba-149	117.7	56.2%
	F	213.0	
	F-LDH	211.7	0.6%
	F-LDH-149	204.1	4.2%
	F	258	
	F-Sa	259	0%
	F-Sa-149	247.9	3.9%

These results show that $BaCl_2$ can remove more sulfate than LDH-500C and LDH-granular. This explains why using CCT-149 with $BaCl_2$ was better than when using CCT-149 with LDH for removing Se. Also, the % S removal is about two times higher in site E than in site F. This is consistent with the results that Se in site E is easier to remove than in site F, and also confirms that the high TDS and competing ions in site F could decrease the efficiency of removing selenium on the sorbents.

7.5. Conclusions

In summary, sulfate is the most challenging competing species among ions investigated in SRP waters that decreases the selenate adsorption ability of sorbents. By using $BaCl_2$ pretreatment to remove sulfate, the selenate removal efficiency of both CCT-149 and LDH in well water (Site E) can be increased.

8. Small Scale Column Tests

Small scale column tests were performed using the two promising sorbent materials CCT-149/OCI-B and LDH-granular (commercially obtained from Sasol) to evaluate their Se removal ability in dynamic conditions and to obtain critical data for designing pilot tests. OCI-B is the functionalized biopolymer sorbent prepared using the same synthesis procedure as CCT-149, but with a large scale production. Hence, CCT-149 and OCI-B are supposed to have same properties, and it is the case according to the previous pre-screening results (Figure 38). For LDH-500C, the commercial powder obtained from Aldrich that was used in the jar tests was not suitable for column tests because of the small particle sizes that required high pressure for water to go through. To avoid channeling, the minimum column diameter should be at least 20 times the particle effective size; since the column diameter is fixed as 1.1 mm, LDH-granular was mechanically ground into small particles ranging 250 – 500 μm that we needed for the small scale column tests using sieve mesh No.35 and No.60.

8.1. Small Scale Column Procedures

Small scale column tests [146-147] were performed in a 1.1 cm diameter column 30 cm in height (Ace Glass) with Teflon end caps. Table S2 (appendix) shows a list of materials and equipment employed for the column tests. Figure 45 shows a photograph of the column setup. The sorbent media was immersed in DI water to remove any air before pack and allow for media expansion. The sorbent bed was packed in the middle part that occupied about one third of the column. Glass wools (Sigma-Aldrich) was placed above above and below the media bed as well as in both ends of column as a support and to retain all of the sorbent media inside the column. Glass beads (Ace Glass, 5 mm diameter) were placed on either side of the glass wools to disperse the influent flow.[146] Both of the glass wools and glass beads were pre-heated at 500 ^{o}C for 1 h to remove any contaminants and immersed in DI water before use. A peristaltic pump (NE-9000G, SyringePump) was used to set the flow rate according to the bed volume and desired empty bed contact time (EBCT) and food grade tubing was used. Test waters were pumped with upflow mode to avoid channeling. After packing the column, backwashing was performed using DI water to remove fine particles in countercurrent (upflow) mode until the effluent water ran clear.[147] The initial design of the empty bed contact time (EBCT) was obtained from the biopolymer-based sorbents CCT-149/OCI-B and LDHs jar test results. DI water and SRP A well water (site E) with or without 0.2 ppm selenate spiking were used as the water matrices. Barium chloride pretreatment was also being investigated by dropping 1 M $BaCl_2$ solution (Sigma-Aldrich, product no. 34252-1L-R) into the water matrix. $BaCl_2$ was used at a Ba : S mole ratio of 3 in order to fully remove all the sulfate from SRP waters. Samples were collected at regular intervals, once every

several bed volumes (BVs) (time period adjusted depending on the flow rate), and discarding the effluent in between the samplings. After the column test, the sorbent was removed and dried at 50 ^{o}C for one week and the mass measured for calculation of the selenate capacity.

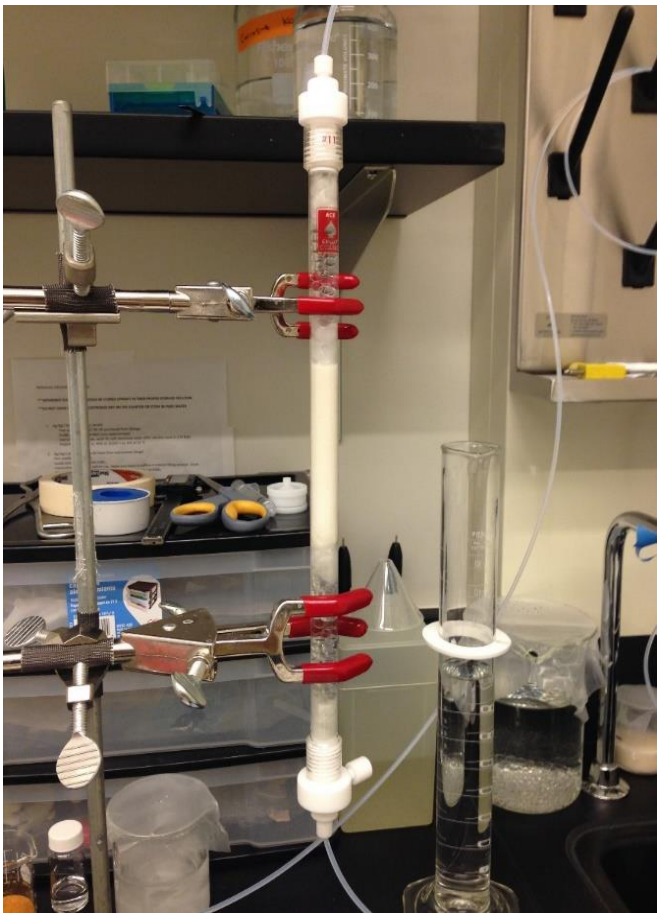

Figure 45. Photograph of the small scale column test setup at ASU.

The exhaustion capacity Q_e (µg/g) of the sorbent was calculated using Equation (6) where C_0 (ppm) is the initial Se(VI) concentration in the influent; C (ppm) is the Se(VI) concentration in the effluent after leaving the column; m (g) is the dried sorbent bed mass in the column; and V_e is the water volume (L) that was treated at exhaustion.[107]

$$Q_e = \frac{\int_{V=0}^{V=V_e}(C_0 - C)dV_e}{m} \quad (6)$$

In this work, Q_e was estimated from the breakthrough curve as illustrated in Figure 46. The adsorbent exhaustion rate (AER) can be estimated as shown in Equation (7).[107]

$$AER = \frac{m}{V_e} \quad (7)$$

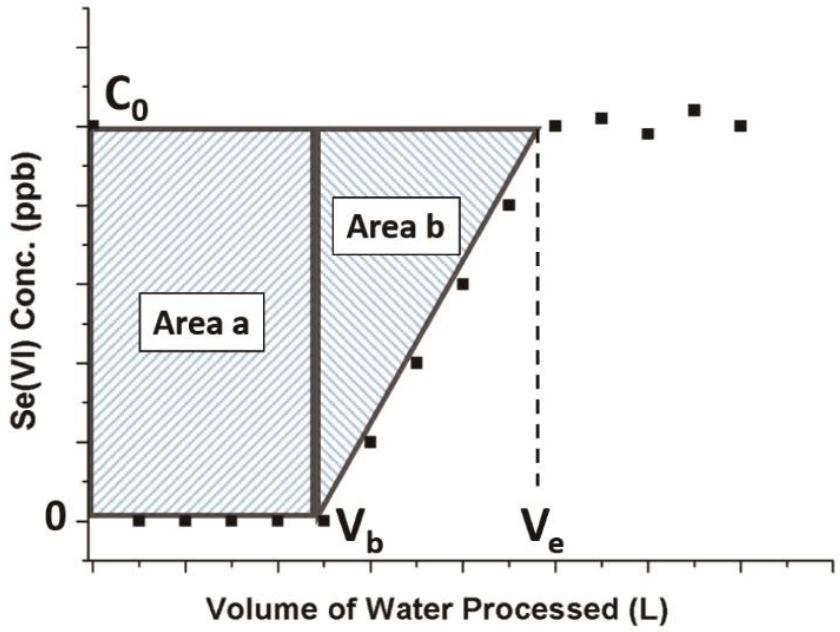

Figure 46. Method used to estimate exhaustion capacity (Q_e) from column test breakthrough curve using the area of the blue shaded region below C_0. The total area is equal to the area of the rectangle (Area a) + the area of the triangle (Area b), in which Area a = $C_0 \times V_b$; Area b = $\frac{1}{2} C_0 \times (V_e - V_b)$. V_b is the volume of water that passed through the column until breakthrough and V_e is the water volume that was treated at exhaustion. Q_b also can be estimated as Area a.

8.2. Biopolymer-based Sorbents CCT-149/OCI-B

After packing OCI-B in the column, back washing using about 7.5 L DI water from top to bottom in a downflow mode was performed to remove any unstable or loosely bound functional groups from OCI-B to avoid any further influence in the breakthrough results, so this sample was labelled as OCI-Bw. The small scale column tests were performed for OCI-Bw in simulated DI water spiked with sodium selenate to study the performance in removing Se in a dynamic mode. Small scale column tests for CCT-149 with different empty bed contact times (EBCT) were also performed in spiked SRP (starting concentration 0.2 ppm Se) well water (E site) to determine the optimum EBCT. Barium chloride was used as a chemical pretreatment to remove the high level of competing sulfate to further improve the capacity of removing Se in SRP well water.

8.2.1. Results in Simulated DI Water Spiked with 2 ppm Se

DI water was spiked with 2 ppm Se(VI) as the source water flow and fed into the column in an upflow mode to investigate the loading capacity of OCI-Bw in a dynamic mode. The EBCT was chosen as 5 min, since the jar test results in spiked DI water showed that CCT-149 is able to reach equilibrium in 5 min. The bed height shrunk after back washing and the bed volume was calculated to be 6.41 cm^3. Each sample was collected every 2.5 h for first 12.5 h (750 min) and then every 1.5 h thereafter. Figure 47 shows the breakthrough curve obtained. Breakthrough was observed to begin at the time point of 2210 minutes, corresponded to 2.83 L (441 Bed Volumes) of water that was treated. The last 7 points showed a shift to a lower Se concentration level than expected and did not continue along the slope of the previous points. This may be due to the

column test being stopped over two weeks at the point of 3830 min after 5 L of water treated. The exhaustion point was the estimated based on a linear fitting to the slope without those discord points. The exhaustion point relative to 4.92 L of water that was fully treated according to the calculation. This corresponded to a total amount of Se that was removed, which is 8.71446 g. After the column test, the sorbent was removed and dried under 50 ^{o}C for one week. The mass of the dried sorbent was determined to be 0.87 g. Based on the breakthrough data, the adsorption ability of the sorbent was calculated using the method shown in Figure 46, which is 10 mg Se/g OCI-Bw in spiked 2 ppm DI water. This is a relative high adsorption ability for removing selenium using the biopolymer-based sorbent.

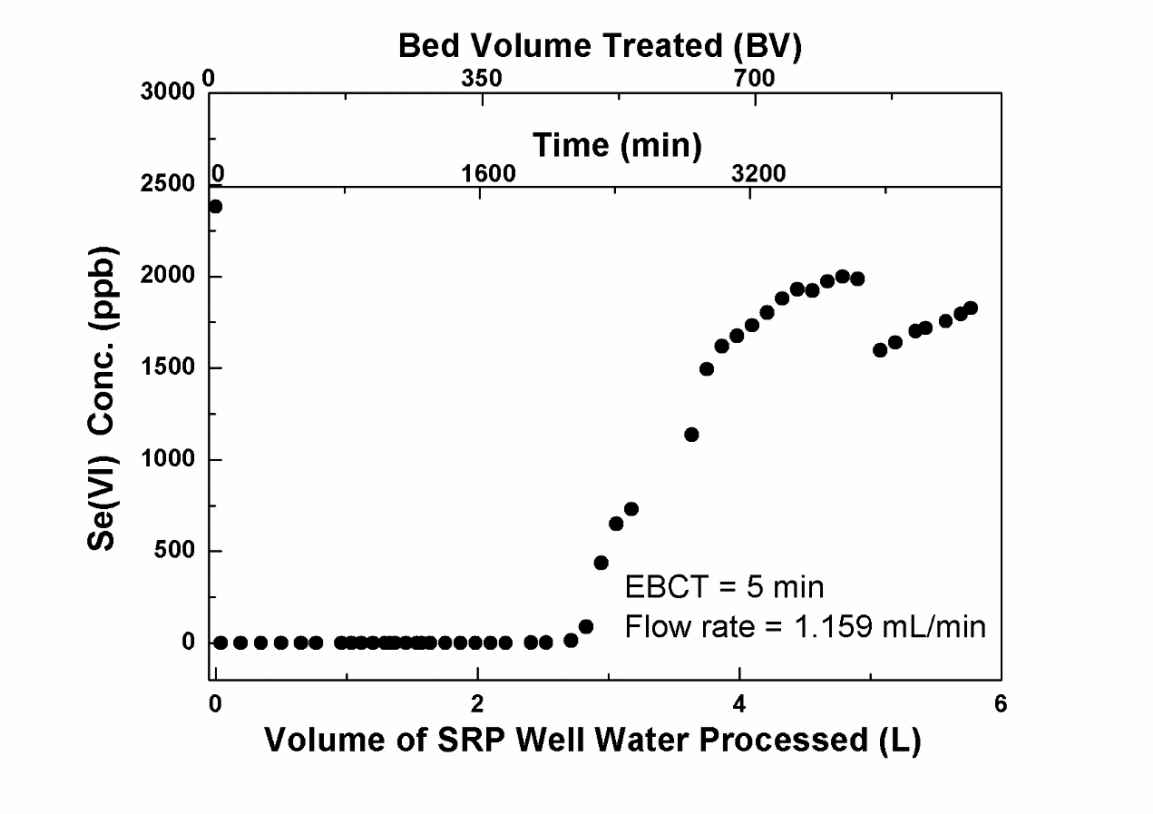

Figure 47. Breakthrough curve of OCI-Bw with 5 min EBCT in DI water spiked with 2 ppm sodium selenate. Adsorption ability was 10 mg Se/g OCI-Bw.

8.2.2. Results in Simulated DI Water Spiked with 2 ppb Se

As the SRP well water only contains Se at a very low level, which is only around 2 ppb, DI water was spiked with sodium selenate to about 2 ppb used as the water feed for the small scale column test to simulate the real water condition, and to see how the biopolymer-based sorbents work at trace Se levels. Figure 48 shows the breakthrough results. The breakthrough was first observed to begin at 4080 min, corresponding to 5.26 L (859 Bed Volumes) of water that were treated; howerer the media was still able to continue to treat even more than 16 L of water. Because of the low selenate levels, much more water can be treated before the OCI-Bw was fully exhausted. Therefore, new batches of water solutions needed to be prepared after one batch was used up. For different water feed batches, the initial selenate concentration displayed fluctuations due to the solution preparation system error each time, shown in Figure 48 as several different separate points labelled from a-e. However, we still can estimate how much selenate was absorbed in total using the method as shown in Figure 46 by calculating the areas of the drawn rectangles and trapezoids. The total estimated Se removed is 99.12 μg from the calculation of the total areas. Due to the time consuming test, the column test was stopped after treating 17.5 L of spiked DI water, and this was still before the sorbent exhaustion. At this point, the adsorption ability was 123.5 μg Se/g OCI-Bw according to the dried bed mass which is 0.80 g. The much lower adsorption ability compare to the one using 2 ppm spiked DI water is due to the lower initial Se concentration in the water that is only 2 ppb. Also, since the final batch of water had an initial Se concentration of 12.5 ppb (point e, Figure 48) while the final sample point had a Se concentration still below 10 ppb, the bed did not reach full exhaustion.

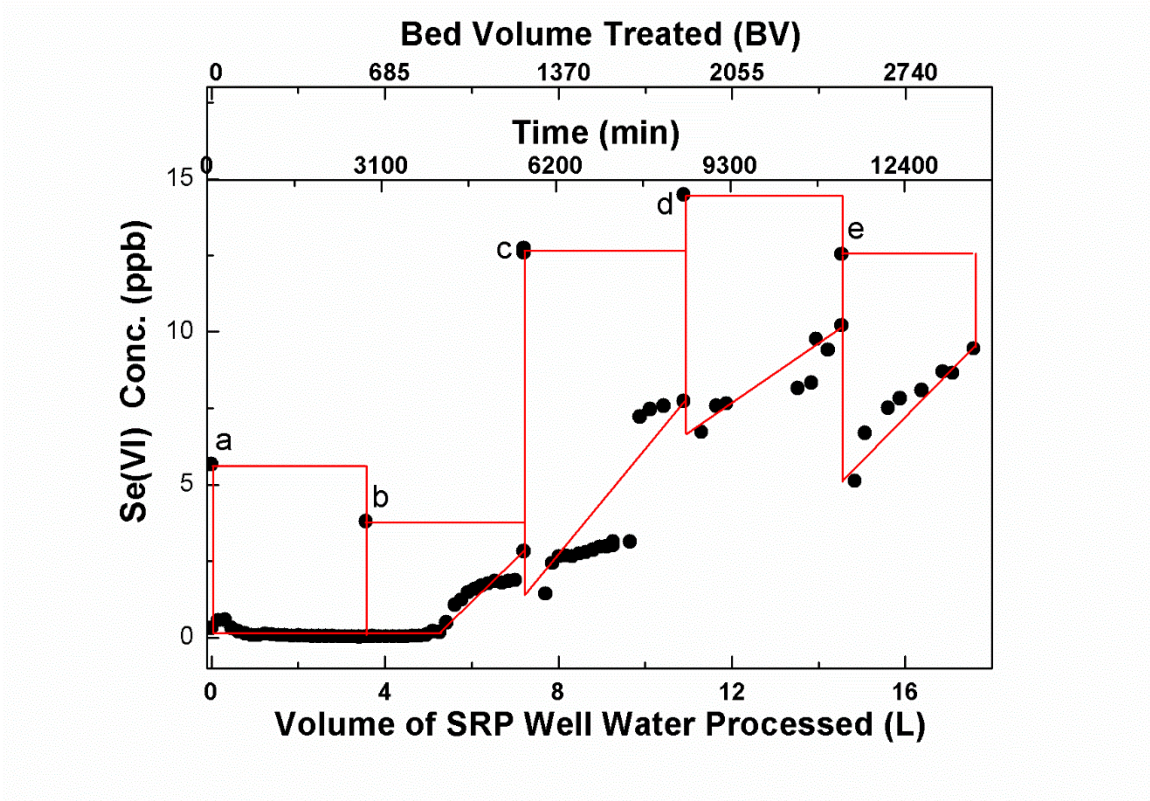

Figure 48. Breakthrough curve of OCI-Bw with 5 min EBCT in DI water spiked with 2 ppb sodium selenate. Adsorption ability was 123.5 µg Se/g OCI-Bw.

8.2.3. Results for 5 min EBCT in Spiked Well Water

SRP well water was spiked with 0.2 ppm selenate as the water feed to study the effect of different empty bed contact time (EBCT). The breakthrough curve for the small scale column test with 5 min EBCT is shown in Figure 49. In this test, the bed height was 8.5 cm and the bed volume was calculated to be 8.074 cm^3. Breakthrough was observed to begin at the time point of 350 minutes. The last point before breakthrough corresponded to 0.744 L of water that was fully treated. The mass of the dried sorbent was determined to be 1.1957 g. Based on the breakthrough data, the adsorption ability of

the sorbent was 110 µg Se/g CCT-149. Comparing to the jar test data in spiked well water (Figure 36 and 37), this is a little bit higher than the adsorption ability of CCT-149 in the jar tests (0.1 mg/g for 45 % removal at 1 g/L loading and 0.05 mg/g for 100 % removal at 5g/L loading).

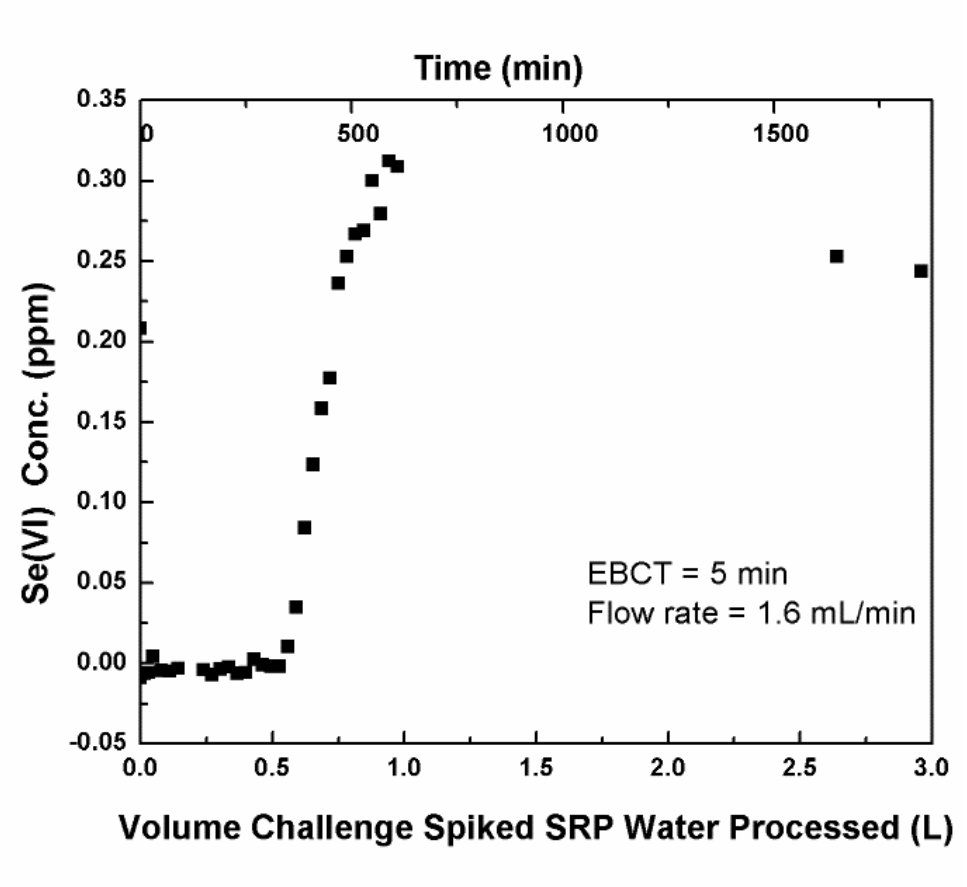

Figure 49. Breakthrough curve of CCT-149 with 5 min EBCT in SRP well water (E site) spiked with 0.2 ppm sodium selenate. Adsorption ability was 110 µg Se/g CCT-149.

8.2.4. Results for 15 min EBCT in Spiked Well Water

To see if the amount of Se removed on CCT-149 could be increased with a longer contact time, the flow rate was reduced to achieve 15 min EBCT. The bed height was

measured to be 9.8 cm, which correspond to a bed volume of 9.308 cm^3. The flow rate was thus set as 0.62 mL/min according to the EBCT and bed volume.

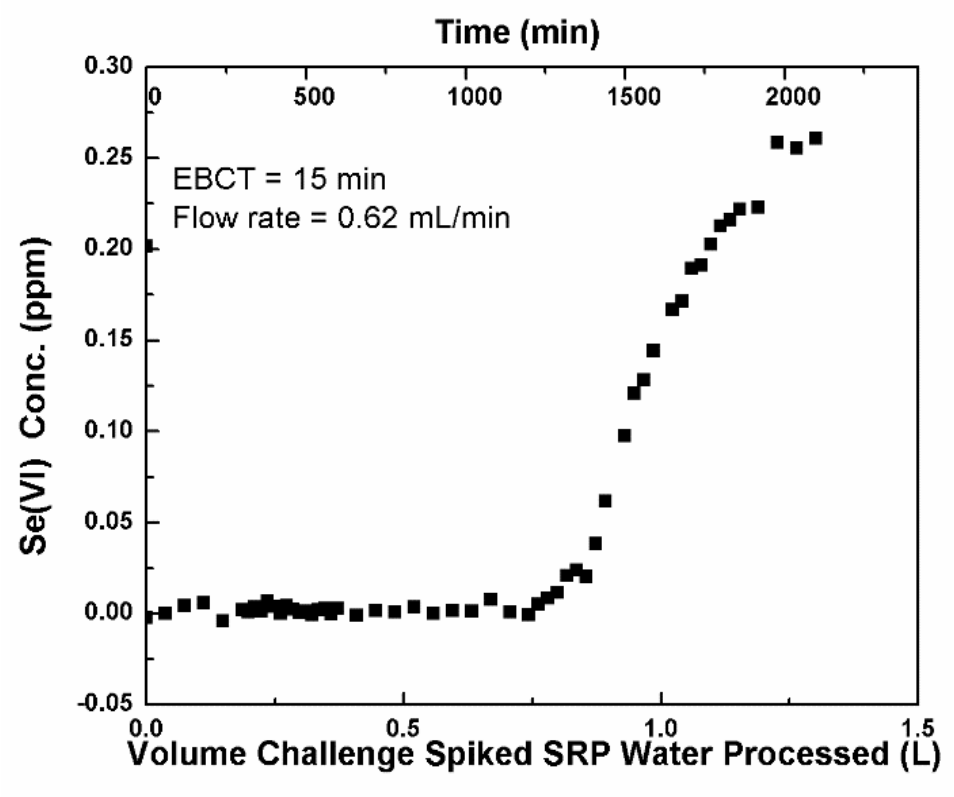

Figure 50. Breakthrough curve of CCT-149 with 15 min EBCT in SRP well water (E site) spiked with 0.2 ppm sodium selenate. Adsorption ability was 114.5 µg Se/g CCT-149.

Figure 50 shows the breakthrough curve for the small scale column test with 15 min EBCT. Breakthrough was observed to begin at the time point of 1200 minutes. The breakthrough point corresponded to 1.106 L of water that was fully treated. The mass of the dried sorbent was determined to be 1.628 g. Based on the breakthrough data, the adsorption ability of the sorbent was 114.5 µg Se/g CCT-149. Comparing to the data in Figure 49, this is similar to the adsorption ability of CCT-149 with shorter EBCT. This indicates that a longer EBCT did not increase the amount of Se removed on CCT-149. In

other words, shorter contact time will not decrease the adsorption ability of CCT-149. Therefore, it is worth to know if the EBCT can be decreased to lower than 5 min to obtain a faster flow rate. In this way, the anticipated total time used for small scale column tests using unspiked well water matrix will be much shorter instead of running several months.

8.2.5. Results for 1.5 min EBCT in Spiked Well Water

The EBCT was set at 1.5 min to obtain the faster flow rate of 4.68 mL/min. The bed height was measured to be 7.39 cm, which corresponds to a bed volume of 7.02 cm^3.

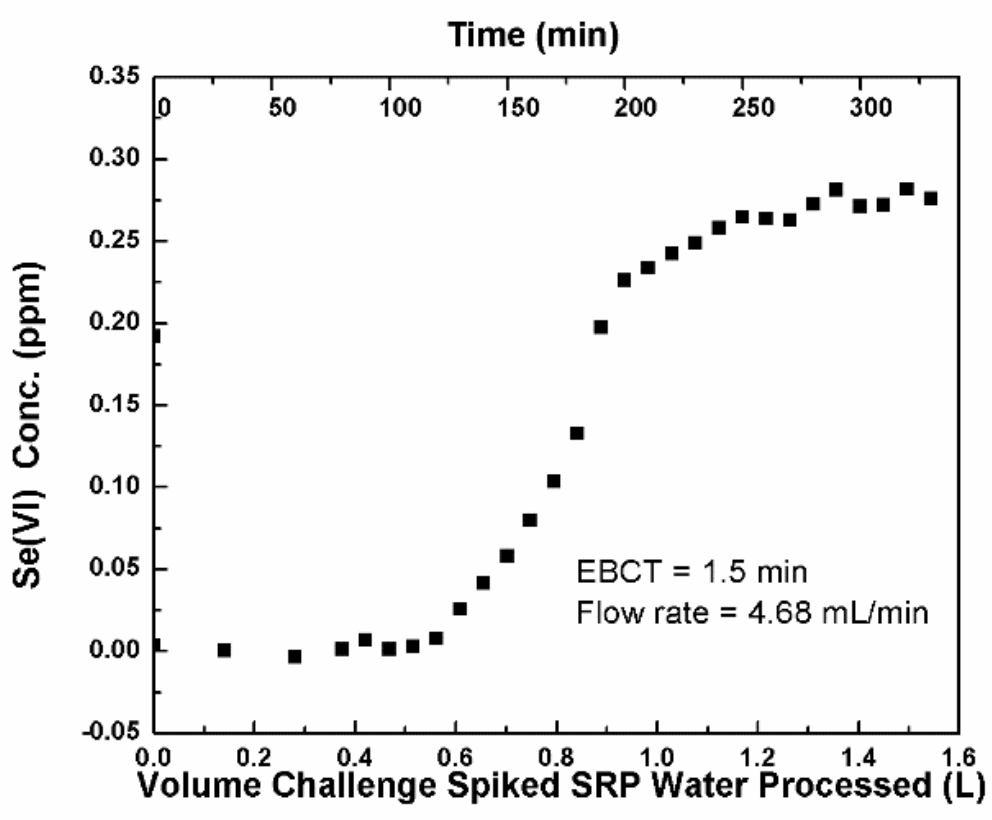

Figure 51. Breakthrough curve of CCT-149 with 1.5 min EBCT in SRP well water (E site) spiked with 0.2 ppm sodium selenate. Adsorption ability was 114.6 µg Se/g CCT-149.

The breakthrough curve for small scale column test with 1.5 min EBCT is shown in Figure 51. Breakthrough was observed to begin at the time point of 110 minutes. The breakthrough exhaustion point corresponded to 0.924 L of water that was fully treated. The total amount of Se removed was 138 µg, according to the dried CCT-149 bed mass which is 1.2041 g, the adsorption ability was 114.6 µg Se/g CCT-149. Therefore, EBCT of 1.5 min, 5 min, and 15 min didn't affect the adsorption ability of CCT-149 on loading Se in spiked DI water. The measured adsorption ability in all the column tests performed in spiked well water were similar to that observed in the jar tests (0.1 mg Se/g for 45% removal at 1 g/L loading).

8.2.6. Results for 5 min EBCT in Non-Spiked Well Water

Based on the small scale column test results of CCT-149 in spiked SRP well water, we found that the different EBCTs did not have a big effect on the adsorption ability. Thus, a 5 min EBCT was chosen for the small scale column test in unspiked SRP well water to keep a stable running. The breakthrough curve using 5 min EBCT is shown in Figure 52. In this test, the bed height was 8.78 cm and the bed volume was calculated to be 8.339 cm^3. Breakthrough was observed to begin at the time point of 490 minutes. The last point before breakthrough corresponded to 1.02 L of water that was fully treated. The total amount of Se removed was 1.53 µg. After the column test, the sorbent was removed and dried for one week. The mass of the dried sorbent was determined to be 1.275 g. Based on the breakthrough data, the adsorption ability of the sorbent was 1.2 µg Se/g CCT-149. Comparing to the data in Table 20, this is lower than the adsorption ability of CCT-149 in the spiked SRP water with relatively high Se concentration. This is

likely due to the low concentration of Se in the water compared to competing sulfate anions. Therefore, pretreatment of the water using $BaCl_2$ to remove the sulfate followed by Se removal with CCT-149 was considered for future column tests.

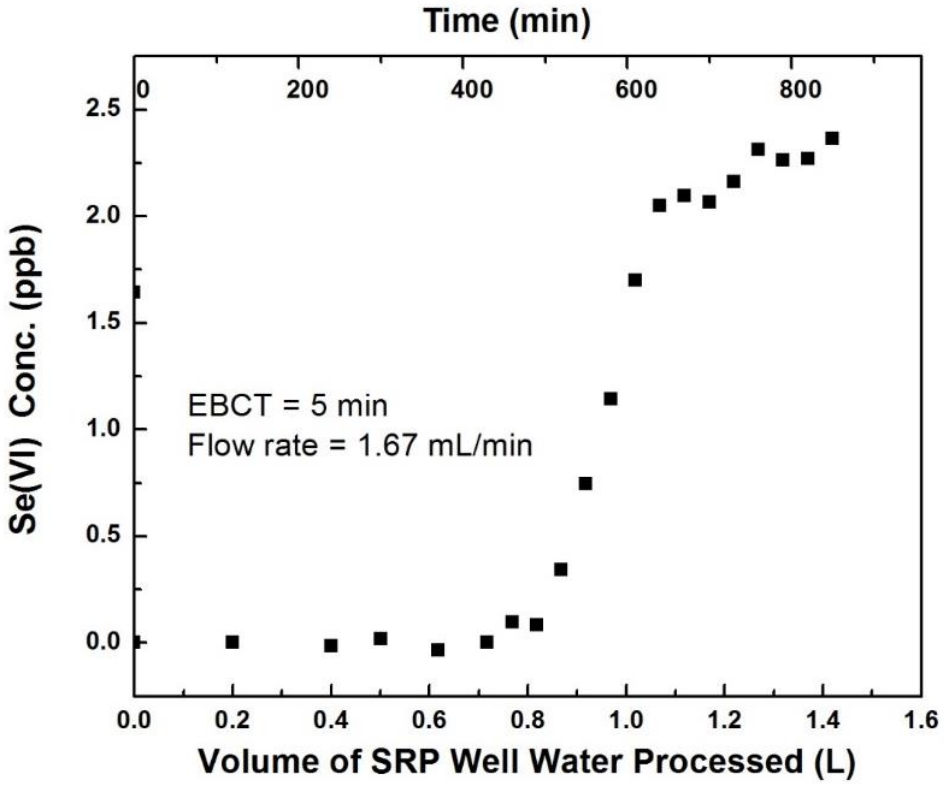

Figure 52. Breakthrough curve of CCT-149 with 5 min EBCT in non-spiked well water. Adsorption ability was 1.2 µg Se/g CCT-149.

8.2.7. Results for 5 min EBCT in Non-Spiked Well Water with $BaCl_2$ Pretreatment

Small jar tests regarding how much barium chloride is needed to remove all the sulfate in SRP well water were performed prior to the small scale column tests. By

dropping 1 M $BaCl_2$ solution into SRP well water, Ba/S mole ratio was calculated to be 0.7, 1.47, 3, 7.62, and 15.3 as shown in Figure 53. By using a Ba/S mole ratio of 0.7, the sulfate remaining was still high. After increasing the Ba/S mole ratio to about 3, the sulfate remaining concentration in the water did not decrease too much and the sulfate left was less than 2.8 ppm.

Table 20. Small scale column test results for CCT-149/OCI-B in SRP well water.

Water matrices	**EBCT (min)**	**Flow rate (mL/min)**	**Volume (L) at Breakthrough**	**Volume (L) at Exhaustion**	**Se Adsorbed (µg)**	**Adsorption Ability (µg Se/ g)**
Well water spiked with 0.2 ppm Se6	1.5	4.68	0.515 (73.4 BV)	0.924 (131.6 BV)	138	114.6
	5	1.6	0.528 (65BV)	0.744 (92 BV)	132	110.0
	15	0.62	0.744 (79.9 BV)	1.106 (118.8 BV)	186.4	114.5
Well water	5	1.67	0.8183 (98 BV)	1.0187 (122.16 BV)	1.5	1.2
Well water, $BaCl_2$ pretreatment	5	1.538	1.938 (252 BV)	2.03 (264 BV)	3.3	3.78

* OCI-B used as a replacement of CCT-149
BV – Bed Volume

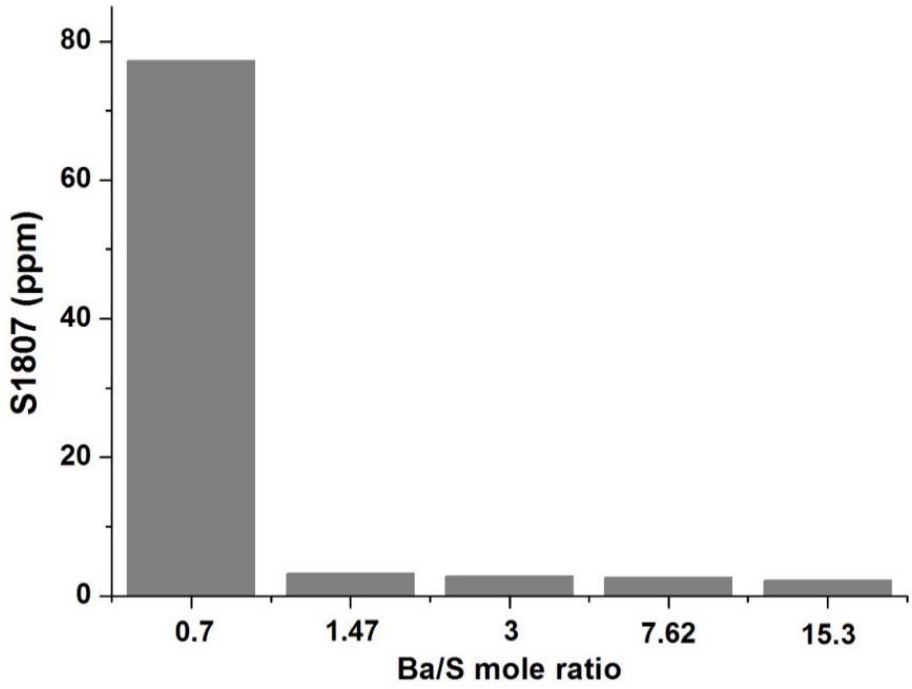

Figure 53. S remaining in SRP well water with different Ba/S mole ratio using $BaCl_2$.

According to the small jar tests results, $BaCl_2$ was used at a mole ratio of Ba/S equal to 3 in order to fully remove most of the sulfate from well water. After $BaCl_2$ pretreatment, a white precipitate formed and settled down on the bottom of 1-gal container overnight. OCI-B was used as the sorbent bed considering it has the same synthesis procedure with CCT-149. The bed height was 8.1 cm and the bed volume was calculated to be 7.69 cm^3. Therefore, the flow rate was set to be 1.54 mL/min to achieve the 5 min EBCT (Table 20). From Figure 54, we can see the breakthrough began at the point that about 1.938 L water was treated, corresponding to 252 bed volume (BV) that treated. The last point before breakthrough corresponded to 2.03 L of water that was fully treated. According to the dried OCI-B bed mass, 0.866 g, the adsorption ability of OCI-B

was 3.78 µg Se/g OCI-B, which is about 3 times higher than the one that without $BaCl_2$ pretreatment (Table 19).

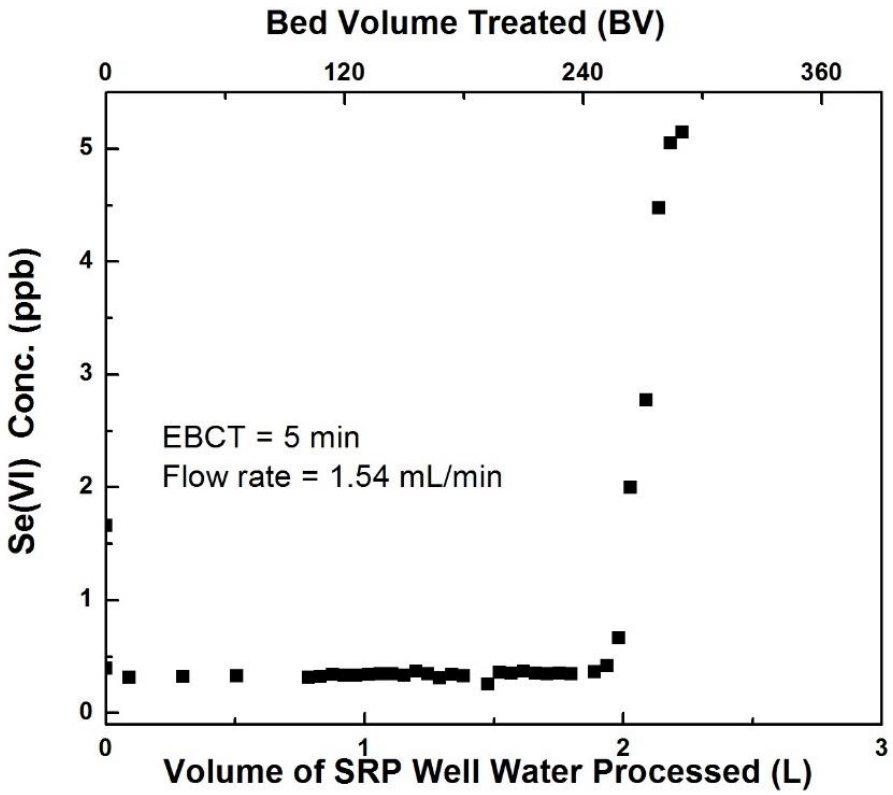

Figure 54. Breakthrough curve of OCI-B with 5 min EBCT in non-spiked well water with $BaCl_2$ pretreatment flow in upflow mode. Adsorption ability was 3.78 µg Se/g OCI-B.

All of the above small scale column tests were run in an upflow mode to avoiding channeling. We also tried one with downflow mode to confirm that upflow mode is better. Figure 55 shows the small scale column test result for OCI-B in $BaCl_2$ pretreated well water with a downflow mode. The flow rate was set to be 1.38 mL/min to achieve the 5 min EBCT. The breakthrough began at about 1 L water that treated. The Se loading capacity is 3 µg Se/g OCI-B according to the calculation based on 0.6757g dried sorbent

used. This was a little bit worse than using upflow mode with all the other conditions the same (Figure 54). This confirms that using upflow mode can get a better result.

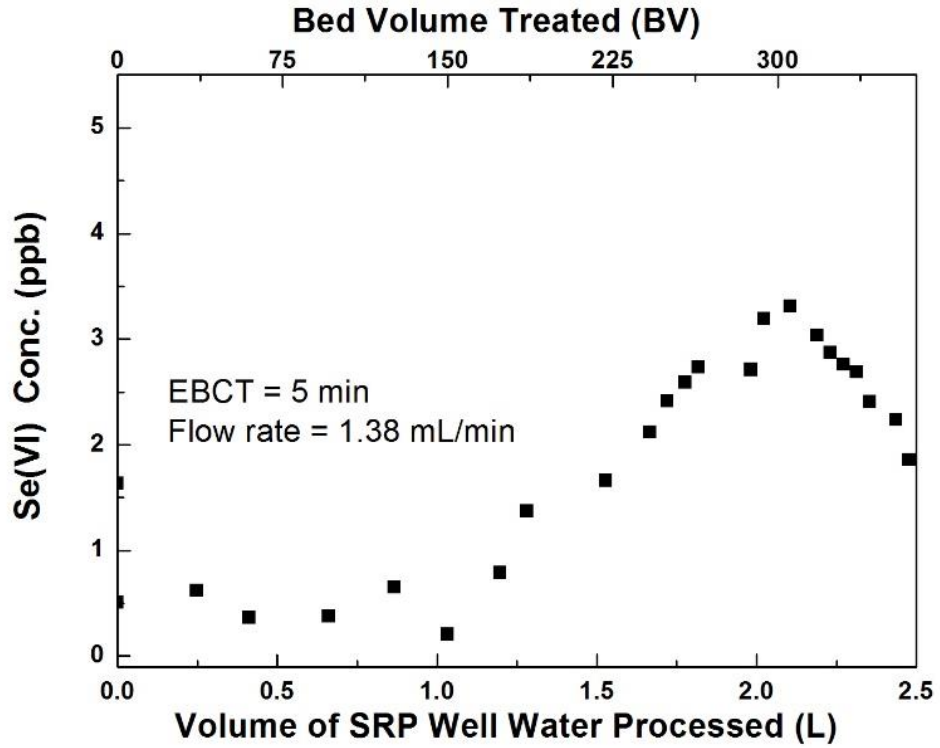

Figure 55. Breakthrough curve of OCI-B with 5 min EBCT in non-spiked well water with $BaCl_2$ pretreatment flow in downflow mode. Adsorption ability was 3 µg Se/g OCI-B.

8.2.8. Conclusions

In summary, biopolymer-based sorbent OCI-Bw was tested in small scale column tests using spiked DI water to study the Se loading capacity in a dynamic mode. In 2 ppm spiked DI water, OCI-Bw demonstrates a high adsorption ability of 10 mg Se/g OCI-Bw. Different empty bed contact time (EBCT) were studied for CCT-149 in spiked well water

small scale column tests. The results show no big influence on the adsorption ability of Se onto CCT-149 using different EBCTs. Small scale column tests of CCT-149/OCI-B with and without barium chloride pretreatment for SRP well water were investigated. By removing sulfate first with $BaCl_2$, the adsorption ability of Se onto CCT-149/OCI-B increased about three times, from 1.2 µg Se/g to 3.78 µg Se/g.

8.3. Layered Double Hydroxides (LDH)

LDH-granular was gently ground into small particles using a mortar and a pestle, and sieved to the specified mesh size using sieves NO. 35 and NO. 60 to obtain the suitable particle sizes ranging 250 – 500 µm. Based on the jar test results, LDH-granular requires longer retention time (2 h) to reach 100% Se removal. For this reason, 30 min was first set as the EBCT to ensure that sufficiently long exposure times were used, considering the flow rate would be very slow for small scale column tests if using 2 h as the EBCT. Non-spiked well water (SRP A well, site E) was used as the water feed.

8.3.1. Results in Non-Spiked Well Water without $BaCl_2$ Pretreatment

In this test, the bed height was measured to be 9.668 cm, which corresponds to a bed volume of 9.18 cm^3. The flow rate was accordingly set as 0.3 mL/min. Figure 56 shows the breakthrough curve of LDH-granular using the as-obtained well water (initial [Se] = 1.75 ppb) without $BaCl_2$ pretreatment. Breakthrough was observed to begin at time point of 8344 min, which correspond to a breakthrough volume of V_b = 2.5 L (272 Bed Volumes, BVs) water treated. The last point before breakthrough corresponded to an exhaustion volume, V_e, was equal to 3 L (326.8 bed volumes, BVs) of water that was fully treated. After the column test, the sorbent was removed and dried for one week

under 50 ºC. The mass of dried LDH-granular was determined to be 7.7 g. Based on the breakthrough data, the adsorption ability of the sorbent was calculated as Q_e = 0.65 µg Se/g LDH-granular (Table 21). This low adsorption capacity is consistent with the interference of sulfate with the selenium binding sites on the LDH, and also the much lower level of [Se] in the water compared to the amount of sulfate (from [S]). The [S] during the column test was also monitored and the breakthrough curve is shown in Figure 56. The V_b for [S] was similar to the one observed for [Se], but with a loading of 18 mg S/g LDH, which suggests that the Se binding sites were saturated by sulfate. Comparing to the results of CCT-149 (Table 20), the Se adsorption ability is lower than that of CCT-149 in unspiked well water, which is due to the relatively high density of LDH-granular. Although the value of Se removed per gram LDH-granular is lower than CCT-149, the total amount of Se removed was 5 µg, which is more than three times higher than CCT-149 (1.5 µg Se adsorbed, Table 20). Considering the cost of LDH-granular is cheaper than CCT-149, LDH-granular is still a promising sorbent material for removing Se in SRP power plant waters.

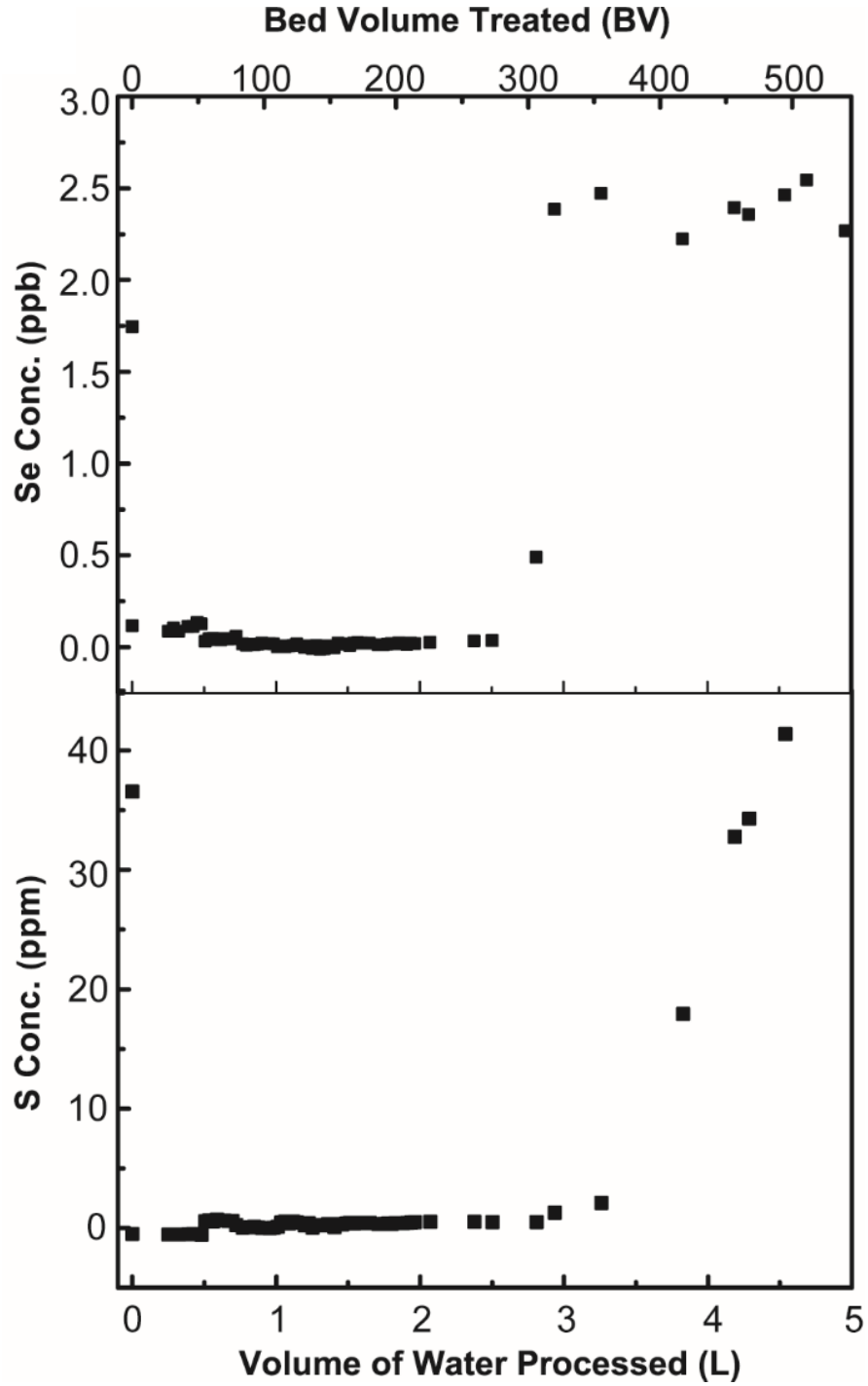

Figure 56. Breakthrough curve of LDH-granular with 30 min EBCT in non-spiked well water. Adsorption ability was 0.65 µg Se/g LDH-granular.

8.3.2. Results in Non-Spiked Well Water with $BaCl_2$ Pretreatment

To increase the adsorption ability of LDH-granular in non-spiked well water, $BaCl_2$ pretreatment was also applied to remove the competing ion sulfate. The same procedure as for OCI-B, $BaCl_2$ was used at a mole ratio of 3 to S in order to fully remove all of the sulfate from well water. After $BaCl_2$ pretreatment, white precipitate formed and settled down on the bottom of container overnight. The bed height was 9.2 cm and the bed volume was calculated to be 8.74 cm^3. The flow rate was set to be 0.3 mL/min to achieve the 30 min EBCT (Table 21). The initial selenium concentration in the water decreased slightly from 1.64 ppb to 1.3 ppb after $BaCl_2$ was added, suggesting that some of the selenium was removed by co-precipitation. The initial [S] in the water was 41.5 ppm; after $BaCl_2$ addition it decreased to 1.9 ppm. The [S] in the water in the sample of the effluent after 135 BVs was 0.9 ppm, suggesting that there may still have been some sulfate adsorption on the LDH media. The column test results using the pre-treated water are shown in Figure 57. Compared with the column test performed using water without $BaCl_2$ pre-treatment, breakthrough occurred much later, with the V_b = 9.75 L and V_e = 15.55 L (1779 BVs) (Table 21), which is much higher than without $BaCl_2$ pre-treatment. The last point before breakthrough corresponded to 15.549 L (1779 BV) of water that was fully treated. It is almost six times of the one without $BaCl_2$ pretreatment, which is 326.8 BV. Based on the breakthrough data, the exhaustion capacity of LDH-granular was Q_e = 1.90 µg Se/g LDH-granular. This indicates that $BaCl_2$ pre-treatment can help decrease the amount of sulfate in the water, leading to a roughly 3X increase in the amount of Se(VI) removed by granular LDH. The adsorption exhaustion rate (AER) also decreased from 2.57 to 0.51 g/L. The [S] concentration did not increase at the V_b

observed for Se, suggesting that sulfate adsorption was not as large of a contributor to the exhaustion of the Se(VI) binding sites on the LDH. Nonetheless, the exhaustion capacity of Q_e = 1.90 µg Se/g obtained in the $BaCl_2$-treated water is still much lower than what was observed by Chubar *et. al* (Q_b = 481.1 µg/g) when performing the column test in background electrolyte containing only NaCl.[107]

Table 21. Small scale column test results for LDH-granular in SRP well water (E); BV is the bed volume; Q_b is the capacity of loading selenate at breakthrough; Q_e is the exhaustion capacity; AER is the adsorbent exhaustion rate.

Water	**BV (cm^3)**	**Sorbent Mass (g)**	V_b **(L)**	BV_b	Q_b **(µg/g)**	V_e **(L)**	BV_e	Q_e **(µg/g)**	**AER (g/L)**	**V (L) by 1 g**
Well water	9.18	7.7	2.50	272	0.57	3.00	327	0.65	2.57	0.39
Well water with $BaCl_2$ pre-treatment	8.74	7.9	9.75	1115	1.6	15.55	1779	1.9	0.51	1.97

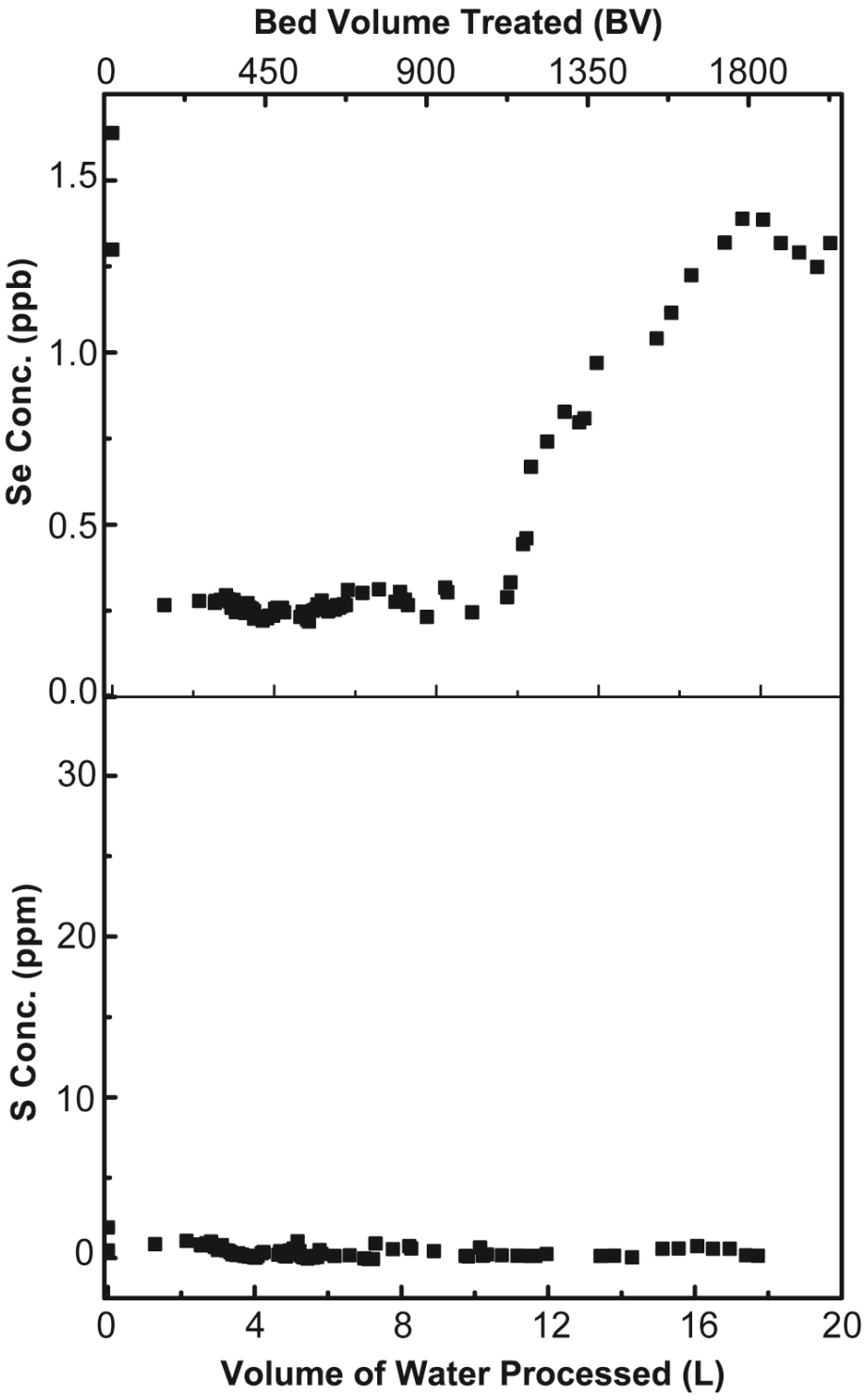

Figure 57. Breakthrough curve of LDH-granular with 30 min EBCT in non-spiked well water with $BaCl_2$ pretreatment. Adsorption ability was 1.9 µg Se/g LDH-granular.

To identify other potentially interfering species in our groundwater samples, ICP-MS analysis was performed on the effluent water at breakthrough from the column test conducted using the $BaCl_2$-treated groundwater. Figure 58 shows the influent and effluent concentrations for various metal species analyzed. Other than removing selenium, the LDH was also effective for completely removing chromium and uranium (initial concentrations < 10 ppb) and removing some of the magnesium, calcium, and strontium (initial concentrations between 10 – 100 ppm) present in the groundwater. On the other hand, slight increases in arsenic and aluminum concentrations were observed.

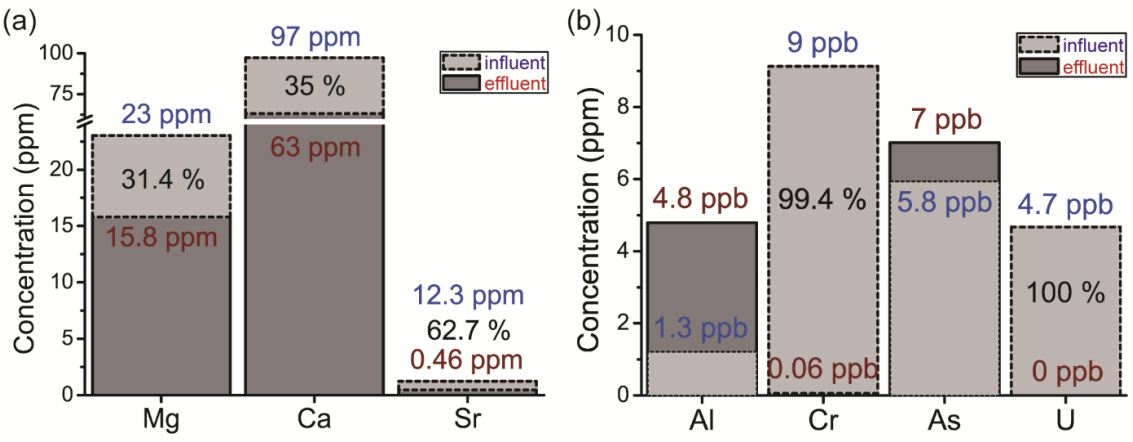

Figure 58. Metals concentration in $BaCl_2$ pre-treated groundwater with blue and red text indicating the influent and effluent concentrations, respectively. The removal percentage is also shown.

Since LDHs have already been shown to be effective for adsorption of chromium and arsenic oxoanions through a similar mechanism as for selenium,[1,103,117,148-149] the changes in these concentrations can be explained by the simultaneous removal of these species on the LDH. The slight increase in the [As] could be from desorption of the

arsenic oxoanions due to exhaustion of the LDH, but this could not be confirmed without having the corresponding breakthrough curve for [As].

Regarding the changes in the cation concentrations in the effluent, studies have also shown that certain metal cations can interact with anions adsorbed on the LDHs and become removed,[150] despite LDHs being anionic clays with positively charged surfaces. Specifically, uranium cationic species were shown to be removed on Mg-Al LDHs through the formation of complexes with the carbonates adsorbed on the LDHs,[151-152] although previous studies focused on much higher uranium levels (80 ppb – 750 ppm) than observed here. Previous studies also showed that calcined LDH, which releases hydroxide anions during rehydration and reconstruction of the layered structure according to equation (8), can remove Mg^{2+} and Ca^{2+} from solution through its reaction with these OH^- species and precipitation of $Mg(OH)_2$ and $Ca(OH)_2$.[120,153]

$$Mg_{1-x}Al_xO_{1+x/2} + x/n\ A^{n-} + (1+x/2)\ H_2O \rightarrow Mg_{1-x}Al_x(OH)_2A_{x/n} + xOH^- \qquad (8)$$

Since the pH of the effluent at breakthrough was measured to be 9.3, only a little higher than the influent pH of 8.3, it is possible that the divalent cations in the groundwater could act to buffer the increase in pH resulting from the reaction in equation (8) by forming the hydroxide precipitates. This mechanism could explain the lower levels of Ca^{2+}, Mg^{2+}, and Sr^{2+} in the effluent. Since Mg-Al LDHs typically do not undergo dissolution unless below pH 5,[154] the slight increase in [Al] observed in the effluent is not yet understood. Previous studies have observed Al^{3+} leaching from LDHs even at pH 7 though the formation of complexes with organic compounds,[155] but further detailed study

of the composition of the groundwater samples would be needed in order to determine if this were occurring.

8.3.3. Characterization of LDH after Small Scale Column Tests

The exhausted granular LDH from the column test performed with $BaCl_2$ treated groundwater was further characterized using BET, XRD, and FTIR. The BET surface area for the LDH decreased to 41 m^2/g after the column test (Table 5), confirming the surface adsorption processes. The XRD analysis showed the exhausted LDH adopted the rhombohedral crystal structure (Figure 12c-d). This indicates that the water molecules together with the anions were incorporated back into the LDH to form the crystalline layered structure.[101,117] However, the XRD patterns for the LDH recovered from the column test using groundwater pre-treated with $BaCl_2$ (Figure 12d) looked similar as the one obtained for the LDH used in the groundwater without pre-treatment (Figure 12c). Both of these XRD patterns also looked similar, although with slightly larger peak widths, to the one obtained from the LDH reconstructed in DI water (Figure 12b). The reflections for all of the reconstructed granular LDH samples were broad, suggesting a low crystallinity. These results indicate that XRD is not able to distinguish between the different intercalated anion species in the reconstructed granular LDH.

FTIR characterization of the exhausted granular LDH from the column test performed with $BaCl_2$ treated groundwater also confirmed the recovery of the LDH crystal structure and also provide evidence of oxoanion adsorption. As shown in Figure 14c, the LDH bands associated with interlayer carbonate and Mg,Al-OH bonds could be observed, in addition to a new band at 861 cm^{-1} that was not seen in the spectrum from

the LDH reconstructed in DI water (Figure 14b). Previous studies observed a band at 849-862 cm^{-1} attributed to the ν(Se-O) vibrations of Se(VI)-O-Mg,Al-LDH complexes,[108] so this is the likely origin of this feature. However, the adsorption of arsenate and chromate on Mg-Al-LDH was observed at 852 cm^{-1} [156] and 887 cm^{-1},[119] respectively. Since this is in the same range, it is possible that the observed band could have contributions from the adsorption of the arsenic and chromium oxoanions as well. Additionally, the exhausted LDH-granular spectrum exhibited features between 1000 – 1300 cm^{-1}, which are not observed in the LDH reconstructed in DI water. These could be attributed to interlayer surface adsorbed sulfate [107,157] since the $BaCl_2$ may not have completely removed all the sulfate in the water.

8.4. Conclusions

In summary, different empty bed contact time (EBCT) were studied for CCT-149 in spiked well water small scale column tests. The results show no big influence on the adsorption ability of Se onto CCT-149 using different EBCTs. Small scale column tests of CCT-149/OCI-B with and without barium chloride pretreatment for SRP well water were investigated. By remove sulfate first with $BaCl_2$, the adsorption ability of Se onto CCT-149/OCI-B increased about three times, from 1.2 µg Se/g to 3.78 µg Se/g.

Small scale column tests were also performed using the SRP well water containing [Se] < 2 ppb Se and 20,000 times higher [S] with and without $BaCl_2$ pre-treatment for LDH-granular. Using the $BaCl_2$ pre-treatment resulted in about three times higher loading of selenium with an adsorption capacity of 1.9 µg Se/g, indicating that sulfate removal will help to improve the sorption capacities of the LDH. Other methods

for sulfate removal may also be effective and more appropriate for large-scale demonstrations in the field. Characterization of the effluent water and exhausted media confirmed that selenium was adsorbed onto the LDH. Other constituents in the water, such as chromium, arsenic, uranium, strontium, magnesium, and calcium were also removed, although not all of these species may have necessarily adsorbed onto the LDH. These results show that although the selenium concentration in the groundwater was very low compared to the other background ions, the granular LDH was an effective sorbent for its removal. While the observed adsorption capacities in the column tests were low, the results are promising considering the trace levels of selenium in the SRP well water.

9. Pilot Testing Onsite at SRP Power Plant

To assist SRP evaluate the efficacy and efficiency of the promising adsorptive media for the removal of selenium in actual field conditions, a pilot test was prepared with LDH-granular for total selenium removal at SRP's Santan Generating Station. The primary objective of the pilot test is to evaluate the sorbents under actual field conditions to determine the flux rate as measured in gallons per minute per square foot ($gpm/ft.^2$), empty bed contact time (EBCT) to validate the lab results, and the overall capacity of the sorbent material in (mg Se removed per gram of sorbent material) when treating larger volumes of water. The ultimate goals of the pilot test are to: (1) determine the number of bed volumes that can be treated in 6 ft long columns (diameter 4"), and (2) to obtain realistic cost estimates for decreasing the selenium discharge at the Santan Generating Station to < 1 ppb.

9.1. Pilot Testing Set-up

The pilot system contained four identical columns that are 3” diameter by 60” high with 4” of underlayment and not exceeding a 5-foot height, which is the straight side shell height of a commercial vessel (Figure 59). Each column set (lead-lag) had a flow meter/totalizer with an in-line flow meter to visually set the required flow rate.

A commercial pilot system will typically run 70% of the height of a column, which in our case is 42” (from 60”). The bed volume (BV) was then calculated to be 0.17 $ft.^3$, corresponding to 4.8 L (1.27 gal). For LDH-granular commercially obtained from Sasol with a density of around 39.33 $lb/ft.^3$, about 6.74 lb (3060 g) LDH-granular was needed as the sorbent bed for each column. Considering an EBCT of 30 min, the flow rate needed was determined to be 0.161 L/min (0.043 gpm). One 250 mL effluent sample per day was obtained and analysis was performed using inductively coupled plasma – mass spectrometry (ICP-MS) in the geology department at ASU.

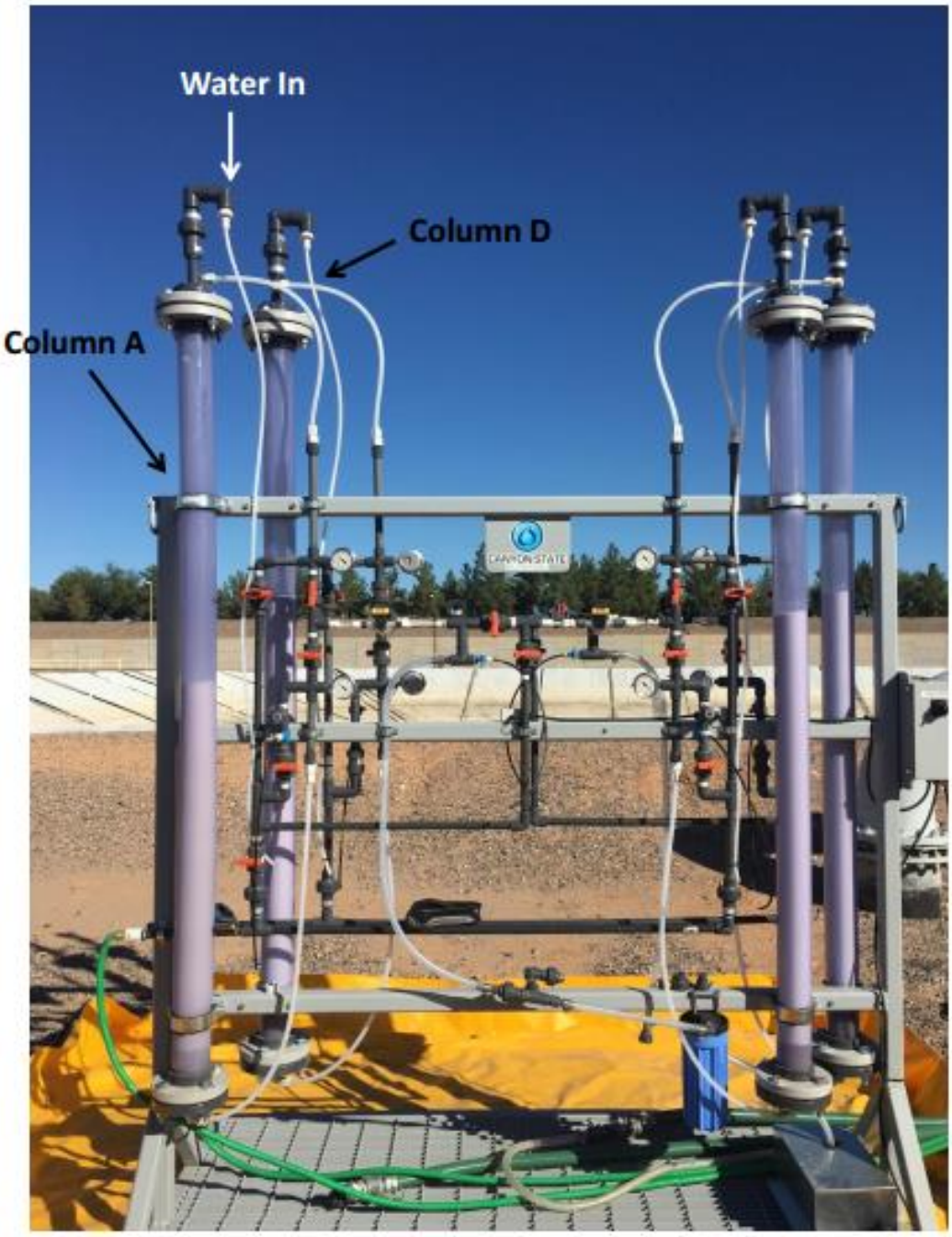

Figure 59. Photograph of the pilot testing columns setup on site at SRP santan generating station.

9.2. Pilot Test Results

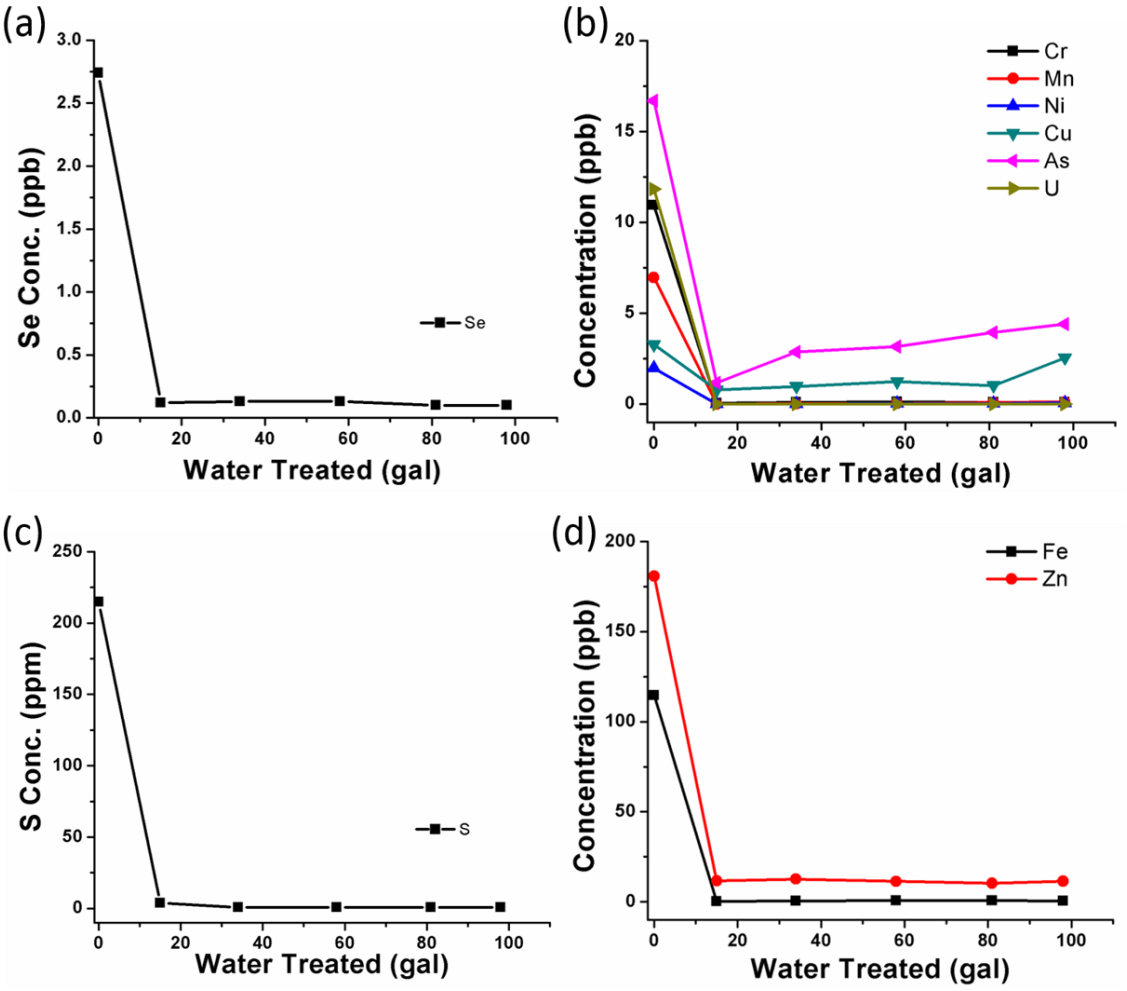

Figure 60. Pilot testing results of (a) Se; (b) Cr, Mn, Ni, Cu, As, and U; (c) S, and (d) Fe and Zn at SRP Santan generating station.

Cooling tower 5 (CT-5) was preliminarily used as the water feed to consider the on-site pilot testing set up location and feasibility. The influent water contained 2.74 ppb Se, according to sampling on Nov. 4, 2016 (Figure 60a). After running for 20 min, the effluent water contained only 0.05 ppb Se, demonstrating the total Se in the SRP CT-5

water was successfully removed by LDH-granular in only 20 min. S was also detected (presumably as sulfate) in the CT-5 water at a level of 214.9 ppm, more than 78000X of Se level. It was also removed by LDH-granular with an effluent concentration of 0.16 ppm (Figure 60c). The LDH-granular was able to treat more than 98 gal (370 L) of CT-5 water in removing Se even with such a high competing S level. Due to the approach of the winter season, SRP was not able to continue running the CT-5 water facility, so we were not able to obtain more samples to reach out breakthrough. But in Figure 60a, it demonstrates the success of removing Se from CT-5 water using LDH-granular in actual field condition. Some other ions were also analyzed, as shown in Figure 60b-d, showing that Cr, Mn, Fe, Ni, Cu, Zn, As, and U were also removed.

9.3. Conclusions

The pilot test onsite at SRP demonstrates the efficiency and efficacy of LDH-granular used under actual field condition for SRP cooling tower 5 (CT-5) water reducing selenium from 2.74 ppb to around 0.1 ppb with 20 min EBCT. Despite the high total dissolved solids contained and algae grown observed, the high level competing ions sulfate and other regulated metals such as Cr, As, U, and etc. were also been successfully removed by LDH.

10. Continuous-Stirred Tank Reactor Experiments

The continuous flow stirred tank reactor (CSTR) is a common ideal reactor type in chemical engineering. The behavior of a CSTR is often approximated or modeled by a

Continuous Ideally Stirred-Tank Reactor (CISTR).[158] A CSTR often refers to a mathematical model that describes an important class of continuous reactors — continuous, steady, well-agitated tank reactors. The mathematical model works for all fluids: liquids, gases, and slurries.[158] It can be used to estimate the key unit operation variables when using a continuous agitated-tank reactor to reach a specified output.

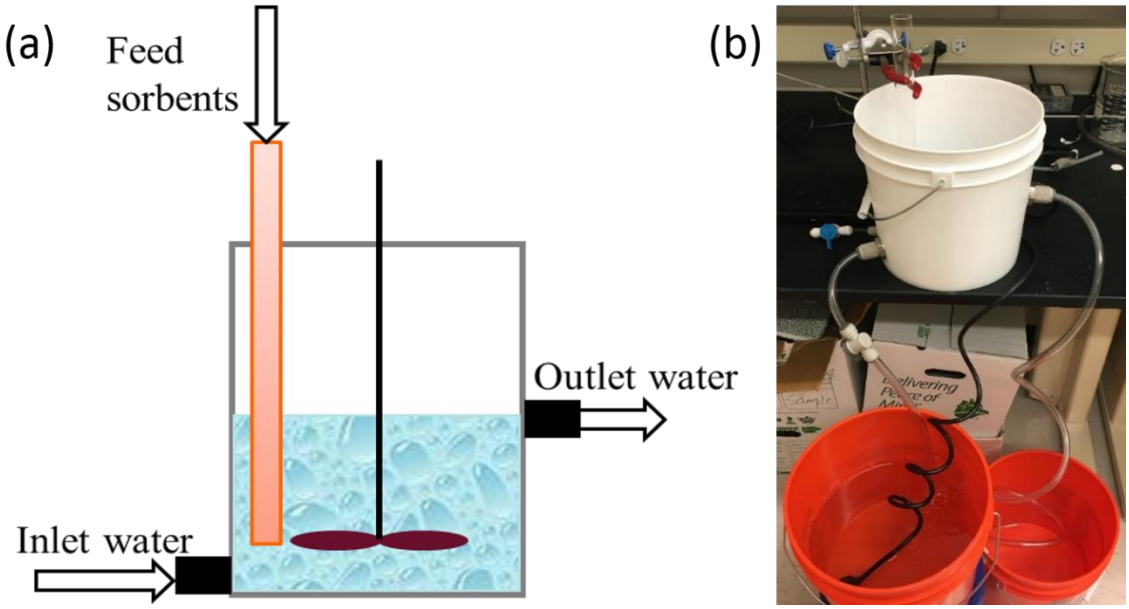

Figure 61. a) Schematically of liquid-phase CSTR; b) Lab set up of a small-scale CSTR.

The CSTR model is based on two assumptions: 1) Steady-state operation, i.e. Run at steady state with a continuous flow of reactants and products; 2) Perfect mixing that result in uniform conditions (concentrations and temperature). In a perfectly mixed reactor, the feed assumes a uniform composition throughout the reactor, namely the output composition is the same as the composition inside in the tank, which is a function of the residence time and rate of reaction.[159]

10.1. CSTR Experiments

OCI-B offered by Crystal Clear Technologies was used as the sorbent feed with a dosage of 2.5 g/L. The empty bed contact time (EBCT) was designed to be 15 min according to previous jar tests results. A total 5.28 gal of water was prepared with 1 gal in the white bucket (Figure 61b) to start with and the other 4.28 gal water was pumped in from the bottom inlet hole with a flow rate set as 252 mL/min to maintain the 15 min EBCT (water flow rate = 1 gal divided by 15 min). 9.5 g OCI-B was firstly added into the 1 gal water (2.5 g/L), with stirring at 400 rpm for 15 min using a magnetic stir plate and large stir bar. Sampling was peformed every 5 min from the white bucket and the samples filtered using a single use syringe filter (Sartorius Stedim, Minisart, 17764-ACK, 0.2 µm regenerated cellulose) unless otherwise noted. After 15 min stirring, fresh influent water was pumped into the white bucket and in the meanwhile, OCI-B was fed at a rate of 0.63 g/min (feed rate = water flow rate × dosage) into the white bucket to keep the dosage at 2.5 g/L since the sorbents will flow away from the top outlet tube together with the water. In this way, there was always 1 gal of water and 2.5 g/L sorbent materials in the white bucket reactor. Effluent sampling was performed every 5 min from the outlet tube and filtered. Samples were acidified using 2% trace metal nitric acid and analyzed using ICP-MS.

10.2. CSTR Preliminary Results

10.2.1. DI Water Spiked with 2 ppb Se(VI)

As shown in Table 22, Sample 1 and Sample 2 were taken from the bucket before starting the flow and were filtered using a reusable syringe filtration unit. The higher Se

concentration than initial Sample 0 may come from the cross contamination of the reusable filtration unit. The later samples were filtered using the single use filtration units and showed that Se was removed, with the level lower than 1 ppb until Sample 9, which is the last sample of the total 5.28 gal of water that treated.

Table 22. Results of DI water spiked with 2 ppb Se(VI).

Sample#		**Se ppb**	**comments**		**S ppm**
0	Initial (spiked DI water)	1.93			-0.13
1	5 min from bucket	5.12	reusable filtration	1 gal	1.53
2	10min from bucket	13.40			1.81
3	15min from outlet tube	0.12	single use filtration		1.64
4	20min	0.52		4.28 gal	1.09
5	25min	0.60			0.96
6	30min	0.61			0.69
7	35min	0.63			0.72
8	40min	0.63			0.73
9	45min	0.55			0.61
1 gal + 9.5 g OCI-B stir @ 400 rpm 15min					
After 15min, starts to flow @ 250mL/min, 0.63g OCI-B was added into bucket every minutes					
But actually, real flow rate is 4.28 gal/30min = 536 mL/min					

Although the desired flow rate was 250 mL/min to achieve the 15 min EBCT, the real flow rate when starting the testing happened to be 536 mL/min (4.28 gal divided by 30 min), which equals to 7 min EBCT, as the pump is not accurate and was hard to control. Nonetheless, OCI-B was still able to lower the Se(VI) levels to below 1 ppb within 7 min EBCT. The average Se that been removed can be calculated as follow:

$$Se_{ave} = inlet\ conc. - outlet\ conc.$$

$$= 1.934\ \text{ppb} - 0.59\ \text{ppb}$$

$$= 1.343\ \text{ppb} = 0.0013\ \mu\text{g/L}$$

Outlet conc. 0.59 ppb is the average from Sample 4 to 9. Consider flow rate of 536 mL/min, the removal rate of Se equal to:

$$Se_{rate} = 0.0013\ \mu\text{g/L} \times 536\ \text{mL/min}$$

$$= 0.6968\ \mu\text{g Se/min}$$

Consider the media adding rate is 0.63 g OCI-B/min, then the Se removal capacity is:

$$Capacity = 0.6968\ \mu\text{g Se/min} \div 0.63\ \text{g OCI} - \text{B/min}$$

$$= 1.1\ \mu\text{g Se/g OCI} - \text{B}$$

So the Se loading capacity is 1.1 µg Se/g OCI-B.

10.2.2. SRP Well Water

The CSTR using SRP well water without spiking (~2 ppb Se) was also performed using the same procedured as the one in spiked DI water. 5.28 gal of water was prepared for 10 samples. The OCI-B media ran out before all the water was treated, with 1.528 gal left. The result is similar as the one for spiked DI water, with the Se level decreased to about 0.5 ppb. The concentration of S in the SRP well water were also lowered.

Table 23. Results of SRP well water (site E). (originally with ~2 ppb Se)

Sample#		Se ppb		S ppm	comments
0	Initial (SRP well water)	1.82		42.94	all use disposal filtration
1	5 min from bucket	0.28	1 gal	8.20	
2	10min from bucket	0.52		6.86	
3	15min from outlet tube	25.37		6.97	
4	20min	0.42	4.28 gal	10.21	
5	25min	0.46		11.70	
6	30min	0.51		11.91	
7	35min	0.46		12.02	
8	40min	0.49		12.06	
9	45min	0.50		12.53	
10	50min	0.53		12.77	
1 gal + 9.5 g OCI-B stir @ 400 rpm 15min					
After 15min, starts to flow @ 250mL/min, 0.63g OCI-B was added into bucket every minute					
All of the OCI-B was used up in 50 min and 1.528 gal (5.785 L) was left					
So real flow rate is 10.415 /35min = 297.57 mL/min					

Although the desired flow rate was 250 mL/min to achieve the 15 min EBCT, the real flow rate when starting the testing was 297.57 mL/min according to calculation (4.28 gal – 1.528 gal divided by 35 min), which equals to 12.6 min EBCT.

The calculation procedure is the same as the one in spiked DI water. The average Se removed = 1.34 ppb = 0.0013 µg/mL. Considering the flow rate = 297 mL/min, the removal rate of Se = 0.3861 µg Se/min. Considering the media addition rate is 0.63 g OCI-B/min, then the Se removal capacity is 0.6 µg Se/g OCI-B.

The relatively lower value of mg Se/g media for treating SRP water compared with spiked DI water is due to the lower flow rate; thus less water was processed in the same period of time, meaning less Se can be treated. In SRP water, the flow rate (actually 297 mL/min) is closer to the expected values (250 mL/ min to achieve 15 min EBCT).

Figure 62 compares the Se results in spiked DI water and SRP well water. (The unreasonable points and contaminated points from the use of the reusable syringe filtration have been excluded from the plots)

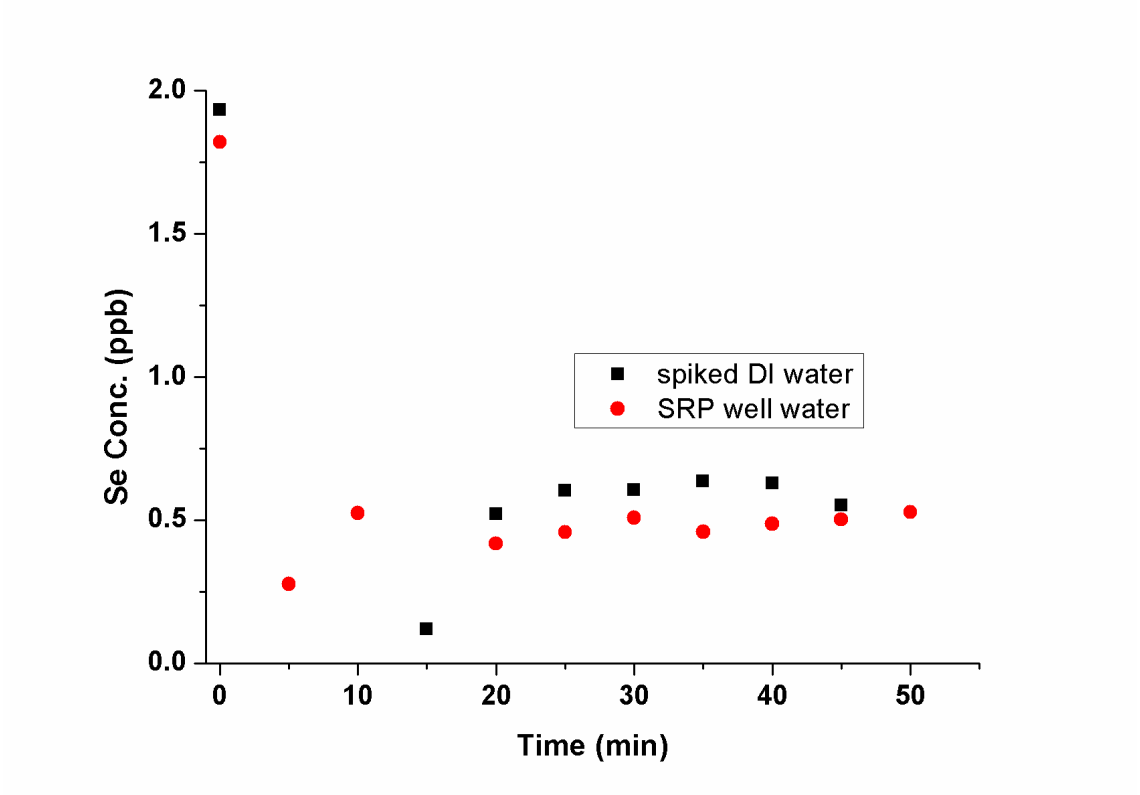

Figure 62. Selenium concentration in spiked DI water and SRP well water.

10.2.3. SRP Well Water Spiked with 50 ppb Se(VI) and Pretreated

SRP well water (assumed to contain 50 ppm sulfate) was pretreated by adding $BaCl_2$ with a Ba:S mole ratio of 3:1 and sitting for 4 days to try to precipitate all the sulfate out. The water was then spiked with about 50 ppb Se(VI). The CSTR result (Table 24) showed that 60.7 ppm S was lowered to 7.4 ppm by $BaCl_2$. But with the higher initial

Se concentration, which is 57 ppb instead of 1.8 ppb, the effluent Se concentration is relatively high, at ~8.8 ppb as an average. After running for 65 min, there was ~2.75 L water left, so the actual flow rate was 269 mL/min, and the loading capacity was 20 µg Se/g OCI-B.

Table 24. Results of SRP well water (site E). (originally with ~2 ppb Se)

Sample#		**Se ppb**		**S ppm**	**comments**
0	Initial (SRP well water)	0.02		0.21	all use disposal filtration
1	Pretreat with BaCl2	2.32		60.70	
2	Spiked with Se(VI)	2.04		7.40	
3	5 min from bucket	57.39	1 gal	7.71	
4	10min from bucket	11.20		5.50	
5	15min from outlet tube	5.05		5.00	
6	20min	2.82	4.28 gal	4.85	
7	25min	9.88		4.54	
8	30min	10.60		4.00	
9	35min	10.31		3.72	
10	40min	9.56		3.71	
11	45min	9.05		3.72	
12	50min	8.66		3.72	
13	55min	8.37		3.61	
14	60min	7.81		3.71	
15	65min	7.22		3.87	
1 gal + 9.5 g OCI-B stir @ 400 rpm 15min					
After 15min, starts to flow @ 250mL/min, 0.63g OCI-B was added into bucket every minutes					
After 65 min, ~2.75 L was left					
So real flow rate is 13.45 /50min = 269 mL/min					

Figure 63 shows the Se concentration and S concentration for the CSTR tested with spiked SRP water. The Se(VI) was lowered by OCI-B, while most of the S was removed after $BaCl_2$ pretreatment.

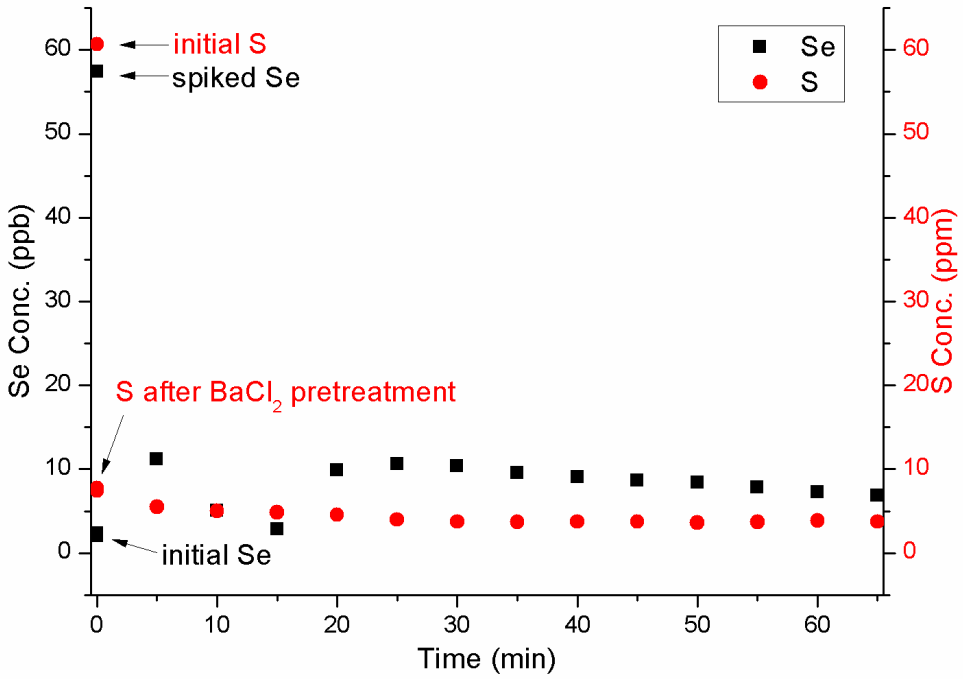

Figure 63. Se (ppb) and S (ppm) concentration spiked SRP well water with pretreatment.

10.3. Conclusions

The CSTR set-up in our lab was used to simulate the full engineered system to confirm that Se can be removed in such engineering conditions. The results in both spiked DI water and SRP well water showed OCI-B was able to lower Se down to 0.5 ppb, demonstrating the adsorption ability of OCI-B in CSTR system. Detailed study will be needed in future work to optimize the flow rates and dosages.

11. Summary

Carbon nanospheres (CNS) prepared using a facile spray pyrolysis method displays good activity for arsenate and selenate adsorption in synthetic DI water solution. In water solutions composed of canal and well water from SRP at pH > 8, the CNS could outperform PAC likely due to the presence of basic functional groups, higher surface area, and suitable microporous structure as a result of the formation mechanism arising from the synthesis method. However, competing anions in these waters completely inhibited selenate adsorption on the CNS.

The functionalized biopolymer-based sorbent made by Crystal Clear Technologies (CCT-149/OCI-B) and layered double hydroxides (LDH-500C/LDH-granular) were the two most promising materials for removing selenate in SRP waters among the sorbents screened. In jar tests, CCT-149 was able to remove 100% selenate in 30 min (starting concentration 0.2 ppm Se, 1 g/L CCT-149). The maximum loading observed for CCT-149 in DI water by fitting in Langmuir model was 90.9 mg Se/g. It could also remove 100% of the selenate spiked in A well discharge water (site E) and reduce the level to below 2 ppb in non-spiked samples. LDH-500C could remove 100% of the spiked selenate in all of the SRP water matrices tested, except the cooling tower 5 and 6 blowdown (Site C) due to interference of high concentration of competing ions like sulfate. Both materials were effective in small scale column tests for removing the selenium below 1 ppb for SRP well water. Due to the similar chemical structure and adsorption properties of sulfate and selenate, the high concentration of sulfate relative to selenate makes the selective removal of selenate difficult. Removing sulfate using a

pretreatment step with barium chloride result in about three times higher of selenate loading onto both sorbent materials.

12. Future Work and Preliminary Results

Although CCT-149/OCI-B and LDH exhibit good efficacy and efficiency in selenate removal, they have their strengths and weaknesses. Although the functionalized biopolymer CCT-149/OCI-B showed fast adsorption with 5 min EBCT, the materials are flaky and did not display good self-packing properties in the small scale column tests. That is the reason the CSTR was used for large scale testing instead of using a large column. Further, the small particle size of the sorbents is not feasible for a full-engineered system. LDH-granular, with a relatively larger particle size about 1.5 mm that facilitates the use in the pilot study, was observed to break apart into fine particles and undergo attrition in the pilot testing. Therefore, further studies will focus on exploring the formation of LDH composites that are stable in size under dynamic condition, and the development of combination with larger substrates so that to enable the performance in actual field application.

12.1. LDH/Chitosan Composites

While the high adsorption efficiency of LDH is very attractive, once breaking apart, similar to other nanocrystalline metal oxide (NMO) sorbents, it may require energy intensive filtration to separate the adsorbent from solution as post-treatment thus increasing the overall cost of use and regeneration.[160,122] To overcome this barrier,

engineered adsorbents with NMO embedded in various substrates have been developed.[161-165] In the last few years, polymer-clay composites have attracted a great deal of attention, including studies developed composites used as sorbents for non-ionic and anionic pollutants,[166] or organic pollutants.[167] Among them, chitosan-clay nanocomposites have been well investigated for the adsorption of anionic pollutants.[168-169]

Chitosan, a derivative of chitin, is a waste byproduct of the shellfish processing industry.[170] It can be isolated from the several million tons of shellfish waste generated globally per year[171] so that offers the advantages of being inexpensive.[172] The chitosan biopolymer can be formulated into films and beads[171] and can behave as a hydrogel in non-acidic aqueous solutions.[173] This characteristic can facilitate post-treatment removal, potentially creating a system that can be operated with minimal equipment and training.[174] As an ideal material for simple water treatment processes, chitosan has an environmental and economic advantages over other sorbents because it is plentiful,[175] renewable, biodegradable,[176] and non-toxic.[170] Chitosan has shown the effectiveness for metal removal including chromium, cadmium, mercury, and copper, [171,177] and can served as a passive and green matrix.[122] Previous work by Julie Zimmerman's group[165,174,178] successfully demonstrated a novel technology, NMO-impregnated chitosan beads (MICB), to remove arsenic from water. Their group also studied the MICB for selenite and selenate combined systerm.[122] Bleiman et al.[127] designed chitosan-clay composites that reported Se(VI) capacities of 18.4 mg/g.

Herein, we proposed the combination of LDH with the biopolymer, chitosan, as a substrate to develop the composites. The particle size and shape can be controlled in the synthesis process to achieve the desired composite size and shape, resulting in a sorbent that is capable to be used in the full-engineering system for selenium removal as well as simplified post-treatment. In order to synthesize the LDH/chitosan composites, different methods can be considered, such as: 1) physical agglomeration of chitosan and LDH, 2) direct synthesis of LDH onto chitosan using co-precipitation, and 3) spray deposition of LDH suspensions onto chitosan materials to combine with LDH-granular by directly mixing or in-situ synthesizing. The objective of this work is to optimize the composite preparation for the selenium adsorption capacity.

12.1.1. LDH/Chitosan Composite Beads Synthesis

Chitosan flakes (Dungeness Environmental, L/N CMP02P79, Alaskan Crab Chitosan) were used as chitosan beads source. The method used to synthesize chitosan beads or composite beads is based on the beads development of Miller and Zimmerman.[174-178] Typically, 1 g chitosan flakes are dissolved in 60 mL 0.1 M HCl solution, then stirred for four hours to make it clear chitosan gel. To make the pure chitosan beads, a 19G needle was fitted on a syringe and 20 mL of the chitosan gel was pushed into 100 mL of 0.1 M NaOH in droplets. The chitosan gel droplets in the alkaline solution were soft and clear and in the size around 3 mm in diameter (Figure 64). The droplets solution was stirred overnight slowly to form chitosan beads. The soft beads were washed using DI water and dried at room temperature in the fume hood for 3 days to form solid beads and shrunk into size around 1 mm (Figure 65). To make

LDH/chitosan composite beads, two approaches were investigated. The first was to use direct mixing of 0.1414 g of ground LDH-granular (Sasol Germany GmbH, PURALOX MG 63 HT – Granulate) into 20 mL of chitosan gel, followed by stirring overnight to make uniform composite gel. The gel turned white and sticky after being mixed with LDH. The second was to synthesize LDH "in-situ" by adding $MgCl_2$ and $AlCl_3 \cdot 6H_2O$ as precursors with a Mg/Al mole ratio of 3:1 (total mass of combined precursors = 0.1414 g, or otherwise noted) into 20 mL chitosan gel, followed by stirring overnight to make the gel mixture. The mixture gel was still light yellow and clear as pure chitosan gel. Composite beads were also formed by pushing the gel from a syringe fitted with a 19G needle into the NaOH solution. After stirring overnight in the alkaline solution, the clear mixture gel beads turned white. The amount of LDH in the in-situ LDH/chitosan beads was controlled by adjusting the total amount of precursor to obtain LDH weight percentages of 20%, 30%, 40%, 50%, and 60%. When the LDH wt% increased to 60%, most of the beads were observed to be broken (Figure 66, broken beads), indicating that the amount of chitosan was not sufficient to serve as substrate for all of the LDH to assemble into uniform round beads. For comparison, pure LDH without chitosan was also prepared. Briefly, 0.33 g $MgCl_2$ and $AlCl_3 \cdot 6H_2O$ precursors were added into 20 mL 0.1 M HCl solution, then dropped into 0.1 M NaOH using a syringe. The suspension was stirred overnight and filtered to form pure LDH and dried at 50 ^oC.

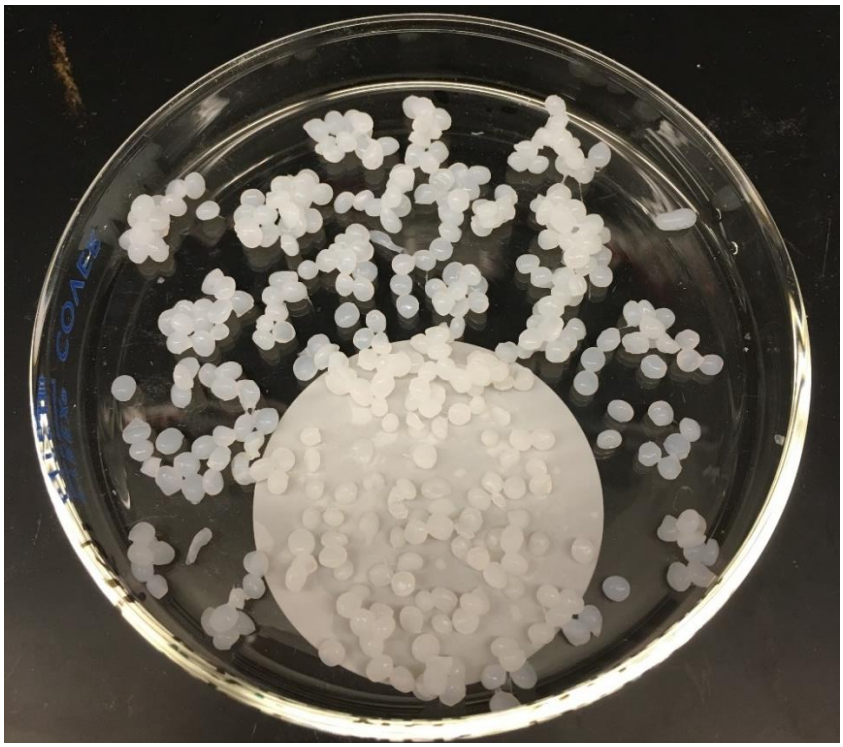

Figure 64. Picture of soft LDH/chitosan composite beads before drying.

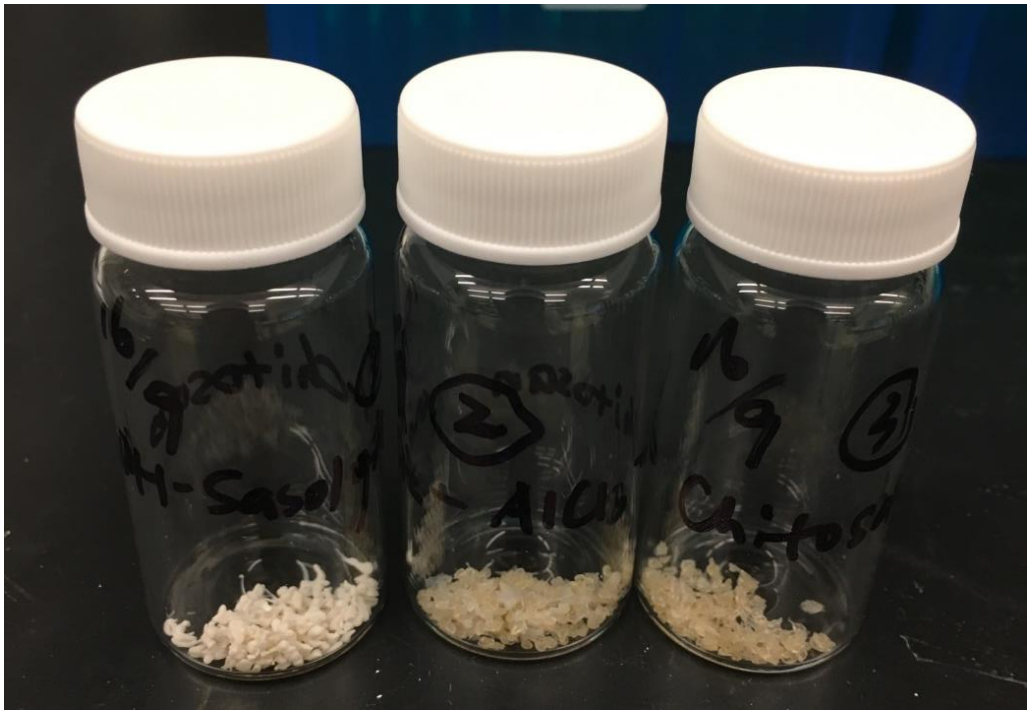

Figure 65. Picture of synthesized LDH/chitosan composite beads. Left: directly mixing beads, mixing 30% LDH-granular; middle: in-situ beads with 30% precursors as LDH part; right: pure chitosan beads.

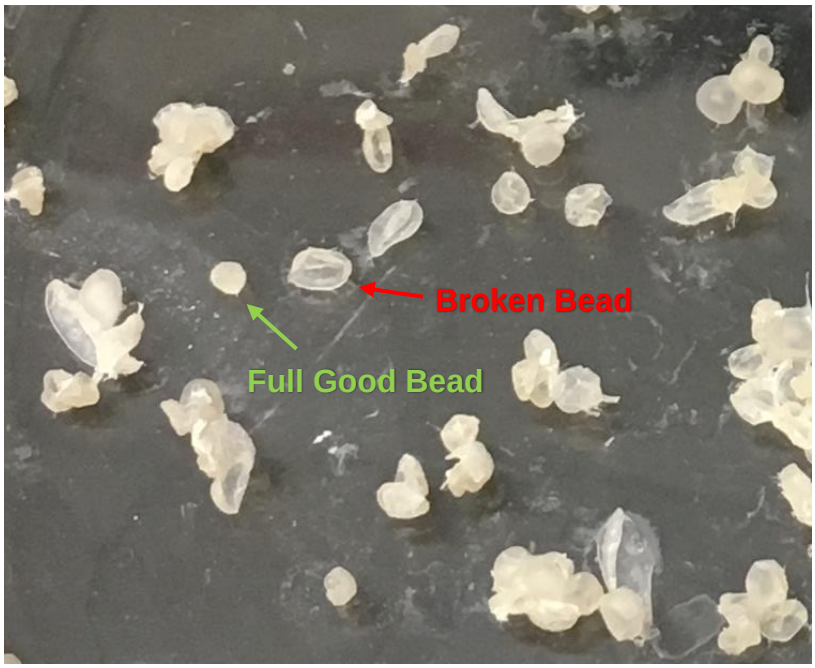

Figure 66. Picture of in-situ synthesized LDH/chitosan composite beads with 60% precursors as LDH part. Most of the beads were broken.

12.1.2. LDH/Chitosan Composite Beads Preliminary Tests

XRD of the composite beads showed both chitosan peaks, shown as the blue star, and the LDH characteristic peaks, which matched the LDH reference pattern (Figure 67), confirming that the LDH/chitosan composite beads are successfully synthesized using either the direct mixing method or the in-situ synthesis. For the beads prepared by directly mixing with 30 wt% of LDH-granular, the peak intensity was lower than the in-situ synthesized 30 wt% composite beads. This may be because some of the LDH-granular particles were not successfully embedded into the chitosan gel. Hence, there might actually be less than 30 wt% LDH inside the composite beads, but this requires further study to confirm how much LDH is really embedded into the beads. For the in-

situ synthesized composite beads, the precursors were able to be dissolved into the chitosan to make a uniform gel. As the LDH domain increased from 30 wt% to 50 wt%, the LDH peaks were more obvious compared with the chitosan peaks (blue star). However, the LDH peak intensity decreased greatly for the 60 wt% in-situ beads, which indicated that when increasing LDH domain to 60 wt%, the chitosan was not effective to adhere to the LDH and form a full bead. Most of the beads were broken and the LDH was observed in the suspension when synthesizing. This also suggested that 50 wt% is the optimum LDH ratio in making the in-situ LDH/chitosan beads.

Figure 68 shows the jar test results of selenate removal from 1 ppm spiked DI water using the composite beads with 1 g/L of the chitosan domain. For the in-situ composite beads, the wt% number indicates the nominal amount of LDH precursors added to the gel. Pure chitosan beads (0%) showed no Se(VI) removal at all, but in-situ LDH/chitosan composite beads showed increasing Se(VI) removal percentage as the ratio of LDH precursors increased (Figure 68a). The beads with 50 wt% LDH could remove more than 80% of the selenate. This indicates that the Se removal is attributed to the synthesized LDH domains inside the composite beads, since native chitosan does not display good selenium removal properties. The beads prepared by direct mixing with 30% LDH-granular showed 50% Se(VI) removal after 48 h (Figure 68b), as did the 30% in-situ beads but with slower adsorption rate. Both LDH/chitosan beads prepared had higher selenate removal efficacy compared to the native pure chitosan beads. However, comparing the directly mixed beads with same amount of LDH-granular, more than 80% Se(VI) removal can be reached by LDH-granular itself, higher than the directly mixed beads. The synthesized LDH also showed about 80% Se(VI) removal compared with the

30% in-situ beads, which is about 50% more Se(VI) that can be removed. Considering pure chitosan showed no removal at all, this may due to some of the LDH inside the chitosan beads that are not accessible to Se.

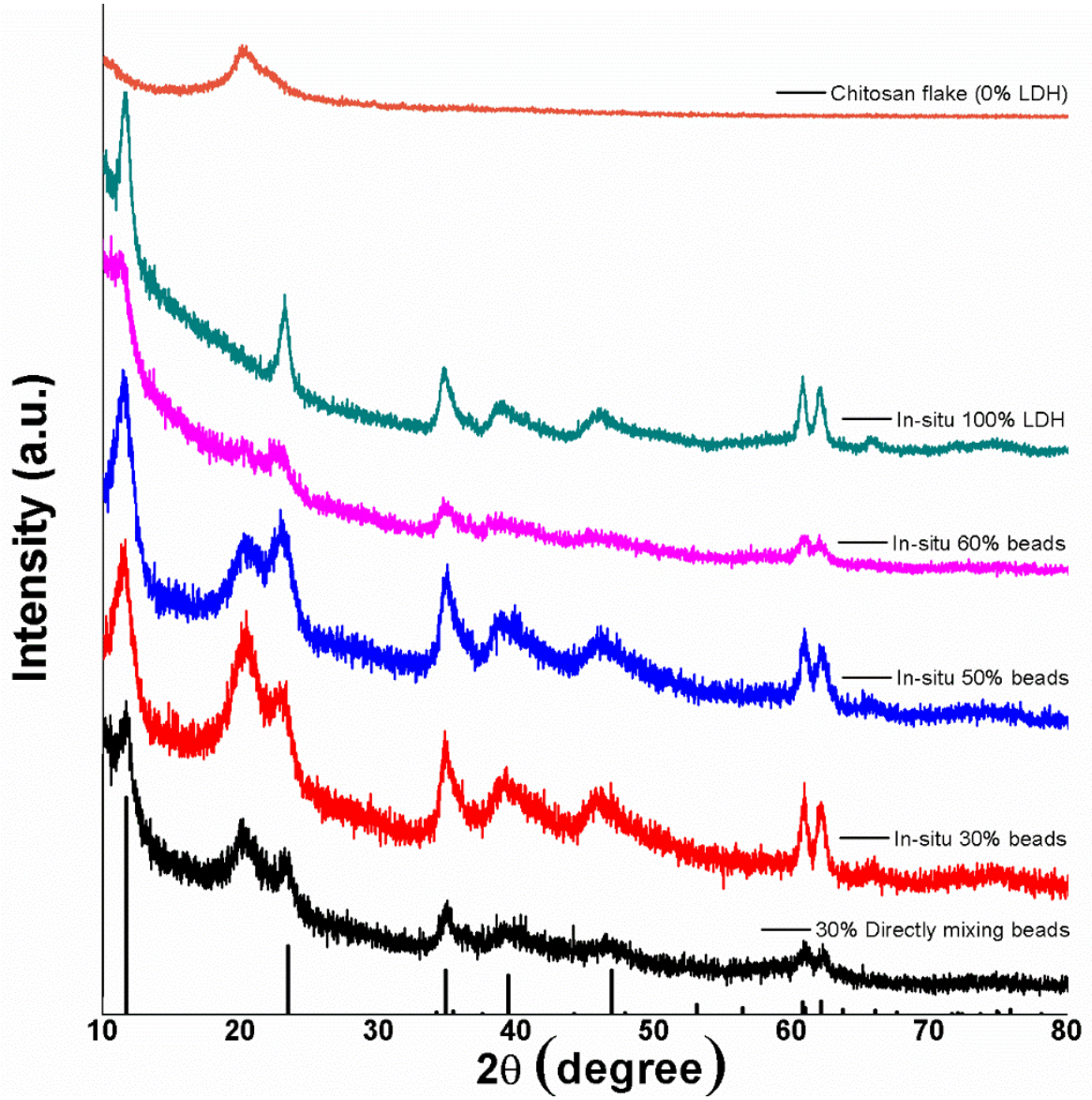

Figure 67. XRD patterns of different in-situ or directly mixed synthesized LDH/chitosan beads with percentage indicating the ratio of LDH part inside the beads, and reference pattern of $Mg_{0.667}Al_{0.333}(OH)_2(CO_3)_{0.167}(H_2O)_{0.5}$ from PDF 01-089-0460 (bottom).

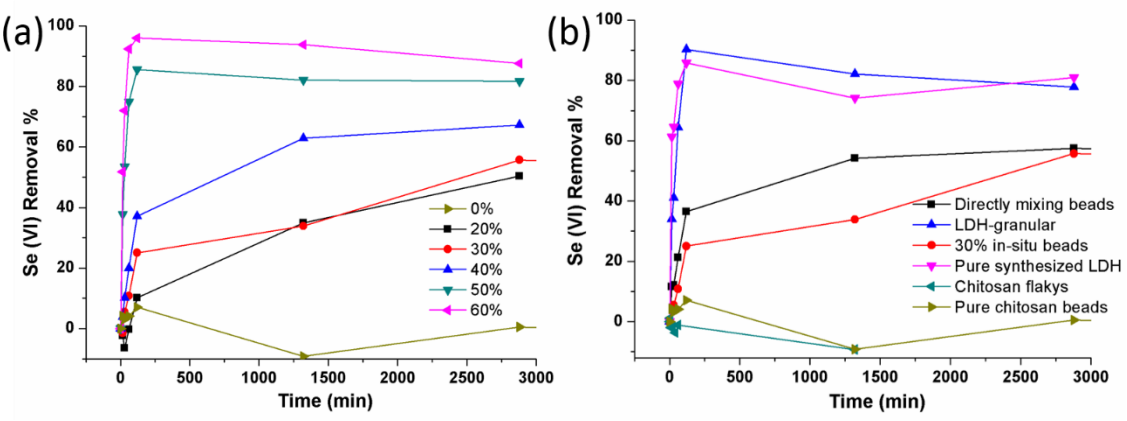

Figure 68. Percent removal of 1 ppm selenate from spiked DI water using (a) in-situ LDH/chitosan composite beads with different weight ratio of LDH precursors, and (b) different synthesis ways of making LDH/chitosan beads with 30 wt% LDH part compared with pure chitosan, pure synthesized LDH and LDH-granular. Sorbents used at a 1 g/L dosage of chitosan domain.

12.1.3. LDH/Chitosan Composite Beads Next Steps

The next steps would be to study the maximum loading capacity of the composite beads in spiked DI or SRP waters, and perform characterization such as BET, FTIR to study the binding mechanisms. As the chitosan could be interfering with some of the binding sites on the LDH, we anticipate that this could be remedied by making the chitosan porous. The selenium removal efficacy of the composites will be evaluated in small scale column tests using water obtained from SRP's Santan facility and compared to our previous data obtained on LDH media used individually. Using the breakthrough curves from the column tests, the overall capacity of the composite material (in mg Se removed per gram of sorbent material) will be obtained.

12.2. LDH/Ahlstrom Membranes

To combine LDH onto polymer membranes could be a promising way to immobilize the nanostructured LDH into a larger form factor while maintaining the high surface area of the active media. It could also enable adsorption properties for filter membranes that typically just remove particles. The membrane concept was applied to prepare composites of LDH with some commercial membranes, such as cellulose fibers. The cellulose would act as an inert substrate and scaffold for the LDH nanosheets and enable the nanosheets to be sufficiently separated from each other to maintain a high surface area. Formation of the composite is facilitated by the presence of negatively charged carboxylic acid groups in the cellulose, which can bind to the positively charged LDH, as shown in Figure 69.

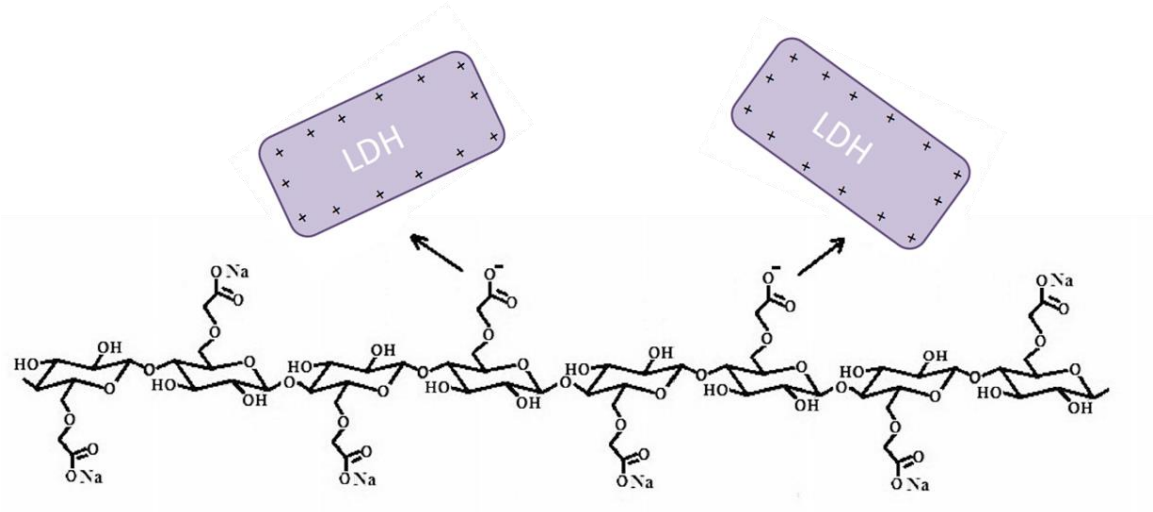

Figure 69. Depiction of LDH sequestered on a carboxymethylcellulose scaffold through electrostatic interactions between the negatively charged caroboxylic acid groups.

Ahlstrom is a high-performance fiber-based materials company, partnering with leading businesses around the world.[179] They offered us their filter membrane products made of different substrates such as cellulose filters, microglass/alumina, and activated carbon. Detailed membranes grade and type are shown in Table 25.

Table 25. Different grade of Ahlstrom filter membranes and the main components.

Grade	Type
4601	unlaminated cellulose
5281	microglass, activated alumina
5283	5281 with addition of about 70 gsm of activated carbon, heat-sealable
5284	PAC; some sheath/core synthetic fibers, heat-sealable

12.2.1. LDH/Ahlstrom Membranes Preparation

LDH-granular was dispersed in DI water and sonicated to make it into a nanosheet suspension. Ahlstrom membranes were cut into 25 mm discs and dipped in the LDH-granular suspension for 5 min so that the LDH nanosheets could bind to the surface of the membrane. The as-prepared LDH/Ahlstrom membranes were dried at 50^{o}C for a week.

12.2.2. LDH/Ahlstrom Membranes Preliminary Tests

The Se(VI) solution was prepared by spiking DI water or SRP well water (E site) with 100 ppb Se(VI). The LDH/Ahlstrom membrane (blank membrane substrates are named as the grade number XXXX; the membrane combined with LDH are named as grade number followed by LDH, i.e. XXXX-LDH) was placed on the frit in the vacuum

filtration system (Figure 70) with a valve to control the filter flow rate. 10 mL Se(VI) solution was filtered through the membrane each time, and the filtrate was collected and acidified for ICP-MS analysis.

Figure 70. Photograph of the vacuum filtration setup at ASU.

After filtering the Se(VI) spiked DI water, the results of using different membranes with or without LDH are shown in Table 26. Substrates 4601 and 5281 could only remove 30% selenate from spiked DI water, while 4601-LDH showed 85% and 5281-LDH shows 89.5% Se removal respectively. This indicates that the LDH was successfully retained on the membrane substrates, and the combined LDH helped increase the Se removal percentage. 5283 and 5284 without LDH were able to show almost 100% Se removal, which may be due to the activated carbon from the membranes. Therefore, it is hard to tell whether Se was removed by LDH or the membrane substrate itself. So, further testing would focus on 4601 and 5281.

Table 26. Results of Se(VI) concentration and Se(VI) removal percentage from spiked DI water after filter using different Ahlstrom membranes with or without coating LDH.

	Filter flow rate	**Se (ppb)**	**Removal %**
DI with Se(VI)		108.54	0
4601	fast	76.03	29.95
5281	slow	77.15	28.92
5283	medium	0.22	99.80
5284	fast	0.10	99.91
DI with Se(VI)		88.61	0
4601-LDH	fast	12.89	85.46
5281-LDH	slow	9.31	89.50
5283-LDH	medium	0.70	99.21
5284-LDH	fast	0.26	99.70

Spiked SRP well water (E site) was used for evaluating 4601 and 5281 with or without LDH. However, the filtrate results showed that the combined LDH on both of the membranes cannot markedly increase the Se removal percentage (Table 27). This may due to the very small amount of LDH deposited on the membrane by dipping, which may not be enough for removing Se from SRP water that contains very high level of other competing ions and TDS. Another possibility is that the exposure time of the filter to the water was very short and may not be sufficiently long for LDH as it requires a relatively longer retention time. Exploring this possibilities will require further study.

Table 27. Results of Se(VI) concentration and Se(VI) removal percentage from spiked SRP well water (E site) after filter using different Ahlstrom membranes with or without coating LDH.

	Filter flow rate	**Se (ppb)**	**Removal %**
E water with Se(VI)		89.76	
4601	fast	81.68	8.99
4601-LDH	slow	82.85	7.69
5281	medium	85.47	4.77
5281-LDH	Medium but slower than above	84.70	5.63

12.2.3. LDH/Ahlstrom Membranes Next Steps

The as-obtained composite membranes will need to be characterized using scanning electron microscopy to evaluate the morphology, energy dispersive X-ray spectroscopy composition mapping to identify the distribution of the LDH, X-ray diffraction to check the crystallinity of LDH was maintained, and BET analysis for surface area. The selenium removal efficacy of the combined membranes should be evaluated with longer retention time by controlling the filter flow rate or to retain more LDH onto the substrates with quantity control. Furthermore, different types of cellulose such as nanocellulose, carboxymethyl cellulose, and lignocellulose could be investigated to prepare composites in different form factors, including powders, granules, spherical beads, and sheets.

REFERENCES

(1) Yang, L.; Shahrivari, Z.; Liu, P. K. T.; Sahimi, M.; Tsotsis, T. T. Removal of Trace Levels of Arsenic and Selenium from Aqueous Solutions by Calcined and Uncalcined Layered Double Hydroxides (LDH). *Ind. Eng. Chem. Res.* **2005**, *44* (17), 6804–6815.

(2) Feeley, T. J.; Skone, T. J.; Stiegel, G. J.; McNemar, A.; Nemeth, M.; Schimmoller, B.; Murphy, J. T.; Manfredo, L. Water: A Critical Resource in the Thermoelectric Power Industry. *Energy* **2008**, *33* (1), 1–11.

(3) Wu, L. Review of 15 Years of Research on Ecotoxicology and Remediation of Land Contaminated by Agricultural Drainage Sediment Rich in Selenium. *Ecotoxicol. Environ. Saf.* **2004**, *57* (3), 257–269.

(4) Diehl, S. F.; Goldhaber, M. B.; Koenig, A. E.; Lowers, H. A.; Ruppert, L. F. Distribution of Arsenic, Selenium, and Other Trace Elements in High Pyrite Appalachian Coals: Evidence for Multiple Episodes of Pyrite Formation. *Int. J. Coal Geol.* **2012**, *94*, 238–249.

(5) Yudovich, Y. E.; Ketris, M. P. Selenium in Coal: A Review. *Int. J. Coal Geol.* **2006**, *67* (1), 112–126.

(6) Smith, K.; Lau, A. O.; Vance, F. W. Evaluation of Treatment Techniques for Selenium Removal. *70th Annu. Int. Water Conf.* **2009**, 75–92.

(7) Santos, S.; Ungureanu, G.; Boaventura, R.; Botelho, C. Selenium Contaminated Waters: An Overview of Analytical Methods, Treatment Options and Recent Advances in Sorption Methods. *Sci. Total Environ.* **2015**, *521–522* (1), 246–260.

(8) Mandal, S.; Mayadevi, S.; Kulkarni, B. D. Adsorption of Aqueous Selenite [Se(IV)] Species on Synthetic Layered Double Hydroxide Materials. *Ind. Eng. Chem. Res.* **2009**, *48*, 7893–7898.

(9) Sharrad, M. O. M.; Liu, H.; Fan, M. Evaluation of FeOOH Performance on Selenium Reduction. *Sep. Purif. Technol.* **2012**, *84*, 29–34.

(10) Lemly, A. D. Aquatic Selenium Pollution Is a Global Environmental Safety Issue. *Ecotoxicol. Environ. Saf.* **2004**, *59* (1), 44–56.

(11) Dudas, J. W. *US EPA, 2003, EPA-HQ-OW-2002-0061, FRL-8046-5*; **2006**; Vol. 71.

(12) Environmental Protection Agency. *Effluent Limitations Guidelines and Standards for the Steam Electric Power Generating Point Source Category: Final Rule*; **2015**; Vol. 80.

(13) Frankenberger, T. W.; Engberg, A. R. *Environmental Chemistry of Selenium*; CRC

Press, 1998.

(14) Torres, J.; Pintos, V.; Domínguez, S.; Kremer, C.; Kremer, E. Selenite and Selenate Speciation in Natural Waters: Interaction with Divalent Metal Ions. *J. Solut. Chem.* **2010**, *39* (1), 1–10.

(15) Nishimura, T.; Hata, R.; Hasegawa, F. Chemistry of the M (M=Fe, Ca, Ba)-Se-H2O Systems at 25 °C. *Molecules* **2009**, *14* (9), 3567–3588.

(16) Karen, H.; Mudder, T. I. Selenium Treatment Technologies & Case Studies. In *Supplemental Proceedings*; 2009.

(17) Zhang, Y.; Amrhein, C.; Frankenberger, W. T. Effect of Arsenate and Molybdate on Removal of Selenate from an Aqueous Solution by Zero-Valent Iron. *Sci. Total Environ.* **2005**, *350* (1–3), 1–11.

(18) Myneni, S. C. B.; Tokunaga, T. K.; Brown, G. E. Abiotic Selenium Redox Transformations in the Presence of Fe(II,III) Oxides. *Science (80-.).* **1997**, *278* (5340).

(19) Elrashidi, M. A.; Adriano, D. C.; Workman, S. M.; Lindsay, W. L. Chemical Equilibria of Selenium in Soils: A Theoretical Development. *Soil Sci.* **1987**, *144* (2), 141–152.

(20) Balistrieri, L. S.; Chao, T. T. Selenium Adsorption by Goethite. *Soil Sci. Soc. Am. J.* **1987**, *51* (5), 1145.

(21) Wijnja, H.; Schulthess, P. C. Vibrational Spectroscopy Study of Selenate and Sulfate Adsorption Mechanisms on Fe and Al (Hydr)oxide Surfaces. *J. Colloid Interface Sci.* **2000**, *229*, 286–297.

(22) Rovira, M.; Giménez, J.; Martínez, M.; Martínez-Lladó, X.; de Pablo, J.; Martí, V.; Duro, L. Sorption of selenium(IV) and selenium(VI) onto Natural Iron Oxides: Goethite and Hematite. *J. Hazard. Mater.* **2008**, *150* (2), 279–284.

(23) Holmes, A. B.; Gu, F. X.; Dash, G. P.; Parida, K. M.; Jin, S.; Heister, K.; Man, P.; Fraissard, J.; Reuther, H.; Soda, S.; et al. Emerging Nanomaterials for the Application of Selenium Removal for Wastewater Treatment. *Environ. Sci. Nano* **2016**, *3* (5), 982–996.

(24) Cotton, F. A. (Frank A.; Wilkinson, G.; Gaus, P. L. *Basic Inorganic Chemistry*; J. Wiley, **1995**.

(25) Yamaguchi, N. U.; Okazaki, M.; Hashitani, T. Volume Changes Due to SO_4^{2-}, SeO_4^{2-}, and $H_2PO_4^-$ Adsorption on Amorphous Iron(III) Hydroxide in an Aqueous Suspension. *J. Colloid Interface Sci.* **1999**, *209* (2), 386–391.

(26) Takeno, N. *Atlas of Eh-pH Diagrams Intercomparison of Thermodynamic Databases*; **2005**.

(27) CH2M HILL. *Review of Available Technologies for the Removal of Selenium from Water*; **2010**.

(28) Pickett, T.; Sonstegard, J.; Bonkoski, B. *Using Biology to Treat Selenium - Power Engineering*; **2006**.

(29) Lalvani, S. B. *Selenium Removal from Agricultural Drainage Water: Lab Scale Studies*; Sacramento, CA, **2004**.

(30) Jeffers, T. H.; Ferguson, C. R.; Bennett, P. G. Biosorption of Metal Contaminants Using Immobilized Biomass-A Laboratory Study.

(31) Qian, S.; Huang, G.; Jiang, J.; He, F.; Wang, Y. Studies of Adsorption Behavior of Crosslinked Chitosan for Cr(VI), Se(VI). *J. Appl. Polym. Sci.* **2000**, *77* (14), 3216–3219.

(32) Trussell, R. A.; Trussell, A.; Kreft, P. *Selenium Removal from Ground Water Using Activated Alumina*; USEPA: Washington,DC., 1980.

(33) Trussell, R. A.; Trussel, A.; Kraft, P. Selenium Removal with Activated Alumina. *AWWA Res. Found. Water Qual. Res. News* **1991**, *19*, 4–5.

(34) Su, C.; Suarez, D. L. Selenate and Selenite Sorption on Iron Oxides. *Soil Sci. Soc. Am. J.* **2000**, *64* (1), 101.

(35) Hagelstein, K.; Mudder, T. I. Selenium Treatment Technologies and Case Studies. *TMS 2009 138th Annu. Meet. Exhib. Suppl. Proc.* **2009**, *3*, 77–88.

(36) Séby, F.; Potin-Gautier, M.; Giffaut, E.; Borge, G.; Donard, O. F. . A Critical Review of Thermodynamic Data for Selenium Species at 25°C. *Chem. Geol.* **2001**, *171* (3), 173–194.

(37) Tchounwou, P. B.; Patlolla, A. K.; Centeno, J. A. Carcinogenic and Systemic Health Effects Associated with Arsenic Exposure--a Critical Review. *Toxicol. Pathol.* **2003**, *31* (6), 575–588.

(38) Mohan, D.; Pittman Jr, C. U. Arsenic Removal from Water/wastewater Using Adsorbents - a Critical Review. *J. Hazard. Mater.* **2007**, *142* (1), 1–53.

(39) Brunauer, S.; Emmett, P. H.; Teller, E. Adsorption of Gases in Multimolecular Layers. *J. Am. Chem. Soc.* **1938**, *60* (2), 309–319.

(40) Langmuir, I. The Adsorption of Gases on Plane Surfaces of Glass, Mica and Platinum. *J. Am. Chem. Soc.* **1918**, *40* (9), 1361–1403.

(41) Montgomery, J. M. *Water Treatment Principles and Design* ; John Wiley & Sons: New York, **1985**.

(42) Huang, C. P.; Wu, M. H. The Removal of Chromium (VI) from Dilute Aqueous Solution by Activated Carbon. *Water Res.* **1977**, *11* (8), 673–679.

(43) Rivera-Utrilla, J.; Sánchez-Polo, M.; Gómez-Serrano, V.; Alvarez, P. M.; Alvim-Ferraz, M. C. M.; Dias, J. M. Activated Carbon Modifications to Enhance Its Water Treatment Applications. An Overview. *J. Hazard. Mater.* **2011**, *187* (1–3), 1–23.

(44) Asadullah, M.; Jahan, I.; Ahmed, M. B.; Adawiyah, P.; Malek, N. H.; Rahman, M. S. Preparation of Microporous Activated Carbon and Its Modification for Arsenic Removal from Water. *J.Ind.Eng.Chem.* **2014**, *20* (3), 887–896.

(45) Hu, Z.; Lei, L.; Li, Y.; Ni, Y. Chromium Adsorption on High-Performance Activated Carbons from Aqueous Solution. *Sep.Purif.Technol.* **2003**, *31* (1), 13–18.

(46) Chandra, V.; Kim, K. S. Highly Selective Adsorption of Hg2+ by a Polypyrrole–reduced Graphene Oxide Composite. *Chem. Commun.* **2011**, *47* (13), 3942–3944.

(47) Chandra, V.; Park, J.; Chun, Y.; Lee, J. W.; Hwang, I.-C.; Kim, K. S. Water-Dispersible Magnetite-Reduced Graphene Oxide Composites for Arsenic Removal. *ACS Nano* **2010**, *4* (7), 3979–3986.

(48) Vadahanambi, S.; Lee, S. H.; Kim, W. J.; Oh, I. K. Arsenic Removal from Contaminated Water Using Three-Dimensional Graphene-Carbon Nanotube-Iron Oxide Nanostructures. *Environ. Sci. Technol.* **2013**, *47* (18), 10510–10517.

(49) Di, Z. C.; Ding, J.; Peng, X. J.; Li, Y. H.; Luan, Z. K.; Liang, J. Chromium Adsorption by Aligned Carbon Nanotubes Supported Ceria Nanoparticles. *Chemosphere* **2006**, *62* (5), 861–865.

(50) Jabeen, H.; Chandra, V.; Jung, S.; Lee, J. W.; Kim, K. S.; Kim, S. B. Enhanced Cr (VI) Removal Using Iron Nanoparticle Decorated Graphene. *Nanoscale* **2011**, *3* (9), 3583–3585.

(51) Fu, Y.; Wang, J.; Liu, Q.; Zeng, H. Water-Dispersible Magnetic Nanoparticle–graphene Oxide Composites for Selenium Removal. *Carbon N. Y.* **2014**, *77*, 710–721.

(52) Jia, G.; Wang, H.; Yan, L.; Wang, X.; Pei, R.; Yan, T.; Zhao, Y.; Guo, X. Cytotoxicity of Carbon Nanomaterials: Single-Wall Nanotube, Multi-Wall Nanotube, and Fullerene. *Environ. Sci. Technol.* **2005**, *39* (5), 1378–1383.

(53) Seabra, A. B.; Paula, A. J.; de Lima, R.; Alves, O. L.; Durán, N. Nanotoxicity of Graphene and Graphene Oxide. *Chem.Res.Toxicol.* **2014**, *27* (2), 159–168.

(54) Hu, X.; Kang, J.; Lu, K.; Zhou, R.; Mu, L.; Zhou, Q. Graphene Oxide Amplifies the Phytotoxicity of Arsenic in Wheat. *Sci. Rep.* **2014**, *4*.

(55) Wang, C.; Wang, Y.; Graser, J.; Zhao, R.; Gao, F.; O'Connell, M. J. Solution-Based Carbohydrate Synthesis of Individual Solid, Hollow, and Porous Carbon Nanospheres Using Spray Pyrolysis. *ACS Nano* **2013**, *7* (12), 11156–11165.

(56) Zhao, Q. L.; Zhang, Z. L.; Huang, B. H.; Peng, J.; Zhang, M. Facile Preparation of Low Cytotoxicity Fluorescent Carbon Nanocrystals by Electrooxidation of Graphite. *Chem. Commun.* **2008**, No. 41, 5116–5118.

(57) Zhang, R.; Liu, Y. B.; Sun, S. Q. Preparation of Highly Luminescent and Biocompatible Carbon Dots Using a New Extraction Method. *J. Nanopart. Res.* **2013**, *15* (10), 1–12.

(58) Cooper, A. M.; Hristovski, K. D.; Möller, T.; Westerhoff, P.; Sylvester, P. The Effect of Carbon Type on Arsenic and Trichloroethylene Removal Capabilities of Iron (Hydr)oxide Nanoparticle-Impregnated Granulated Activated Carbons. *J. Hazard. Mater.* **2010**, *183* (1), 381–388.

(59) Jain, A. Fabrication and Evaluation of Hematite Modified Granular Activated Carbon (GAC) Media for Arsenic Removal from Groundwater, Arizona State University, 2011.

(60) Sandoval, R.; Cooper, A. M.; Aymar, K.; Jain, A.; Hristovski, K. Removal of Arsenic and Methylene Blue from Water by Granular Activated Carbon Media Impregnated with Zirconium Dioxide Nanoparticles. *J. Hazard. Mater.* **2011**, *193*, 296–303.

(61) Wang, C.; O'Connell, M. J.; Chan, C. K. Facile One-Pot Synthesis of Highly Porous Carbon Foams for High-Performance Supercapacitors Using Template-Free Direct Pyrolysis. *ACS Appl. Mater. Interfaces* **2015**, *7* (16), 8952–8960.

(62) Hanigan, D.; Zhang, J.; Herckes, P.; Krasner, S. W.; Chen, C.; Westerhoff, P. Adsorption of N-Nitrosodimethylamine Precursors by Powdered and Granular Activated Carbon. *Environ. Sci. Technol.* **2012**, *46* (22), 12630–12639.

(63) Sing, K. S. W.; Everett, D. H. Reporting Physisorption Data for Gas/solid Systems with Special Reference to the Determination of Surface Area and Porosity (Recommendations 1984). *Pure Appl. Chem.* **1985**, *57* (4), 603–619.

(64) Li, M.; Wang, C.; O'Connell, M. J.; Chan, C. K.; Huang, C. P.; Wu, M. H.; Rivera-Utrilla, J.; Sánchez-Polo, M.; Gómez-Serrano, V.; Alvarez, P. M.; et al. Carbon Nanosphere Adsorbents for Removal of Arsenate and Selenate from Water. *Environ. Sci. Nano* **2015**, *2* (3), 245–250.

(65) Corapcioglu, M. O.; Huang, C. P. The Surface Acidity and Characterization of Some Commercial Activated Carbons. *Carbon N. Y.* **1987**, *25* (4), 569–578.

(66) Chingombe, P.; Saha, B.; Wakeman, R. J. Surface Modification and Characterisation of a Coal-Based Activated Carbon. *Carbon N. Y.* **2005**, *43* (15), 3132–3143.

(67) Boehm, H. P. Surface Oxides on Carbon and Their Analysis: A Critical Assessment. *Carbon N. Y.* **2002**, *40* (2), 145–149.

(68) Jordan, N.; Foerstendorf, H.; Weiß, S.; Heim, K.; Schild, D.; Brendler, V. Sorption of selenium(VI) onto Anatase: Macroscopic and Microscopic Characterization. *Geochim. Cosmochim. Acta* **2011**, *75* (6), 1519–1530.

(69) Jegadeesan, G.; Mondal, K.; Lalvani. Selenate Removal from Sulfate Containing Aqueous Solutions. *Environ. Technol.* **2005**, *26* (10), 1181–1188.

(70) Montes-Navajas, P.; Asenjo, N. G.; Santamaría, R.; Menendez, R.; Corma, A.; García, H. Surface Area Measurement of Graphene Oxide in Aqueous Solutions. *Langmuir* **2013**, *29* (44), 13443–13448.

(71) Dreyer, D. R.; Park, S.; Bielawski, C. W.; Ruoff, R. S. The Chemistry of Graphene Oxide. *Chem. Soc. Rev.* **2010**, *39* (1), 228–240.

(72) Johns, J. E.; Hersam, M. C. Atomic Covalent Functionalization of Graphene. *Acc. Chem. Res.* **2013**, *46* (1), 77–86.

(73) Szabo, T.; Tombacz, E.; Illes, E.; Dekany, I. Enhanced Acidity and pH-Dependent Surface Charge Characterization of Successfully Oxidized Graphite Oxides,. *Carbon N. Y.* **2006**, *44* (3), 537–545.

(74) US EPA. Arsenic Treatment Technology Evaluation Handbook for Small Systems. 2003, p 151.

(75) Hu, J.; Chen, C.; Zhu, X.; Wang, X. Removal of Chromium from Aqueous Solution by Using Oxidized Multiwalled Carbon Nanotubes. *J. Hazard. Mater.* **2009**, *162* (2), 1542–1550.

(76) Mandich, N. V; Lalvani, S. B.; Wiltkowski, T.; Lalvani, L. S. Selective Removal of Chromate Anion by a New Carbon Adsorbent. *Met. Finish.* **1998**, *96* (5), 39–44.

(77) Eguez, H. E.; Cho, E. H. Adsorption of Arsenic on Activated Charcoal. *JOM-US* **1987**, *39* (7), 38–41.

(78) Lorenzen, L.; van Deventer, J. S. J.; Landi, W. M. Factors Affecting the Mechanism of the Adsorption of Arsenic Species on Activated Carbon. *Miner. Eng.* **1995**, *8* (4), 557–569.

(79) Peng, X.; Luan, Z.; Ding, J.; Di, Z.; Li, Y.; Tian, B. Ceria Nanoparticles Supported on Carbon Nanotubes for the Removal of Arsenate from Water. *Mater. Lett.* **2005**, *59* (4), 399–403.

(80) Gu, Z.; Fang, J.; Deng, B. Preparation and Evaluation of GAC-Based Iron-Containing Adsorbents for Arsenic Removal. *Environ. Sci. Technol.* **2005**, *39* (10), 3833–3843.

(81) Chang, Q.; Lin, W.; Ying, W. Preparation of Iron-Impregnated Granular Activated Carbon for Arsenic Removal from Drinking Water. *J. Hazard. Mater.* **2010**, *184* (1), 515–522.

(82) Balistrieri, L. S.; Chao, T. T. Selenium Adsorption by Goethite. *Soil Sci. Soc. Am. J.* **1987**, *51* (5), 1145.

(83) Montes-Moran, M. A.; Suarez, D.; Menéndez, J. A.; Fuente, E. On the Nature of Basic Sites on Carbon Surfaces: An Overview. *Carbon N. Y.* **2004**, *42* (7), 1219–1225.

(84) Posselt, H. S.; Anderson, F. J.; Weber, W. J. Cation Sorption on Colloidal Hydrous Manganese Dioxide. *Environ. Sci. Technol.* **1968**, *2* (12), 1087–1093.

(85) Hanson, A.; Bates, J.; Heil, D.; Bristol, A. Arsenic Removal from Water Using Manganese Greensand: Laboratory Scale Batch and Column Studies. *Water Treat. Technol. Rep.* **1999**, *41*.

(86) Patrick, H.; Jannie, M.; Jacqueline, B. Barium Carbonate Process for Sulphate and Metal Removal from Mine Water. In *9th International Mine Water Congress*; **2007**; Vol. 26, pp 11–20.

(87) Geldenhuys, A. J.; Maree, J. P.; de Beer, M.; Hlabela, P. An Integrated Limestone/lime Process for Partial Sulphate Removal. *J. South African Inst. Min. Metall.* **2003**.

(88) Das, J.; Patra, B. S.; Baliarsingh, N.; Parida, K. M. Adsorption of Phosphate by Layered Double Hydroxides in Aqueous Solutions. *Appl. Clay Sci.* **2006**, *32* (3–4), 252–260.

(89) Ookubo, A.; Ooi, K.; Hayashi, H. Preparation and Phosphate Ion-Exchange Properties of a Hydrotalcite-like Compound. *Langmuir* **1993**, *9* (5), 1418–1422.

(90) Miyata, S. Anion-Exchange Properties of Hydrotalcite-like Compounds. *Clays Clay Miner.* **1983**, *31* (4), 305–311.

(91) Parker, L. M.; Milestone, N. B.; Newman, R. H. The Use of Hydrotalcite as an Anion Absorbent. *Ind. Eng. Chem. Res.* **1995**, *34* (4), 1196–1202.

(92) Cavani, F.; Trifirò, F.; Vaccari, A. Hydrotalcite-Type Anionic Clays: Preparation, Properties and Applications. *Catal. Today* **1991**, *11* (2), 173–301.

(93) de Roy, A.; Forano, C.; Malki, K. El; Besse, J.-P. Anionic Clays: Trends in Pillaring Chemistry. In *Expanded Clays and Other Microporous Solids*; Springer US: Boston, MA, **1992**; pp 108–169.

(94) Hou, W.-G.; Su, Y.-L.; Sun, D.-J.; Zhang, C.-G. Studies on Zero Point of Charge and Permanent Charge Density of Mg−Fe Hydrotalcite-like Compounds. *Langmuir* **2001**, *17* (6), 1885–1888.

(95) You, Y.; Vance, G. F.; Zhao, H. Selenium Adsorption on Mg–Al and Zn–Al Layered Double Hydroxides. *Appl. Clay Sci.* **2001**, *20* (1), 13–25.

(96) Palmer, S. J.; Frost, R. L.; Nguyen, T. Hydrotalcites and Their Role in Coordination of Anions in Bayer Liquors: Anion Binding in Layered Double Hydroxides. *Coord. Chem. Rev.* **2009**, *253* (1), 250–267.

(97) Sato, T.; Wakabayashi, T.; Shimada, M. Adsorption of Various Anions by Magnesium Aluminum Oxide of ($Mg_{0.7}Al_{0.3}O_{1.15}$). *Ind. Eng. Chem. Prod. Res. Dev.* **1986**, *25* (1), 89–92.

(98) Theiss, F. L.; Palmer, S. J.; Ayoko, G. A.; Frost, R. L. Sulfate Intercalated Layered Double Hydroxides Prepared by the Reformation Effect. *J. Therm. Anal. Calorim.* **2012**, *107* (3), 1123–1128.

(99) Theiss, F. L.; Ayoko, G. A.; Frost, R. L. Thermogravimetric Analysis of Selected Layered Double Hydroxides. *J. Therm. Anal. Calorim.* **2013**, *112* (2), 649–657.

(100) Miyata, S. Physico-Chemical Properties of Synthetic Hydrotalcites in Relation to Composition. *Clays Clay Miner.* **1980**, *28* (1), 50–56.

(101) Goh, K. H.; Lim, T. T.; Dong, Z. Application of Layered Double Hydroxides for Removal of Oxyanions: A Review. *Water Res.* **2008**, *42* (6–7), 1343–1368.

(102) Châtelet, L.; Bottero, J. Y.; Yvon, J.; Bouchelaghem, A. Competition between Monovalent and Divalent Anions for Calcined and Uncalcined Hydrotalcite: Anion Exchange and Adsorption Sites. *Colloids Surfaces A Physicochem. Eng. Asp.* **1996**, *111* (3), 167–175.

(103) Carja, G.; Nakamura, R.; Niiyama, H. Tailoring the Porous Properties of Iron Containing Mixed Oxides for As (V) Removal from Aqueous Solutions. *Microporous Mesoporous Mater.* **2005**, *83* (1–3), 94–100.

(104) Lazaridis, N. K. Sorption Removal of Anions and Cations in Single Batch Systems by Uncalcined and Calcined Mg-Al-CO_3. *Water. Air. Soil Pollut.* **2003**, *146* (1/4), 127–139.

(105) Chubar, N.; Gerda, V.; Megantari, O.; Mičušík, M.; Omastova, M.; Heister, K.; Man, P.; Fraissard, J. Applications versus Properties of Mg–Al Layered Double Hydroxides Provided by Their Syntheses Methods: Alkoxide and Alkoxide-Free Sol–gel Syntheses and Hydrothermal Precipitation. *Chem. Eng. J.* **2013**, *234*, 284–299.

(106) Das, D. P.; Das, J.; Parida, K. Physicochemical Characterization and Adsorption Behavior of Calcined Zn/Al Hydrotalcite-like Compound (HTlc) towards Removal of Fluoride from Aqueous Solution. *J. Colloid Interface Sci.* **2003**, *261* (2), 213–220.

(107) Chubar, N.; Szlachta, M. Static and Dynamic Adsorptive Removal of Selenite and Selenate by Alkoxide-Free Sol-Gel-Generated Mg-Al-CO_3 Layered Double Hydroxide: Effect of Competing Ions. *Chem. Eng. J.* **2015**, *279*, 885–896.

(108) Chubar, N. EXAFS and FTIR Studies of Selenite and Selenate Sorption by Alkoxide-Free Sol–gel Generated Mg–Al–CO_3 Layered Double Hydroxide with Very Labile Interlayer Anions. *J. Mater. Chem. A* **2014**, *2* (38), 15995–16007.

(109) Hussein, M. Z. Bin; Zainal, Z.; Choong, E. M. Structure and Surface Transformations of Humic-Adsorbed Synthetic Hydrotalcite-like Materials. *J. Porous Mater.* **2001**, *8* (3), 219–226.

(110) Costantino, U.; Marmottini, F.; Nocchetti, M.; Vivani, R. New Synthetic Routes to Hydrotalcite-like Compounds − Characterisation and Properties of the Obtained Materials. *Eur. J. Inorg. Chem.* **1998**, *1998* (10), 1439–1446.

(111) Lee, J.; Rhee, S.; Jung, D.-Y. Orientation-Controlled Assembly and Solvothermal Ion-Exchange of Layered Double Hydroxide Nanocrystals. *Chem. Commun. (Camb).* **2003**, No. c, 2740–2741.

(112) Bellotto, M.; Rebours, B.; Clause, O.; Lynch, J.; Bazin, D.; Elkaïm, E. A Re-Examination of Hydrotalcite Crystal Chemistry. *J. Phys. Chem.* **1996**, *10* (96), 8527–8534.

(113) Dékány, I.; Berger, F.; Imrik, K.; Lagaly, G. Hydrophobic Layered Double Hydroxides (LDHs): Selective Adsorbents for Liquid Mixtures. *Colloid Polym. Sci.* **1997**, *275* (7), 681–688.

(114) Hu, G.; Wang, N.; O'Hare, D.; Davis, J. One-Step Synthesis and AFM Imaging of Hydrophobic LDH Monolayers. *Chem. Commun. (Camb).* **2006**, *1* (3), 287–289.

(115) Rattanaoudom, R.; Visvanathan, C.; Boontanon, S. K. Removal of Concentrated PFOS and PFOA in Synthetic Industrial Wastewater by Powder Activated Carbon and Hydrotalcite. *J. Water Sustain.* **2012**, *2* (4), 245–258.

(116) Yang, W.; Kim, Y.; Liu, P. K. T.; Sahimi, M.; Tsotsis, T. T. A Study by in Situ Techniques of the Thermal Evolution of the Structure of a Mg–Al–CO_3 Layered Double Hydroxide. *Chem. Eng. Sci.* **2002**, *57* (15), 2945–2953.

(117) Khitous, M.; Salem, Z.; Halliche, D. Effect of Interlayer Anions on Chromium Removal Using Mg – Al Layered Double Hydroxides : Kinetic , Equilibrium and Thermodynamic Studies. *Chinese J. Chem. Eng.* **2015**, *In Press,*.

(118) El Gaini, L.; Lakraimi, M.; Sebbar, E.; Meghea, A.; Bakasse, M. Removal of Indigo Carmine Dye from Water to Mg–Al–CO_3-Calcined Layered Double Hydroxides. *J. Hazard. Mater.* **2009**, *161* (2), 627–632.

(119) Martinez-Gallegos, S.; Pfeiffer, H.; Lima, E.; Espinosa, M.; Bosch, P.; Bulbulian, S. Cr(VI) Immobilization in Mixed (Mg,Al) Oxides. *Microporous Mesoporous Mater.* **2006**, *94* (1), 234–242.

(120) Kameda, T.; Yoshioka, T.; Mitsuhashi, T.; Uchida, M.; Okuwaki, A. *The Simultaneous Removal of Calcium and Chloride Ions from Calcium Chloride*

Solution Using Magnesium–aluminum Oxide; 2003; Vol. 37.

(121) Faust, S. D.; Aly, O. M. *Adsorption Processes for Water Treatment*; 1987.

(122) Yamani, J. S.; Lounsbury, A. W.; Zimmerman, J. B. Adsorption of Selenite and Selenate by Nanocrystalline Aluminum Oxide, Neat and Impregnated in Chitosan Beads. *Water Res.* **2014**, *50*, 373–381.

(123) Fu, Y.; Wang, J.; Liu, Q.; Zeng, H. Water-Dispersible Magnetic Nanoparticle–graphene Oxide Composites for Selenium Removal. *Carbon N. Y.* **2014**, *77*, 710–721.

(124) Martínez, M.; Giménez, J.; de Pablo, J.; Rovira, M.; Duro, L. Sorption of selenium(IV) and selenium(VI) onto Magnetite. *Appl. Surf. Sci.* **2006**, *252* (10), 3767–3773.

(125) Gonzalez, C. M.; Hernandez, J.; Parsons, J. G.; Gardea-Torresdey, J. L. A Study of the Removal of Selenite and Selenate from Aqueous Solutions Using a Magnetic Iron/manganese Oxide Nanomaterial and ICP-MS. *Microchem. J.* **2010**, *96*, 324–329.

(126) Gonzalez, C. M.; Hernandez, J.; Parsons, J. G.; Gardea-Torresdey, J. L. Adsorption of Selenite and Selenate by a High- and Low- Pressure Aged Manganese Oxide Nanomaterial. *Instrum. Sci. Technol.* **2011**, *39* (1), 1–19.

(127) Bleiman, N.; Mishael, Y. G. Selenium Removal from Drinking Water by Adsorption to Chitosan–clay Composites and Oxides: Batch and Columns Tests. *J. Hazard. Mater.* **2010**, *183* (1), 590–595.

(128) Chan, Y. T.; Kuan, W. H.; Chen, T. Y.; Wang, M. K. Adsorption Mechanism of Selenate and Selenite on the Binary Oxide Systems. *Water Res.* **2009**, *43* (17), 4412–4420.

(129) Zhong, L.; Cao, Y.; Li, W.; Xie, K.; Pan, W.-P. Selenium Speciation in Flue Desulfurization Residues. *J. Environ. Sci.* **2011**, *23* (1), 171–176.

(130) Lenz, M.; Floor, G. H.; Winkel, L. H. E.; Román-Ross, G.; Corvini, P. F. X. Online Preconcentration-IC-ICP-MS for Selenium Quantification and Speciation at Ultratraces. *Environ. Sci. Technol.* **2012**, *46* (21), 11988–11994.

(131) Jegadeesan, G.; Mondal, K.; Lalvani. Selenate Removal from Sulfate Containing Aqueous Solutions. *Environ. Technol.* **2005**, *26* (10), 1181–1188.

(132) Parker, L. M.; Milestone, N. B.; Newman, R. H. The Use of Hydrotalcite as an Anion Absorbent. *Ind. Eng. Chem. Res.* **1995**, *34* (4), 1196–1202.

(133) Tan, T.; Beydoun, D.; Amal, R. Effects of Organic Hole Scavengers on the Photocatalytic Reduction of Selenium Anions. *J. Photochem. Photobiol. A Chem.* **2003**, *159* (3), 273–280.

(134) Kosmulski, M. The pH-Dependent Surface Charging and the Points of Zero Charge. *J. Colloid Interface Sci.* **2002**, *253* (1), 77–87.

(135) Walcarius, A.; Devoy, J.; Bessière, J. Interactions of Selenate with Copper(I) Oxide Particles. *Langmuir* **2004**, *20* (15), 6335–6343.

(136) Lefèvre, G.; Walcarius, A.; Ehrhardt, J. J.; Bessière, J. Sorption of Iodide on Cuprite (Cu2O). *Langmuir* **2000**, *16* (10), 4519–4527.

(137) Reddy, K. J.; Zhang, Z.; Blaylock, M. J.; Vance, G. F. Method for Detecting Selenium Speciation in Groundwater. *Environ. Sci. Technol.* **1995**, *29* (7), 1754–1759.

(138) Volesky, B.; Holan, Z. R. Biosorption of Heavy Metals. *Biotechnol. Prog.* **1995**, *11* (3), 235–250.

(139) Boddu, V. M.; Abburi, K.; Talbott, J. L.; Smith, E. D. Removal of Hexavalent Chromium from Wastewater Using a New Composite Chitosan Biosorbent. *Environ. Sci. Technol.* **2003**, *37* (19), 4449–4456.

(140) Saifuddin M, N.; Kumaran, P. Removal of Heavy Metal from Industrial Wastewater Using Chitosan Coated Oil Palm Shell Charcoal. *Electron. J. Biotechnol.* **2005**, *8* (1), 43–53.

(141) Deans, J.; Dixon, B. Uptake of Pb2+ and Cu2+ by Novel Biopolymers. *Water Res.* **1992**, *26* (4), 469–472.

(142) Bissen, M.; Frimmel, F. H. Arsenic - A Review. Part II: Oxidation of Arsenic and Its Removal in Water Treatment. *Acta Hydrochim. Hydrobiol.* **2003**, *31* (2), 97–107.

(143) Golder Associates Inc. Literature Review of Treatment Technologies to Remove Selenium from Mining Influenced Water. **2009**.

(144) Adlem, C. J. L.; Maree, J. P.; Plessis, P. DU. Treatment of Sulphate-Rich Mining Effiuents with the Barium Hydroxide Process and Recovery of Valuable by-Products. *4th Int. Miner. Water Assoc. Congr.* **1991**, No. September 1991, 211–222.

(145) Reinsel, M. Sulfate removal technologies: A review http://www.wateronline.com/doc/sulfate-removal-technologies-a-review-0001.

(146) Westerhoff, P.; Highfield, D.; Badruzzaman, M.; Yoon, Y. Rapid Small-Scale Column Tests for Arsenate Removal in Iron Oxide Packed Bed Columns. *J. Environ. Eng.* **2005**, *131* (2), 262–271.

(147) Badruzzaman, M.; Westerhoff, P.; Knappe, D. R. U. Intraparticle Diffusion and Adsorption of Arsenate onto Granular Ferric Hydroxide (GFH). *Water Res.* **2004**, *38* (18), 4002–4012.

(148) Lazaridis, N. K.; Asouhidou, D. D. Kinetics of Sorptive Removal of chromium(VI) from Aqueous Solutions by Calcined Mg–Al–CO_3 Hydrotalcite. *Water Res.* **2003**, *37* (12), 2875–2882.

(149) Álvarez-Ayuso, E.; Nugteren, H. W. Purification of chromium(VI) Finishing Wastewaters Using Calcined and Uncalcined Mg-Al-CO_3-Hydrotalcite. *Water Res.* **2005**, *39* (12), 2535–2542.

(150) Liang, X.; Zang, Y.; Xu, Y.; Tan, X.; Hou, W.; Wang, L.; Sun, Y. Sorption of Metal Cations on Layered Double Hydroxides. *Colloids Surfaces A Physicochem. Eng. Asp.* **2013**, *433*, 122–131.

(151) Sorg, T. J. Methods for Removing Uranium From Drinking Water. *J. / Am. Water Work. Assoc.* **1988**, *80* (7), 105–111.

(152) Zhang, X.; Ji, L.; Wang, J.; Li, R.; Liu, Q.; Zhang, M.; Liu, L. Removal of uranium(VI) from Aqueous Solutions by Magnetic Mg–Al Layered Double Hydroxide Intercalated with Citrate: Kinetic and Thermodynamic Investigation. *Colloids Surfaces A Physicochem. Eng. Asp.* **2012**, *414*, 220–227.

(153) Hamidi, R.; Kahforoushan, D.; Fatehifar, E. The Simultaneous Removal of Calcium, Magnesium and Chloride Ions from Industrial Wastewater Using Magnesium–aluminum Oxide. *J. Environ. Sci. Heal. Part A* **2013**, *48* (10), 1225–1230.

(154) Jobbágy, M.; Regazzoni, A. E. Dissolution of Nano-Size Mg–Al–Cl Hydrotalcite in Aqueous Media. *Appl. Clay Sci.* **2011**, *51* (3), 366–369.

(155) Starukh, G. M. Study of Tetracycline Adsorption by Zn-Al Mixed Oxides and Layered Double Hydroxides. *Chem. Phys. Technol. Surf.* **2015**, *6*, 169–178.

(156) Huang, P.-P.; Cao, C.-Y.; Wei, F.; Sun, Y.-B.; Song, W.-G. MgAl Layered Double Hydroxides with Chloride and Carbonate Ions as Interlayer Anions for Removal of Arsenic and Fluoride Ions in Water. *RSC Adv.* **2015**, *5* (14), 10412–10417.

(157) López, T.; Bosch, P.; Asomoza, M.; Gómez, R.; Ramos, E. DTA-TGA and FTIR Spectroscopies of Sol-Gel Hydrotalcites: Aluminum Source Effect on Physicochemical Properties. *Mater. Lett.* **1997**, *31* (3), 311–316.

(158) Schmidt, L. D. *The Engineering of Chemical Reactions*; **2005**.

(159) Mann, U. *Principles of Chemical Reactor Analysis and Design*; John Wiley & Sons, Inc.: Hoboken, NJ, USA, **2009**.

(160) Michaud, J. S.; Boyle, K. J.; Smith, A. E. Cost Effective Arsenic Reductions in Private Well Water in Maine. *J. Am. Water Resour. Assoc.* **2006**, *42* (5), 1237–1245.

(161) Han, R.; Zou, L.; Zhao, X.; Xu, Y.; Xu, F.; Li, Y.; Wang, Y. Characterization and

Properties of Iron Oxide-Coated Zeolite as Adsorbent for Removal of copper(II) from Solution in Fixed Bed Column. *Chem. Eng. J.* **2009**, *149*, 123–131.

(162) Yadanaparthi, S. K. R.; Graybill, D.; von Wandruszka, R. Adsorbents for the Removal of Arsenic, Cadmium, and Lead from Contaminated Waters. *J. Hazard. Mater.* **2009**, *171* (1–3), 1–15.

(163) Bajpai, S. K.; Chand, N.; Chaurasia, V. Nano Zinc Oxide-Loaded Calcium Alginate Films with Potential Antibacterial Properties. *Food Bioprocess Technol.* **2012**, *5* (5), 1871–1881.

(164) Sarkar, S.; Guibal, E.; Quignard, F.; SenGupta, A. K. Polymer-Supported Metals and Metal Oxide Nanoparticles: Synthesis, Characterization, and Applications. *J. Nanoparticle Res.* **2012**, *14* (2), 715.

(165) Yamani, J. S.; Miller, S. M.; Spaulding, M. L.; Zimmerman, J. B. Enhanced Arsenic Removal Using Mixed Metal Oxide Impregnated Chitosan Beads. *Water Res.* **2012**, *46* (14), 4427–4434.

(166) Churchman, G. J. Formation of Complexes between Bentonite and Different Cationic Polyelectrolytes and Their Use as Sorbents for Non-Ionic and Anionic Pollutants. *Appl. Clay Sci.* **2002**, *21* (3–4), 177–189.

(167) Breen, C. The Characterisation and Use of Polycation-Exchanged Bentonites. *Appl. Clay Sci.* **1999**, *15* (1–2), 187–219.

(168) An, J.-H.; Dultz, S. Adsorption of Tannic Acid on Chitosan-Montmorillonite as a Function of pH and Surface Charge Properties. *Appl. Clay Sci.* **2007**, *36* (4), 256–264.

(169) Li, J.-M.; Meng, X.-G.; Hu, C.-W.; Du, J. Adsorption of Phenol, P-Chlorophenol and P-Nitrophenol onto Functional Chitosan. *Bioresour. Technol.* **2009**, *100* (3), 1168–1173.

(170) Crini, G.; Badot, P.-M. Application of Chitosan, a Natural Aminopolysaccharide, for Dye Removal from Aqueous Solutions by Adsorption Processes Using Batch Studies: A Review of Recent Literature. *Prog. Polym. Sci.* **2008**, *33* (4), 399–447.

(171) Gerente, C.; Lee, V. K. C.; Le Cloirec, P.; Mckay, G. Application of Chitosan for the Removal of Metals From Wastewaters by Adsorption—Mechanisms and Models Review. *Crit. Rev. Environ. Sci. Technol.* **2007**, *37*, 41–127.

(172) Bailey, S. E.; Olin, T. J.; Bricka, R. M.; Adrian, D. D. A Review of Potentially Low-Cost Sorbents for Heavy Metals. *Water Res.* **1999**, *33* (11), 2469–2479.

(173) Shang, J.; Shao, Z.; Chen, X. Electrical Behavior of a Natural Polyelectrolyte Hydrogel: Chitosan/Carboxymethylcellulose Hydrogel. *Biomacromolecules* **2008**, *9* (4), 1208–1213.

(174) Miller, S. M.; Zimmerman, J. B. Novel, Bio-Based, Photoactive Arsenic Sorbent: TiO2-Impregnated Chitosan Bead. *Water Res.* **2010**, *44* (19), 5722–5729.

(175) Berger, J.; Reist, M.; Mayer, J. .; Felt, O.; Gurny, R. Structure and Interactions in Chitosan Hydrogels Formed by Complexation or Aggregation for Biomedical Applications. *Eur. J. Pharm. Biopharm.* **2004**, *57* (1), 35–52.

(176) Muzzarelli, R. A. A.; Muzzarelli, C. Chitosan Chemistry: Relevance to the Biomedical Sciences. In *Polysaccharides I: Structure, Characterisation and Use*; Heinze, T., Ed.; Springer-Verlag: Berlin/Heidelberg, 2005; pp 151–209.

(177) Bassi, R.; Prasher, S. O.; Simpson, B. K. Removal of Selected Metal Ions from Aqueous Solutions Using Chitosan Flakes. *Sep. Sci. Technol.* **2000**, *35* (4), 547–560.

(178) Miller, S. M.; Spaulding, M. L.; Zimmerman, J. B. Optimization of Capacity and Kinetics for a Novel Bio-Based Arsenic Sorbent, TiO2-Impregnated Chitosan Bead. *Water Res.* **2011**, *45* (17), 5745–5754.

(179) Alhstrom homepage http://www.ahlstrom.com/en/.

APPENDIX

TABLE OF SELECT COMMERCIALLY AVAILBLE SELENIUM TREATMENT TECHNOLOGIES AND TABLE OF PARTS/COMPONENTS FOR SMALL SCALE COLUMN TESTS COLUMN SETUP

Table S 1. Select commercially available selenium treatment technologies.

Technology	Company	Description	Tested Water Types	Key Design Considerations	Advantages
Biological: Fixed film, packed bed biological treatment technology	**GE Power & Water/ABMet** http://www.gewater.com/products/abmet-selenium-removal.html	Bioreactor operating in anoxic conditions. As influent gravity flows downward through the submerged biomatrix (support media + biofilm), selenate and selenite are reduced to particulate elemental selenium. When a WASH sequence is automatically performed, elemental selenium is removed from the biofilter.	Power (flue gas desulfurization, FGD) and mining waters. 10 full-scale plants fully compliant. 30 successful pilot demonstrations. Reduced total selenium concentration to below 4.7 ppb. Effluent BOD and TSS as low as 10 ppm.	Reduction and precipitation of selenium requires EBCT of 2 – 16 hours.	ABMet removes nitrate and metals including mercury and arsenic; One time seeding; Fast startup; No post treatment requirements.
Biological: Fluidized bed reactor (FBR) biological treatment technology High efficiency ion exchange technology	**Envirogen Technologies** http://www.envirogen.com/pages/contaminants/selenium-2/	A biologically active reactor utilizing project-specific media (sand or activated carbon) and electron donors, operated upflow in an anoxic state. Selenite and selenate are reduced to insoluble selenium that is removed along with biomass and feed suspended solids by downstream liquid/solids separation (usually filtration).	Mining, power generation, refining, agricultural and groundwater applications. Reported 150 FBRs installed in the U.S. and operated two pilot reactors (2011) for the treatment of coal mining waste. For coal mining applications, achieved < 5 ppb Se.	Biological treatment for handling large flow rates; Ion exchange for low flow rates.	Good handling of large flow rates; Low capital and operating costs; Wide range of influent and discharge limit conditions; offers fast kinetics and long media life.

Technology	Company	Description	Tested Water Types	Key Design Considerations	Advantages
Biological: Electro-biochemical reactor (EBR) technology	**Inotec** http://www.inotec.us/	Bioreactor uses electrical cells to provide electrons to microbes and reduce the nutrient doses needed.	Mining and mineral processing wastewater from metal and coal mines. Pilot test with coal mining wastewater showed selenium reduction below 10 ppb.	Retention times of 12 hours and applied voltage of 3 volts required in EBR.	Can be used for reduction of inorganic contaminants and heavy metals from waste streams.
Biological: Biological treatment technology	**Frontier Water Systems** http://frontierwater.com/	Containerized and mobile bioreactor that contains a proprietary dual stage process configuration that separately reduces and filters particulate selenium reduced by bacteria.	Mining and power (FGD wastewater and combustion residual leachate). Reported effluent selenium < 5 ppb at flow rates of 50 – 500 gpm depending on the reactor model.		Combined treatment of selenate, nitrate, mercury and arsenic in a single process.
Reactive Media: Sulfur modified iron (SMI) and ion-exchange	**Loprest Water Treatment Company** http://loprest.com/2013/06/seleniun-removal/	Uses ion exchange or sulfur modified iron to remove Se to ppt level. Ion exchange: Se is oxidized to selenate and removed by strong base anion exchange resins, which are regenerated with brine. Sulfur modified iron: SMI reacts with the sulfate in water to form jarosite mineral, which has a high affinity for selenate in its crystal structure	Pilot testing using SMI on coal storage runoff water reduced incoming Se > 20 ppb to < 0.06 ppb. SMI results can be achieved in high TDS waters after suspended solids have been removed.		Compared to zero valent iron (ZVI), SMI has greater longevity, releases less iron, remains more permeable, and has less effect on pH. SMI works well in high sulfate environments Once loaded, SMI is less susceptible to selenium release

Technology	Company	Description	Tested Water Types	Key Design Considerations	Advantages
Reactive Media: Selen-IX™: Ion exchange combined with zero valent iron	**BioTeq** http://www.bioteq.ca/technology-solutions/selenium/	Reduces to as low as 1 ppb using resins, operating in carousel mode, the columns treat feed solution and regenerate resin to provide continuous. treatment. In the electrochemical reduction step Fe is added to form an iron-selenium solid.	Mobile pilot plant deployed to mine-impacted surface waters in Canada		Does not require the feed water to be heated, is highly adaptable to fluctuations in selenium concentrations, greatly reduces the volume of waste by-product and stabilizes selenium into an inorganic iron-selenium solid product.
Reactive Media: Perma-Fix Process	**Perma-Fix Environmental Services** http://www.selenium-waste.com/ http://www.perma-fix.com/services/industrial.aspx	Chemically reduces it to an insoluble, non-toxic form , selenium from the waste water stream to the point the water can be disposed of by deep well injection; the remaining filter cake sludge is treated with the Perma-Fix Process so that it meets land ban restrictions to allow inexpensive disposal.			Operated at ambient temperature and atmospheric pressure.
Reactive Media: Ferric Sulfate	**ALTIVIA** http://www.altivia.com/Application-Selenium-Removal.aspx	Remove selenium through adsorption and iron co-precipitation.		It is recommended that selenate be chemically reduced to selenite for better selenium removal.	Selenite is strongly adsorbed to the ferric hydroxide particle.

Technology	Company	Description	Tested Water Types	Key Design Considerations	Advantages
Reactive Media: Elemental metallic iron	**Zero Valent Iron Solutions** http://www.zerovalent.com/zvis/what-is-zero-valent-iron/ http://www.zerovalent.com/images/White-Paper-The-Removal-of-Selenium-from-Water-using-Zero-Valent-Iron-Systems-ZVI-Medium.pdf	Finely divided ZVI fibers are used in polypropylene treatment tanks that can treat up to 20 gpm of constant flow.	Coal mining drainage, industrial wastewater, agriculture, municipal.		
Reactive Media: ZVI Blue™	**Liberty Hydro** http://libertyhydro.com/treatment-systems/selenium-treatment/	. Finely divided ZVI is attached to an open-pore polymer foam. The foam media allows easy flow of water while enabling adequate contact and reaction time with ZVI.	Successfully installed and tested 16 operational sites in West Virginia and Idaho Pilot test at South Fork Sage Creek Springs (Idaho) was not effective for reducing selenium < 5 ppb; treatment effectiveness dropped off after 5 months of operation.	Post treatment required to remove soluble and colloidal iron and increase dissolved oxygen prior to discharge; Iron precipitation quickly overwhelmed settling pond/sand filter.	Porous sponge-like matrix of ZVI eliminates scale and plugging issues typically associated with ZVI systems.
Fixed Bed Adsorption: SeRT® Technology	**Phillips 66's Selenium Removal Technology** http://www.phillips66.com/EN/tech/Pages/index.aspx	Fixed bed chemisorption technology that uses activated carbon to remove selenocyanate anion, selenite, and elemental selenium.	Pilot testing and full scale demonstrations on refinery stripped sour water (SWW). Kinetics are improved by reducing the pH of the SWW. SWW is also negatively affected by high concentrations of high molecular weight organics.		Simple, fixed-bed process.

Technology	Company	Description	Tested Water Types	Key Design Considerations	Advantages
Fixed Bed Adsorption: Sorbster®	**MAR SYSTEMS** http://marsystemsinc.com/Portals/0/MAR%20Systems'%20Sorbster%20%C2%AE%20Shows%20Significant%20Removal%20of%20Selenium.pdf https://mlsvc01-prod.s3.amazonaws.com/25ce0dbb001/d2d1e519-d656-430c-bae6-80ce3536599a.pdf	Enhanced activated alumina substrate coated with various proprietary chemical functional groups to complex selenate and selenite.	Industrial process, ground and wastewater systems; Small column tests in coal mine wastewaters showed <50% selenate removal (influent 54.5 ppb).	Pretreatments utilizing a silica removal media, Sorbster® Si-1, and low inlet water pH are especially effective in maximizing selenate removal rates by Sorbster Se-1 and maintaining selenium removal capacities in higher ionic strength waters.	
Fixed Bed Adsorption: ADSORBSIA™ GTO™ media	**DOW Chemical** http://www.wateronline.com/doc/selenium-removal-with-adsorbsia-0001 http://msdssearch.dow.com/PublishedLiteratureDOWCOM/dh_0920/0901b80380920eb7.pdf?filepath=productsafety/pdfs/noreg/233-00425.pdf&fromPage=GetDoc	Titanium oxide based granular adsorbant.		Disposable/non-regenerative; Works under all typical pH conditions.	Kinetics approximately ten times faster than those of currently available iron-based media; Without limitations to flow or pre-treatment

Table S 2. Parts/components for small scale column tests column setup.

Items	Catalog Number	Source	Price	Quantity	Description
Column	5820-06	ACE Glass	$38.8	1	11mm diam, 300mm height, epoxy coated chromatography column.
Adapter-bottom	5838-45	ACE Glass	$110.83	1	Adapter with flow valve, connect to bottom of the column.
Adapter-top	5838-43	ACE Glass	$52.21	1	Adapter without flow valve, connect to top of the column.
Filter Disc	5848-07	ACE Glass	$14.86	1 Pkg	100 micron polyethylene filter for adapters. One time use. Pkg/6.
O-ring	7855-08	ACE Glass	$11.89	1 Pkg	O-ring,Viton,size 012, Pkg/12.
Screen Support for bottom	5814-42	ACE Glass	$10.01	1 Pkg	0.407" 350 micron polypropylene filter for adapters. One time use. Pkg/12.
PTFE tubing	12684-28	ACE Glass	$16.09	1	2.0 mm diam, 0.4 mm wall, 3 meters.
Connectors (Nuts)-1/8”	5854-09	ACE Glass	$6.51	2	Tubing connection nut only 3.3mm 1/8"
Connectors (Ferrules)-1/8”	5854-26	ACE Glass	$6.51	2	Tubing connection ferrule only 3.3mm 1/8"
Glass Beads	8035-07	ACE Glass	$182.60	1 lb	5 mm diam beads. 500 ^{o}C heat treatment before use.
Glass Wool	18421-500G	Aldrich	$71.20	500 g	500 ^{o}C heat treatment before use.
Peristaltic pump	NE-9000G	syringepump	$575	1	Flow rate ranges: 0.004 mL/min to 75.19 mL/min. Output Pressure: 40~50psi (according to customer services)
Food grade tubing	Q-TP-FDI-1/16	syringepump	$2.5/ft	5 ft	1/16” diameter, connect to pump.